Univerzita Karlova

Přírodovědecká fakulta

Studijní program: Genetika, molekulární biologie a virologie

Studijní obor: Molekulární biologie a genetika eukaryot

PŘÍRODOVĚDECKÁ FAKULTA
Univerzita Karlova

Bc. Johana Brodská

Úloha jadérkových fosfoproteinů v odpovědi leukemických buněk na nukleolární stres

Role of nucleolar phosphoproteins in response of leukemic cells to nucleolar stress

Diplomová práce

Školitel: RNDr. Aleš Holoubek, PhD.

Praha, 2025

Prohlášení:

Prohlašuji, že jsem závěrečnou práci zpracovala samostatně a že jsem uvedla všechny použité informační zdroje a literaturu. Tato práce ani její podstatná část nebyla předložena k získání jiného nebo stejného akademického titulu.

V Praze, dne 30.4.2025

Poděkování:
V prvé řadě děkuji svému školiteli RNDr. Aleši Holoubkovi, PhD. za odborné vedení i za trpělivost a vstřícnost. Mgr. Barboře Brodské, PhD. děkuji za nedocenitelné odborné rady a celkovou podporu. RNDr. Kateřině Kuželové, PhD. a Mgr. Ditě Strachotové, PhD. patří dík za poskytnutí výsledků odborných metod. Také děkuji Mgr. Pavle Röselové, Ing. Kateřině Wolfové a dalším kolegyním z Laboratoře proteomiky za nezbytnou práci "za scénou" v podobě rutinních laboratorních prací. Nakonec děkuji Sofii za to, že pro mě vždycky měla slova podpory i útěchy a dostatek svačinek a kávy.

Abstrakt

V podmínkách buněčného stresu vyvolaného např. chemickými látkami poškozujícími DNA, hypoxií nebo UV ozářením dochází k narušení struktury buněčného jadérka a jeho funkce. Stres způsobující takové narušení integrity jadérka se označuje jako nukleolární. Projevuje se delokalizací proteinů jadérka, zejména fosfoproteinů nukleofosminu (NPM) a nukleolinu (NCL), do nukleoplazmy, potažmo cytoplazmy. Tato práce se zabývá reakcí zmíněných nukleolárních proteinů na jednu složku nukleolárního stresu, oxidativní stres, a je inspirována publikací vyšetřující roli jednoho z cysteinů v molekule NPM, Cys275 (Yang a kol. 2016).

V první části je popsána konstrukce plazmidů pro expresi fluorescenčně značených mutovaných variant NPM a NCL, které se od přirozené formy liší zastoupením cysteinů, a mohly by proto mít změněnou odpověď na oxidativní stres. Pomocí konfokálního mikroskopu jsme sledovali chování těchto proteinů v buňkách linie HeLa opůsobených různými stresory. Z testovaných stresorů jsme pro bližší zkoumání zvolili doxorubicin, který je hojně používán pro léčbu nádorových onemocnění, včetně leukémie, a jedním ze známých mechanismů jeho účinku je právě vyvolávání oxidativního stresu.

Druhá část práce se věnuje analýze vlivu doxorubicinu na morfologii a viabilitu buněk, zaznamenává typické znaky apoptózy a aktivaci nádorového supresoru p53, monitoruje vstup doxorubicinu do buněk, delokalizaci jadérkových proteinů a tvorbu reaktivních forem kyslíku. Tyto jevy byly sledovány jak v buňkách linie HeLa, tak v několika leukemických liniích. Výsledky potvrzují, že reakce buněk na doxorubicin je obecná, tedy že leukemické buňky a buňky linie HeLa odpovídají srovnatelně. Dalším poznatkem je, že exogenní formy NPM a NCL delokalizují v buňkách ošetřených doxorubicinem podobně jako jejich endogenní formy.

V další části jsme testovali vliv vnesených mutací na delokalizaci proteinů z jadérka do nukleoplazmy. Jako parametr pro porovnání efektu jsme zvolili časový vývoj poměru intenzit fluorescence detekované v nukleoplazmě a v jadérku. Tato měření potvrdila výraznější vazbu primárně testované mutace v NPM, C275S, v jadérku ve srovnání s přirozenou formou NPM. Zároveň ale ukázala, že důležitou roli hraje nejen ztráta cysteinu, ale i charakter aminokyseliny, jíž je původní cystein nahrazen. Podobné experimenty na NCL s mutací v jeho jediném cysteinu ukázaly, že v případě NCL nemá záměna pozorovatelný efekt.

V závěru jsme provedli několik pilotních experimentů s konstrukty NPM značenými redox senizitivními fluorescenčními proteiny roGFP1 a roGFP2 a ukázali jsme, že jak přirozená forma vyskytující se převážně v jadérku, tak mutovaná varianta typická pro akutní myeloidní leukémii lokalizovaná v cytoplazmě, reflektují redox změny prostředí vyvolané známými oxidačními a redukčními činidly. Zatímco u cytoplazmatické mutované formy jsme zaznamenali výraznou odpověď, reakce NPM s mutací C275S byla zřetelně slabší.

Předložená práce je základem pro další výzkum v oblasti monitorování vlivu léčiv vyvolávajících nukleolární, a zejména oxidativní, stres na funkci jadérkových proteinů.

Klíčová slova: jadérko; nukleolární stres; nukleofosmin; nukleolin; protein-proteinové interakce; sledování redoxního stavu; AML; p53; molekulární klonování; cílená mutageneze

Abstract

Under cellular stress conditions induced e.g. by chemicals detrimental to DNA, hypoxia or UV irradiation, the nucleolar structure and function is compromised. Stress leading to such damage to the integrity of nucleolus is called nucleolar. It manifests by delocalization of nucleolar protein, namely the phosphoproteins nucleophosmin (NPM) and nucleolin (NCL), to the nucleoplasm or even cytoplasm. This thesis focuses on the aforementioned nucleolar proteins, and a subtype of nucleolar stress – oxidative (redox) stress, and is inspired by a publication examining the role of the cysteines (Cys275) in NPM (Yang et al. 2016).

The first section describes the construction of plasmids for the expression of fluorescently labeled mutated variants of NPM and NCL, which deviate from the wild type in the number of cysteines present and as such may have an altered response to redox stress. Under a confocal microscope, we observed the behavior of these proteins in HeLa cells treated by different types of stressors. We eventually chose doxorubicin from these stressors, which is a chemotherapeutic drug widely used to treat cancers, including leukemia, and one of mechanisms of action is inducing redox stress.

The second part of the thesis analyses the influence of doxorubicin on the morphology and viability of cells, monitors typical markers of apoptosis and activation of the tumor suppressor p53, the entrance of doxorubicin into cells, delocalization of nucleolar proteins and production of reactive oxygen species. The results prove that the reaction of cells to doxorubicin is universal, meaning that leukemic cells react comparably to HeLa cell line. Another finding is that exogenous forms of NPM and NCL in cells treated by doxorubicin delocalize similarly to the endogenous forms.

In the next section, we tested the influence of introduced mutations on delocalization of proteins from nucleolus to nucleoplasm. We selected time evolution of the ratio of fluorescence intensities in both compartments as our method for comparison. These experiments confirmed a stronger bond of the main mutation of focus in NPM (C275S) inside the nucleolus compared to the wild type form, but they also showed that the amino acid substituting the original cysteine plays a part as well as simply the loss of a cysteine. Similar tests on NCL and its only cysteine showed that the substitution has no observable effect in the case of nucleolin.

To finish with, we conducted several pilot experiments with NPM constructs labeled with redox-sensitive fluorescent proteins, roGFP1 and roGFP2, and demonstrated that both the wild type form of NPM and the mutated form typical for acute myeloid leukemia localized in the cytoplasm reflect the redox changes in the environment induced by oxidants and reductants. While the AML-typical mutant reacted strongly, the C275S mutant exhibited notably less reactivity.

This thesis serves as a base for further research in the realm of monitoring of the influence of drugs that create nucleolar (specifically redox) stress on the function of nucleolar proteins.

Key words: nucleolus; nucleolar stress; nucleophosmin; nucleolin; protein-protein interactions; redox sensing; AML; p53; molecular cloning; site-directed mutagenesis

Table of contents

Abbreviations:

A = alanine
aa = amino acids
ALL = acute lymphoid leukemia
AML = acute myeloid leukemia
APE1 = apurinic/apyrimidinic endodeoxyribonuclease 1
ATP = adenosine triphosphate
Bcl-xL = B-cell lymphoma extra large
Bcl-2 = B-cell lymphoma 2
BER = base excision repair
C, Cys = cysteine
CAR = chimeric antigen receptor
DCFDA/H_2DCFDA = 2',7'-dichlorodihydrofluorescein diacetate
DDR = DNA damage response
DFC = dense fibrillar component
DNMT3A = DNA-methyltransferase 3A
DSMZ = Deutsche sammlung von mikroorganismen und zellkulturen (German Collection of Microorganisms and Cell Cultures)
DTT = DL-dithiothreitol
ECIS = Electric Cell-substrate Impedance Sensing
ECL = enhanced chemiluminescence
FACS = fluorescence activated cell sorting
FC = fibrillar center
Flt3-ITD = Fms-like tyrosin kinase 3 – internal tandem duplication
GAR domain = glycine/arginine-rich domain
GC = granular component
GFP = green fluorescent protein, eGFP (indicated as “g”: gNPM, gNCL)
GSH = glutathione
GSSG = glutathione disulfide
γH2A.X = histone H2A.X phosphorylated at S139
H_2O_2 = hydrogen peroxide
HPV = human papilloma virus
HRP = horseradish peroxidase
HSR = heat shock response
IB = immunoblot
IF = immunofluorescence
IP = immunoprecipitation
ISR = integrated stress response
Kan = kanamycin
Mdm2/Hdm2 = murine/human double minute 2
NA = numerical aperture

NCL = nucleolin
NES = nuclear export signal
NoLS = nucleolar localization signal
NOR = nucleolar organizing region
NPM, NPM1 = nucleophosmin variant 1; used interchangeably
$O_2^{\bullet -}$ = superoxide
ODR = oxidative distress response
$OH^{\bullet}$ = hydroxyl radical
PARP = poly (ADP-ribose) polymerase
PBS = phosphate buffered saline
PI = propidium iodide
PVDF = polyvinylidene difluoride
RFP = red fluorescent protein, mRFP1 (indicated as “r”: rNPM, rNCL)
RNA Pol I = RNA-polymerase I
RNS = reactive nitrogen species
roGFP = redox sensitive GFP
ROS = reactive oxygen species
rRNA = ribosomal RNA
RT = room temperature
S = serine
SDS-PAGE = sodium dodecyl sulfate polyacrylamide gel electrophoresis
SRP = signal recognition particle
UPR = unfolded protein response
UV = ultraviolet
W = tryptophane
WB = Western blot
WHO = world health organization
wt = wild type
Y = tyrosine

1 Introduction

The nucleolus and its role in sensing cellular stress has been a popular topic in molecular biology research for many years. Nucleolar phosphoproteins (e.g. nucleophosmin (NPM), nucleolin (NCL)) as multifunctional proteins play a thoroughly studied role in diverse cellular processes such as ribosome genesis (or ribogenesis), cell duplication, DNA repair, apoptosis through regulation of the stability of tumor suppressors (e.g. p53) and many others. Nevertheless, many details of the mechanisms in which nucleolus-related proteins are involved remain elusive. This study pays special attention to the role of these proteins in cellular stress sensing which is connected to the phenomenon of nucleolar stress. It is supposed that nucleolar stress is involved in response of cells to the majority of stressful stimuli, especially to redox changes, UV or genotoxic stress. Since the response of both healthy and cancerous cells to drug treatment is crucial in chemotherapy and in the search for more targeted strategies, this study is devoted to investigating of the role of the two aforementioned nucleolar phosphoproteins in redox sensing. In particular, their characteristic stress-induced delocalization is examined in context of the cysteines in their primary structure, which are known to mediate redox signalization.
For a detailed study of the mechanism of stress response, we selected doxorubicin, an anthracycline drug widely used in chemotherapy. It is known to operate in several ways ultimately leading to apoptosis, including DNA damage and generation of reactive oxygen species (ROS). Importantly, doxorubicin is effective in leukemia treatment, but it often causes severe unwanted responses. A deep understanding of all of its mechanisms is therefore crucial.

Acute myeloid leukemia (AML) is a severe hematologic disease characterized by dysregulation of myeloid cell development. As a consequence, accumulation of nonfunctional blood cells impairs normal hematopoiesis. Highly proliferating malignant clones usually develop from a cell with one or more mutations specific to AML, e.g. type A mutation of NPM1. Resulting mutated protein has an altered expression and frequently also changes its interaction network. Specifically, a crucial interaction between NPM and NCL is disrupted by this mutation. Targeting protein-protein interactions is therefore one of the therapeutic strategies for AML treatment. Inspired by the research of the highly specific AML-linked NPM mutation, we pay special attention to the function of both nucleolar phosphoproteins in leukemic cells.

2 Literature review

2.1 Nucleolus and nucleolar stress

The nucleolus is a compartment within a cell's nucleus. It is not separated by a membrane and its structure is dynamic. One cell can have multiple nucleoli; their number, size and shape depend mainly on the cell's proliferation activity (incl. cancerous proliferation) and differentiation stage (Rodrigues et al., 2023; Smetana et al., 2004). The nucleoli contents are organized around nucleolar organizing regions (NORs), which contain clusters of ribosomal DNA on acrocentric chromosomes (chr13, chr14, chr15, chr21 and chr22) (Henderson et al., 1972). Each nucleolus is comprised of three compartments: a fibrillar center (FC), a dense fibrillar component (DFC), and a granular component (GC) (Boisvert et al., 2007). These compartments can be distinguished based on a characteristic marker protein: RNA polymerase I subunit A for FC, fibrillarin for DFC, and nucleophosmin (NPM or NPM1) for GC (Hua et al., 2022).

The nucleolus' primary function is ribosome biogenesis. Apart from many ribosomal proteins, it also contains non-ribosomal proteins, which have ribosome-genesis associated functions – these include NPM, nucleolin (NCL) and others (Muñoz-Velasco et al., 2025). Ribogenesis is a very energy-intensive process, which means that most signaling pathways have a connection to the nucleolus. Besides ribogenesis, the nucleolus is also responsible for initiating the assembly of SRP – signal recognition particle (Issa et al., 2024), and different small RNAs, including tRNAs. Most importantly for our research, the nucleolus also plays a crucial role in detecting stress within cells (Olson, 2004).

James et al. (James et al., 2014) understand nucleolar stress as any disruption to normal ribogenesis, with the consequence of disruption of cell homeostasis. Abnormalities can occur in different stages of the process – all the way from transcription initiation (even due to faulty nucleotide biosynthesis (Maehama et al., 2023)) to assembly and final release from the nucleolus. Three phenomena are considered as typical markers of nucleolar stress: reduction of the nucleoli size, release of nucleolar proteins into the nucleoplasm, and inhibition of RNA Pol I-regulated ribosomal synthesis (Lu et al., 2018; Ogawa et al., 2021). RNA Pol I transcription is negatively affected by several drugs, including the intercalating agent doxorubicin. Environmental stressors such as oxidative stress or UV irradiation can lead to structural changes in the nucleolus (James et al., 2014).

One of the most important molecules for inducing cell cycle arrest and/or apoptosis is p53 (Olausson et al., 2012). In physiological conditions, p53 is mostly inactivated by polyubiquitinilation by murine double minute 2 (Mdm2; or human double minute 2, Hdm2) and subsequent proteasome degradation (Russo & Russo, 2017). When Mdm2 is prevented from interacting with p53 molecules, these are not ubiquitinylated and can carry out their role in arresting the cell cycle and initiating apoptosis (James et al., 2014; Maehama et al., 2023). The activation of p53 signaling by nucleolar stress has been documented (Lafita-Navarro & Conacci-Sorrell, 2023), however the mechanisms of this activation remain unclear.

Nucleolar stress triggers the transfer of nucleolar proteins (NPM1 and NCL, but also ribosomal proteins) into the nucleoplasm (Maehama et al., 2023). It has been proposed that Mdm2 is inactivated by different proteins under nucleolar stress and that NPM1 may interact directly with the Mdm2/p53 complex (Hua et al., 2022). In cells with defective or lacking p53, apoptosis can be triggered through p53-independent pathways, which may be activated for example by the aforementioned ribosomal proteins (Maehama et al., 2023).
Since ribosomes are crucial for a cell's growth and proliferation, increasing their biogenesis is important for cancer cells to thrive. Disrupting ribogenesis then should logically prevent cancerous cells from proliferating, either by lowering the number of available ribosomes, or by inducing nucleolar stress to activate p53 (if present). However, in some cases, defective ribosome synthesis results in the exact opposite, which is promoting cancerous development (Sulima et al., 2017). It is not yet clear why; current hypotheses consider the possibilities of affected DNA repairs and survival signaling or altering ROS level balance and causing DNA damage (Maehama et al., 2023).
Besides cancer, nucleolus and nucleolar stress have been linked to various neurodegenerative diseases (Rieker et al., 2011), but also to cardiovascular (Hariharan & Sussman, 2014) and developmental diseases (Calo et al., 2018).

2.1.1 Redox stress

Nucleoli ensure ribosomal RNA (rRNA) synthesis and its association with ribosomal subunits, and these processes are prone to be affected by aberrant levels of reactive species (Willi et al., 2018). Sies et al. define oxidative stress as "an imbalance between oxidants and antioxidants in favor of the oxidants, leading to a disruption of redox signaling and control and/or molecular damage" (Sies et al., 2017). They emphasize that the presence of oxidants is not inherently stressful, noting that for example the mitochondria's oxidative conditions are physiological. The key components to oxidative stress are an increased presence of oxidants and formation of GSSG from glutathione (Sies et al., 2024).
In their 2024 review, Sies et al. (Sies et al., 2024) model redox regulation as a series of events creating a feedback loop between input cues and final outcome of cells. In summary, the pathway goes as follows:

1. An input cue is received: either from within the cell/organism (endogenous cues) in the form of hormones, cytokines or other molecules, or from the outside (exogenous cues). Exogenous cues include physical factors (e.g., heat), irradiation (UV), or chemical factors – notably drugs.
2. A signal is generated and transduced: here, reactive species of oxygen, nitrogen and sulphur play a key role. These are produced by different enzymes and pathways. Specifically, three main types of reactive oxygen species (ROS) occur as products of cell metabolism: superoxide ($O_2^{\bullet -}$), hydrogen peroxide (H_2O_2) and hydroxyl radicals ($OH^{\bullet}$) (Schieber & Chandel, 2014).

3. The signal is received by “redox proteome” (Sies et al., 2024): reversible modifications are made to thiol groups of cysteines in different proteins (notably glutathione and other redoxins, but also certain transcription factors).
4. These modifications then alter the genome, proteome, regulatory RNAs and other cellular networks.
5. Different responses are activated: “oxidative distress response (ODR), unfolded protein response (UPR), heat shock response (HSR), integrated stress response (ISR) and the DNA damage response (DDR).” (Sies et al., 2024)
6. These responses finally result in larger outcomes, both on cellular and organismal levels. Cells may differentiate, proliferate, and migrate, but also die. In the full organism, inflammation and ageing can be observed among other phenomena (Sies et al., 2024).

In short, a certain level of imbalance in oxidative states is not only normal, but in fact necessary for signaling in cells; however, disturbing the ratio too much can be damaging – as is the case with most balance-based systems.

2.1.1.1 Glutathionylation and redox sensing

Glutathion, or γ-glutamylcysteinylglycine or GSH, is an almost omnipresent molecule in organisms and it plays a key role in protecting cells from oxidative stress. Its antioxidant effect is executed by creating disulfide bridges between thiol groups of two molecules. The ratio between the reduced form GSH and the oxidized form GSSG in physiological conditions is constant, regardless of the total amount of both forms (Komínková et al., 2015).

Among amino acids, cysteine has a thiol group and is then an important redox sensor inside proteins (Barford, 2004). Some studies show a correlation between evolutionary level of organism and average cysteine ratio in its proteins (Castillo-Villanueva, Reyes-Vivas, and Oria-Hernández 2023; Miseta and Csutora 2000), others note an inverse proportion between the length of a protein and cysteine ratio (Carugo, 2008; Desai & Sun, 2024). Most importantly, the cysteine content of a protein is linked to its function and subsequently to the location of the function’s execution (Desai & Sun, 2024; Go et al., 2015), more specifically, it has been proven that ribosomal proteins have approx. half the amount of cysteines to the organism average (Miseta & Csutora, 2000). Desai et al. even recently classified proteins as C-free, low C-count and C-rich; many ribosomal proteins belong to the first group and as such have zero cysteines (Desai & Sun, 2024).

It then comes as no surprise that NPM, NCL and other nucleolar proteins also have a fairly low number of cysteines (NPM: 3 Cys out of 294 amino acids (aa), NCL 1 Cys out of 710aa), even though they do not reside solely in the nucleolus. Yang et al. (Yang et al., 2016) even explicitly proposed that S-glutathionylation on Cys275 of NPM occurred as a result of redox change (oxidation by ROS) and was responsible for the translocation into nucleoplasm (more in the next chapter).

2.2 Nucleophosmin

NPM has three main variants, the most common one being NPM1 (Fig. 1). NPM1 has 294 aa, and lacks the sequence coded by exon 10. Its N-terminal region is stabilized by hydrophobic interactions and is involved in chaperone activity and oligomerization. C-terminal region has a positive charge thanks to basic residues and binds to nucleic acids and ATP. Tryptophan (W) residues on positions 288 and 290 are crucial for nucleolar localization. Other structures on C-terminus are responsible for chaperone activity, histone binding, nucleosome formation or ribonuclease activity (Brodská et al., 2019).

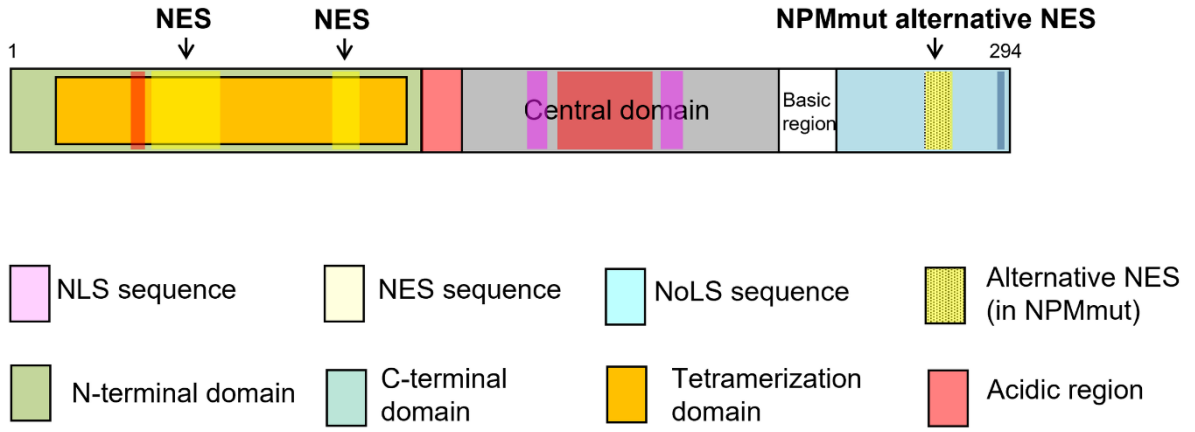

Figure 1: NPM scheme (A. Holoubek et al., 2025)

As illustrated by the examples above, NPM1 has a number of cellular functions in nucleoli, nucleus and cytoplasm. To attend to all of these, it has two nuclear exporter signals (NES) on N-terminus, NLS in central domain, and NoLS in C-terminus with the aforementioned W288 and W290. Its role in ribosome biogenesis in the nucleolus can majorly affect cell growth and proliferation. Further involvement in the cell cycle includes control over centrosome duplication, and indirect modulation of base excision repair (BER) through its interaction with APE1 (Hindley et al., 2021). To cement its importance for maintaining cell health, NPM1 acts as a tumor suppressor: in response to cellular stress, NPM1 is transferred from nucleolus to nucleoplasm, where it binds Mdm2 protein, and thus inhibits its role in mediating the degradation of p53. Increased p53 activity then leads to cell cycle arrest or apoptosis (Kurki et al., 2004).

NPM contains three cysteines: Cys21, Cys104 lie in the oligomerization domain, and Cys275 is found in the second of three C-terminus alpha helixes (Lee et al., 2012) (Fig. 2). Yang et al. (Yang et al., 2016) confidently state that the oxidation of Cys275 is responsible for NPM1 translocation. They experimented with a 3C/S mutant and all 2C/S mutants and concluded that the last cysteine is the important one for translocation. They also state that NPM1 is S-glutathionylated at Cys275 under stress, which they prove by co-immunoprecipitation assay with antibodies against GSH and NPM1 and mass spectrometry (Yang et al., 2016).

Having established the variety of functions, it comes as no surprise that the malfunction of NPM1 is associated not just with AML, but also with different solid tumors (Grisendi et al., 2005).

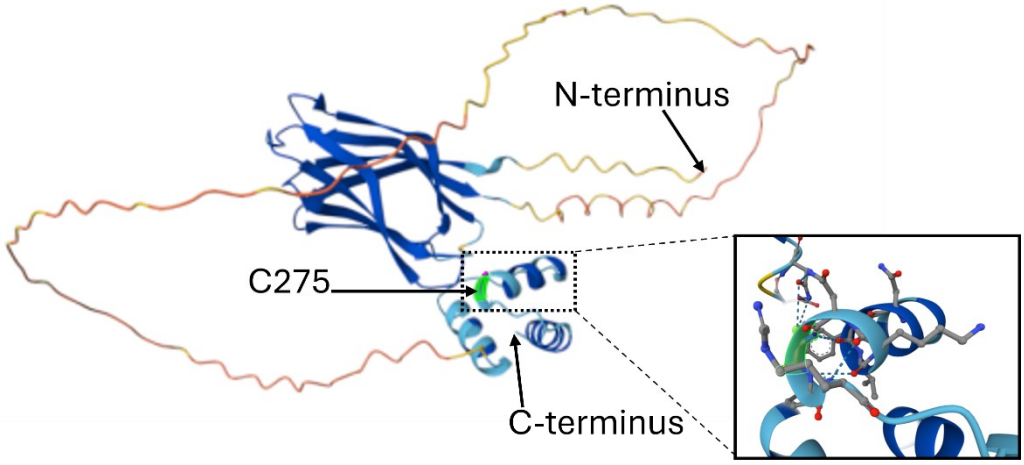

Figure 2: Scheme of Homo sapiens *NPM structure with C275 (green) marked with an arrow (left) and in detail (right); created using AlphaFold2 (Jumper et al., 2021; Varadi et al., 2024)*

2.3 Nucleolin

Similarly to NPM1, nucleolin (NCL) is a phosphoprotein found in the nucleoli, nucleus and cytoplasm of cells (Borer et al., 1989; Scherl et al., 2002), in certain conditions also in the membrane (Christian et al., 2003), and can be shuttled between these. It also has roles in chromatin modeling, ribosome assembly, proliferation and apoptosis (Ginisty et al., 1999), and therefore is a target of cancer-related research. Studies have shown the correlation of overexpressed NCL and poor prognosis not only in AML (Shen et al., 2014), but also breast cancer (Pichiorri et al., 2013), lung cancer (Zhao et al., 2013) and more.

Nucleolin has the ability to interact with a wide range of other proteins, including NPM1, as well as nucleic acids. This has been proven despite researchers not having yet obtained NCL's full 3D structure (Berger et al., 2015).

In her 2015 review, Berger et al. (Berger et al., 2015) concluded that there were no mutations of NCL associated with diseases, and to my knowledge, there are no publications suggesting otherwise even as of 2025. Rather, the involvement of NCL in cancer (incl. leukemia) appears to be in the form of over-expression and/or accumulation of the protein and/or its mRNA (Chen et al., 2023; Otake et al., 2007). This state may be both the result of a pathological state and one of the contributions to its initiation or progression.

NCL is comprised of three structural domains (Fig. 3). The N-terminus has acidic regions and basic stretches, four RNA binding domains are found in the middle, and the C-terminus includes many glycine, phenylalanine and arginine residues (Ginisty et al., 1999).

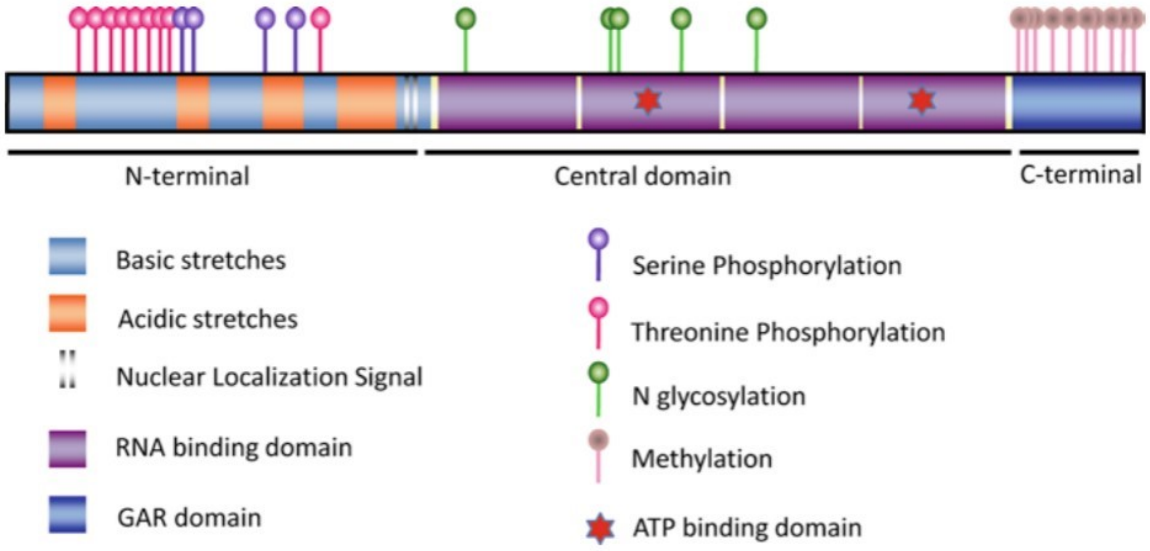

Figure 3: diagram of nucleolin and its domains ((Cong et al., 2011), from book The nucleolus, edited by M. Olson)

Interestingly, no nucleolar localization signal has been identified in the NCL sequence (Créancier et al., 1993; Schmidt-Zachmann & Nigg, 1993). This leaves the question of how such a large fraction (90%) of NCL ends up in the nucleolus. Berger proposes binding to other nucleolar components (possibly to NPM (Li et al., 1996)) after entering the nucleoplasm thanks to its nuclear localization signal (Berger et al., 2015).

Nucleolin also plays a part in ribosome genesis, e.g. by regulating RNA polymerase I transcription (Cong et al., 2012; Rickards et al., 2007), although once again, the mechanisms have not yet been fully elucidated. The roles of NCL in later steps of ribogenesis involve participation in pre-rRNA maturation as well as in assembly of ribosomes (Bouvet et al., 1998; Ginisty et al., 1998, 2000). In addition, Berger calls NCL "a guardian of genome stability", as it is involved in replication, recombination and repair (Berger et al., 2015). To conclude the non-exhaustive list, NCL also appears to be binding to and regulating certain anti-apoptotic mRNAs, such as Bcl-xl or bcl-2 (Otake et al., 2007; Zhang et al., 2008). All of the functions listed above present possible roles of NCL in tumorigenesis.

In terms of drugs targeted to NCL, aiming for the over-expressed cell-surface molecules is the most promising approach due to lower toxicity for healthy cells (Berger et al., 2015).

Nucleolin captured our attention for this thesis due to the fact that its primary structure contains a single cysteine out of 710 amino acids (Cys543; Fig. 4). As mentioned in the chapter on redox stress (part 2.1.1.1), the extremely low number of cysteines may be an indication of their role in redox sensing in the nucleolus.

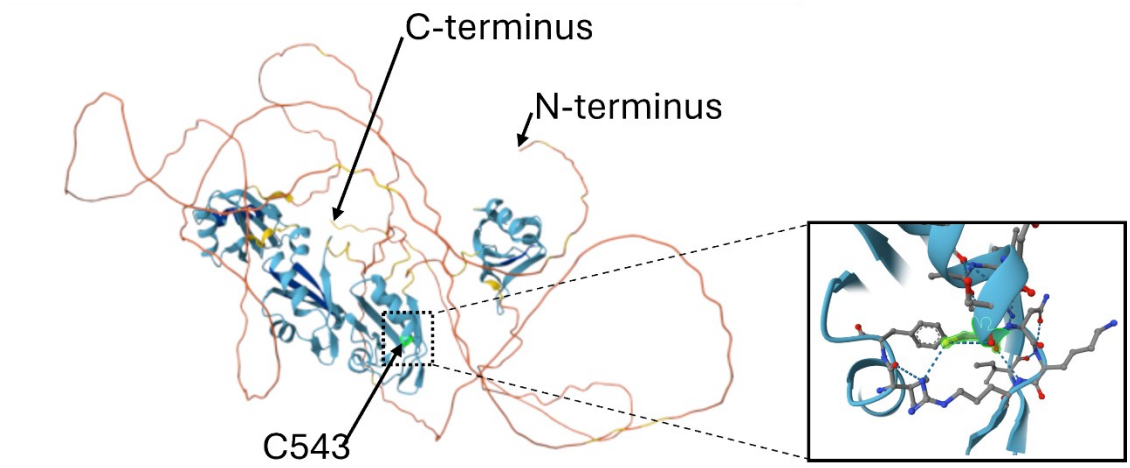

Figure 4: Scheme of Homo sapiens *NCL structure with C275 (green) marked with an arrow (left) and in detail (right;) created using AlphaFold2 (Jumper et al., 2021; Varadi et al., 2024)*

2.4 Leukemia

2.4.1 AML

Acute myeloid leukemia is a hematological disease affecting the myeloid lineage of blood cells, where genetic alterations in stem cells result in overproduction of clonal myeloid cells. A minority of cases hve a causative factor in the form of prior chemotherapy or an effect of other chemical agents, but generally, there is no clear causative agent for AML (Grimwade et al., 2016). According to American Cancer Society, the average age of patients first diagnosed with AML is 69 (ACS web site 2025). Patients may present with various initial symptoms, including fatigue, fever, pallor or bleeding. Some cases may be discovered in routine blood work in asymptomatic patients. The crucial step for final diagnosis is bone marrow examination (Pelcovits & Niroula, 2013).

The WHO (World Health Organization) recognizes 14 types of AML and related neoplasms for risk classification, with mutated NPM1 being identified as AML with favorable or intermediate prognosis (Hindley et al., 2021). The most common base of induction therapy is known as 7+3: seven days of cytarabine infusion plus a dose of an anthracycline, typically daunorubicin, for the first three days (Pelcovits & Niroula, 2013). In general, risk increases and patient performance decreases with age (Appelbaum et al., 2006).

2.4.1.1 AML and mutated NPM1

Most NPM1 mutations in leukemia (over 50) have been identified in exon 12 and these were also pronounced the cause of increased cytoplasmic localization (Alpermann et al., 2016). Over 75% of AML mutations are classified as Type A, characterized by a TCTG duplication. The frameshift nature of the mutation disrupts the NoLS and instead, an NES is created and NPM is therefore transported out of the nucleus and resides in the cytoplasm (Falini et al., 2005). Type A mutated NPM gains one extra cysteine (Cys288) and there is some evidence that it might be responsible for the cytoplasmic localization (Huang et al., 2013). This kind of

mutation appears in around 30% of AML patients (Hindley et al., 2021) and it is mostly found in patients with normal karyotype. It is also associated with high white blood cell, platelet and bone marrow blast count and, interestingly, according to Thiede et al., female patients, despite AML being more prevalent in men (Thiede et al., 2006).
This NPM mutation also has a negative effect on NPM-NCL interaction (Šašinková et al., 2018). NPMmut is always co-expressed with NPMwt, as NPMmut homozygosity is lethal (Grisendi et al., 2005). Both forms can create heterodimers and affect each other's localization (Brodska et al., 2017).
Other mutations, notably Flt3-ITD and DNMT3A (associated with worse prognosis), are more likely to occur in patients with NPMmut (Yao et al., 2024).
Despite hundreds of studies having been published on the topic of NPM1 mutations in AML, the mechanism of tumorigenesis is still not fully understood. This limits the potential of development of targeted therapy (Hindley et al., 2021).

2.4.2 ALL

Acute lymphoid leukemia manifests by proliferation of malignant lymphoid progenitor cells. While AML is more common in older adults (see 2.4.1.), 80% of ALL patients are children. The second largest patient group is then also older adults, specifically over 50 years old. Pediatric patients generally have a hopeful prognosis, especially after the recent development of chimeric antigen receptor (CAR) T cell treatment (Mitra et al., 2023); the prognosis for elderly patients remains unfavorable – long-term remission only occurs in about 30-40% of cases (Terwilliger & Abdul-Hay, 2017).
As of 2016, the WHO recognizes 11 types of B-cell ALL and a single T-cell ALL type. Doxorubicin is a part of the induction chemotherapy treatment, in combination or alteration with other drugs (Terwilliger & Abdul-Hay, 2017). There are no NPM or NCL mutations generally associated with ALL, but there has been some evidence that the overexpression of NCL has negative effects on response to induction chemotherapy treatment (especially anthracyclines, e.g. doxorubicin) and subsequently on overall survival (Chen et al., 2023).

2.5 roGFP

Given their transient nature, it is impossible to accurately observe redox events within cells with probes that lack resolution in the dimensions of time and space. Low invasiveness is also desired. Redox-sensitive GFP, invented by M. Cannon and S. J. Remington (Cannon & Remington, 2006, 2008), provides these qualities – created on the basis of the well-researched and widely used green fluorescent protein, it utilizes sensitivity to oxidation and reduction innate to certain variants of GFP. The structure of GFP is also extremely stable and resistant to adverse conditions, and at the same time allows for insertions, permutations and additions of terminal fusion proteins.
Excitation of GFP produces emission at 508nm, but this emission can be created by exciting either of its two peaks: 400nm (major) or 480nm (minor). Part of the explanation for

the phenomenon is the protonation state of GFP. An anionic form is responsible for the minor excitation peak, a neutral form would normally emit light at the wavelength of approx. 450nm, but it is converted to the anionic form by excited state proton transfer (Cannon & Remington, 2008; Kennis et al., 2004).

It has been shown that certain changes in environment, such as pH or salt concentration changes, influence the equilibrium of the two chromophore states. Naturally, this offers the potential for analyzing environmental changes by observing excitation equilibrium changes – that is creating a ratiometric sensor (Cannon & Remington, 2006, 2008).

Adding cysteine residue pairs in favorable positions on the surface of GFP creates possibilities for disulfide bond formation, which appears as a reaction to ROS and RNS – in other words, as a reaction to redox changes. Disulfide bonds cause slight structure alterations, and since structure is inextricably linked to protonation state, the equilibrium of excitation peaks was thought to possibly be affected by the initial redox changes ((Dooley et al., 2004), Fig. 5). Depending on the original variant of the GFP source and the location of the newly introduced cysteine residues, six roGFP versions were created and eventually confirmed to be reliable indicators of redox potential in different cell compartments (Cannon & Remington, 2006, 2008).

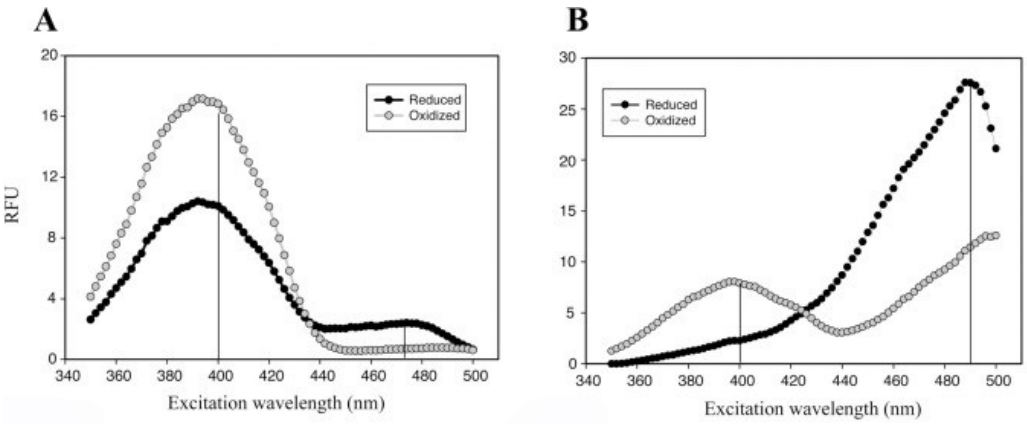

Figure 5: excitation spectra for fully oxidized and fully reduced roGFP1 (A) and roGFP2 (B), as reported by Dooley et al. (Dooley et al., 2004); emission was monitored at 515nm

2.6 Doxorubicin

Doxorubicin was the first anthracycline isolated from *Streptomyces peucetis* (along with daunorubicin) and it is widely used to treat different cancers, including AML (Sherif et al., 2021) and ALL (Kantarjian et al., 2004; Nagura et al., 1994). Doxorubicin is cytotoxic by intercalating into the DNA helix as well as mitochondrial DNA, and by binding proteins involved in replication and transcription. This leads to inhibition of DNA, RNA and protein synthesis and ultimately to cell death. It also interferes with the work of topoisomerase II, more specifically with re-ligation of cleavable complex, resulting in double-strand DNA breaks, and failure to repair them leads to apoptosis (Carvalho et al., 2009; L. F. Liu et al., 1983; Tewey et al., 1984). Doxorubicin-caused DNA damage is also thought to lead to the generation of reactive oxygen species (Thorn et al., 2011), however the exact mechanism of this consequence remains to be

elucidated. It is possible that some of these mechanisms are intertwined, but in the final consequence is definitely a collective effort (Kciuk et al., 2023; Sritharan & Sivalingam, 2021). While doxorubicin (or generally anthracycline) chemotherapy has been a stable choice for its good response rate and overall survival, there are also severe side effects, including but not limited to bone marrow aplasia (increasing the risk of infections and delaying healing (Xu et al., 2023)), leukopenia (Julka et al., 2008), local tissue necrosis (Dorr et al., 1989), cumulative cardiotoxicity (Hortobágyi, 1997), and brain damage (Carvalho et al., 2009), cardiotoxicity being likely induced by doxorubicin's ROS-generating activity (Minotti et al., 1998). Attenuated risk of the side effects is ensured by its administration in lower concentrations, in combination with other drugs (Takeuchi et al., 2002).

Doxorubicin suspension is highly pigmented, with reddish appearance, and it has been shown that its spectral properties allow for its detection by spectrometry. Maximum excitation and emission wavelength were found at 470 and 560nm, respectively (Liang et al., 2018) (Fig. 6). Kauffman et al. determined its detection sensitivity by fluorescence spectrometry less than 0.1µM in buffers and cell lysates (Kauffman et al., 2016).

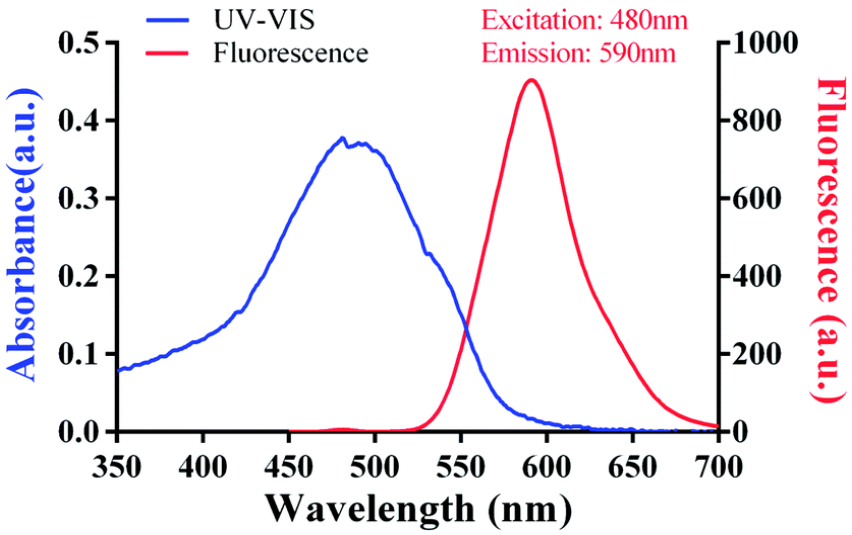

Figure 6: doxorubicin absorption and emission spectra (from (Liang et al., 2018))

3 Aims

1. Construct plasmids for different mutated NPM and NCL variants labeled by eGFP or mRFP1.
2. Subject cells to different stress stimuli in a controlled manner, observe reactions of fluorescently labeled constructs, choose a stressor that induces delocalization of the constructs to nucleoplasm.
3. Verify the works and hypotheses of Yang et al. (Yang et al., 2016) concerning glutathionylation of NPM Cys275 under stress conditions.
4. Examine the impact of studied NPM and NCL mutations on p53 regulation.
5. Construct and test roGFP (NPM) sensors, monitor redox changes in cellular compartments.

4 Methods and materials

4.1 Laboratory equipment

Piece of equipment	**Producer**
Analytic scale AE200 Comesa	Mettler
Agarose DNA electrophoresis E0738 equipment	Sigma
SDS-PAGE equipment	Bio-Rad
Automatic cell-counter	Bio-Rad
Blotcycler W5	Precision Biosystems
MiniSpin centrifuge, rotor F45-12-11	Eppendorf
Biofuge pico centrifuge	Heraeus
Centrifuge 5702	Eppendorf
Rotofix 32A centrifuge	Schoeller
Olympus FV 1000 confocal microscope	Olympus
SafeFast Elite laminar flow box	Faster
Nanodrop ND-1000 Spectophotometer	Thermo Scientific
CFX96 Optics Module PCR cycler	Bio-Rad
LSRFortessa Analyzer flow cytometer	BD Biosciences
G:BOX iChemi XX6 (fluorescence and chemiluminescence detector)	Syngene
Thermoblock TB2	Biometra
Trans-Blot® TurboTM Transfer system	BioRad
Blotboy 3D Rocker	Benchmark Scientific
Sorvall ultracentrifuge, rotors 42.2TI (Beckmann-Coulter) and T476,5 (Sorvall)	Sorvall
Vortex V-1 plus	Biosan

4.2 Materials

4.2.1 Solutions

PBS (Phosphate Buffered Saline):	40g NaCl 1g KCl 14,5g $Na_2HPO_4 \cdot 12\ H_2O$ 1g KH_2PO_4 pH adjusted to 7,4 with H_3PO_4 dH_2O to total volume of 5l
2x reducing sample buffer	0,12g Tris, pH = 6,8 (adjusted with HCl) 8ml dH_{2O} 0,4g SDS 0,31g DTT

	2ml glycerol 50µl 1% BFB (bromophenol blue)
Lytic buffer	10 mM Tris/Cl, pH 7,5 150 mM NaCl 0,5 mM EDTA 0,5% NP-40
Washing buffer for IP	10 mM Tris/Cl pH 7,5 150 mM NaCl 0,5 mM EDTA
STET medium	2g 8% saccharose 1,25g 5% Triton X-100 2,5ml 500mM EDTA – NaOH 1,25ml 500mM Tris – HCl, pH = 8 dH_2O to total volume of 25ml
EDTA – NaOH	14,6g 500 mM EDTA pH adjusted to 8 with 5M NaOH dH_2O to total volume of 100ml
TE (Tris/EDTA) buffer, pH=8	10mM Tris 1mM EDTA
Liquid LB medium	10g Lennox L Broth base 400ml dH_2O 20mg Kan
Agar plates	7,5g LB 5,8g agar 320ml dH_2O 15mg kanamycin (Kan) for approx. 12 plates
LB medium for competent cells	10g bacto-trypton 5g yeast autolysate 5g NaCl 50mg Kan dH_2O to total volume of 1l
TAE	121g TRIS 29ml 99% acetic acid 50ml 0,5M EDTA, pH = 8 dH_2O to total volume of 500ml
SDS buffer for horizontal electrophoresis	4,5g TRIS 21,6g glycine 1,5g SDS 1,5l dH_2O
30% acrylamide gel	29,2g acrylamide

	0,8g bis acrylamide 25ml glycerine 50ml dH2O filtered through filter paper dH_2O to total volume of 100ml
Ammonium persulfate	0,4g ammonium persulfate 1ml dH_2O
Separating gel	5ml dH_2O 3,75ml TRIS/SDS buffer, pH = 8,8 6,25ml 30% acrylamide 10µl TEMED 20µl ammonium persulfate
TRIS/SDS buffer, pH = 8,8	18,1g TRIS 0,4g SDS dH_2O to total volume of 100ml pH adjusted to 8,8 by HCl
Stacking gel	6,2ml dH_2O 2,5ml TRIS/SDS buffer, pH = 6,8 1,3ml 30% acrylamide 10µl TEMED 20µl ammonium persulfate
TRIS/SDS buffer, pH = 6,8	6,06g TRIS 0,4g SDS dH_2O to total volume of 100ml pH adjusted to 8,8 by HCl
Antibiotics	100U/ml penicilin + 100µg/ml streptomycin
DMEM medium with serum	445ml DMEM (Dulbecco´s Modified Eagle´s Medium) with glutamine (Sigma) 5ml antibiotics 50ml fetal calf serum
RPMI medium with serum	440ml RPMI 1640 medium (Roswell Park Memorial Institute) (Sigma) 5ml 200mM L-glutamine 5ml antibiotics 50ml fetal calf serum
Alpha-MEM medium with serum	390ml alpha-MEM (Minimal Essential Medium, alpha modification) (Sigma) 5ml 200mM L-glutamine 5ml antibiotics 50ml fetal calf serum
SOC medium	0,029g 10mM NaCl

	0,0093g 2,5mM KCl 0,102g 10mM $MgCl_2$ 0,123g 10mM $MgSO_4$ 0,198g 20mM glucose 0,25g 0,5% yeast lysate 1g 2% tryptone pH adjusted to 7,0 with NaOH dH_2O to total volume of 50ml
Western blot buffer	200ml buffer concentrate from BioRad kit 200ml 96% ethanol 600ml dH_2O

4.2.2 Enzymes used for molecular cloning

Pfu DNA Polymerase (Promega)
T4 DNA Ligase (NEB)
XhoI Restriction enzyme (10U/µL, Thermo Scientific)
BamHI Restriction enzyme (10U/µL, Thermo Scientific)
EcoRI Restriction enzyme (10U/µL, Thermo Scientific)
HindIII Restriction enzyme (10U/µL, Thermo Scientific)

4.2.3 Primers used for molecular cloning

- NPM:
  - peGFP-C1
    - Fw: AAAAAACTCGAGCTATGGAAGATTCGATGGACATG
  - peGFP-C2
    - Fw: AAAAAACTCGAGCATGGAAGATTCGATGGACATG
    - Rv: AAAAAAGGATCCCTTAAAGAGACTTCCTCCACTGC
- mutated NPM:
  - C275S
    - Rv: AAAAAAGGATCCCTTAAAGAGACTTCCTCCACTGCCAGAGATCTTGAATAG CCTCTTGGTCAGTCATCCGGAAGGAATTCTTCACAT
  - C275A
    - Rv: AAAAAAGGATCCCTTAAAGAGACTTCCTCCACTGCCAGAGATCTTGAATAG CCTCTTGGTCAGTCATCCGGAAGGCATTCTTCACAT
  - MutA
    - Rv: AATTAAGGATCCACTATTTTCTTAAAGAGACTTCCTCCACTGCCAGAGATCT TGAATAGCCTCTTGGTCAG

- NCL:
    - peGFP-C1
        - Fw: AAAAAACTCGAGCTATGGTGAAGCTCGCGAA
    - peGFP-C2
        - Fw: AAAAAACTCGAGCATGGTGAAGCTCGCGAA
        - Rv: AAAAAAGGATCCCCTATTCAAACTTCGTCTTCTTTCCT

4.2.4 Vectors and constructs used for molecular cloning

- originally Clontech:
    - peGFP-C1, -C2
    - pmRFP1-C1, -C2
- constructed by Dr. Holoubek, available in the laboratory:
    - peGFP-C2:NPMwt
    - peGFP-C2:NCLwt
    - pmRFP1-C2:NPMwt
    - pmRFP1-C2:NCLwt
    - peGFP-C2:NPM-Y271C
    - pmRFP1-C2:NPM-Y271C
    - pmVenus-C1:NCL-C543C
    - proGFP1-C1
    - proGFP2-C1

4.2.5 Antibodies

target protein	**type**	**dilution**	**catalogue number**	**producer**
β-Actin	mouse monoclonal	1:500	sc-47778	Santa Cruz Biotechnology, Inc. (=S. Cruz)
Bcl-2	mouse monoclonal	1:500	sc-509	S. Cruz
Caspase-3	mouse monoclonal	1:250	sc-7272	S. Cruz
PARP	mouse monoclonal	1:500	sc-8007	S. Cruz
p53	mouse monoclonal	1:500	sc-126	S. Cruz
p53pS15	rabbit monoclonal	1:500	ab223868	Abcam

p53pS46	rabbit monoclonal	1:500	ab76242	Abcam
p53pS392	rabbit monoclonal	1:1000	ab33889	Abcam
GFP	mouse monoclonal	1:100 - 1:500	sc-9996	S. Cruz
NCL	rabbit monoclonal	1:200 - 1:1000	ab129200	Abcam
NPM	mouse monoclonal	1:100 - 1:500	sc-70392	S. Cruz
HRP-conjugated anti-mouse	goat polyclonal	1:20.000	31430	Invitrogen
HRP-conjugated anti-rabbit	goat polyclonal	1:20.000	31460	Invitrogen
AlexaFluor555-conjugated anti-mouse	goat polyclonal	1:200	A21424	Invitrogen
AlexaFluor448-conjugated anti-rabbit	goat polyclonal	1:200	A11034	Invitrogen

4.3 Cell lines

cell line name	**origin**	**further characteristics**
HeLa	established from cervical cancer cells obtained from 31-year-old patient Henrietta Lacks without her consent	adherent, one of the most widely used cell lines
HEK-293T	est. from human embryonic kidney cells	(weakly) adherent, epithelial, non-functional apoptosis, high expression of exogenous proteins
OCI-AML2	est. from peripheral blood cells of a 65-year-old patient with AML	suspension, mutation in DNMT3A
OCI-AML3	est. from peripheral blood cells of a 57-year-old patient with AML	suspension, mutation (type A) in *NPM* gene and in DNMT3A
Jurkat	est. from peripheral blood of a 14-year-old patient with ALL after relapse	suspension, zero level or activity of p53
MV4-11	est. from peripheral blood cells of a 10-year-old AML patient	suspension, homozygous FLT3-ITD mutation

MOLM-13	est. from peripheral blood cells of a 20-year-old AML patient relapsed after MDS	suspension, heterozygous FLT3-ITD mutation

All cell lines were purchased from DSMZ (German Collection of Microorganisms and Cell Cultures).

4.4 Methods

4.4.1 Working with bacterial and cell cultures

4.4.1.1 Bacterial cultivation and preparation of competent cells

Bacteria *Escherichia coli* Top10 were inoculated into 20ml of LB medium from bacterial stock. The suspension was incubated overnight at 37°C while being shaken at 220rpm. The next day, 1ml of this suspension was inoculated into 100ml LB medium and the mixture was cultivated again at 37°C while shaking until the optic density reached approx. 0,375 at 590nm (OD^{590} ~ 0,375). Then the culture was cooled down for 10min on ice and the suspension was divided into two 50ml centrifuge test tubes and centrifuged for 10min at 1500g and 4°C. Each pellet was resuspended in 25ml of cold, sterile $CaCl_2$ solution (100mM $CaCl_2$, pH = 8) and then they were combined into one 50ml centrifuge test tube and incubated on ice for 20min. Then the suspension was centrifuged again (10min at 1500g and 4°C) and the pellet was resuspended in a mixture of 1,75ml iced $CaCl_2$ solution and 0,75ml glycerol. The final mixture was aliquoted into 1,5ml Eppendorf tubes in 100µl batches, incubated for 30min on ice and then kept at -80°C until needed. Bacterial competence was confirmed by test transformation with plasmid DNA.

4.4.1.2 Transformation of plasmid DNA into competent *E. coli* cells

An Eppendorf tube with competent cells prepared using the aforementioned protocol was placed on ice for about 2min to thaw slightly. Mixing carefully with a tip, 4-10µl of ligation mixture was added and the cells were incubated for 20-40min on ice. Next, the cells were subjected to heat shock by incubating at 42°C for 50s and cooled on ice for several minutes immediately after. 450µl of SOC medium was gently mixed in with the cells and the mixture was incubated on the shaker at 37°C at 180rpm for 1h. Then the suspension was spread onto two agar plates with kanamycin by single-use microbiological cell spreader in volumes of 50-100µl, and the rest to obtain individual cell colonies. The plates were then incubated overnight in the incubator adjusted to 37°C.

4.4.1.3 Preparation of stocks of *E. coli* cultures

Bacterial cultures were incubated overnight in liquid LB medium with an appropriate antibiotic at 37°C while shaking at 220rpm. Batches of 850µl were mixed with 200µl of glycerol. After mixing, they were stored at -80°C.

4.4.2 Working with DNA

4.4.2.1 Construction of plasmids

Plasmids were constructed using standard expression vectors containing sequences of desired fluorescent proteins, peGFP-C1, peGFP-C2, pmRFP1-C1, pmRFP1-C2 (originally Clontech). Fragments and linearized vectors for ligation were prepared by PCR amplification with primers adapted with appropriate restriction sites. For preparation of C275S and C275A NPM mutations, the PCR amplification of NPM fragments was performed using reverse primers containing also accordingly mutated original codon for cysteine 275. NCL fragment with mutation for C543S was PCR amplified from pmVenus-C1:NCL-C543S, plasmid constructed previously in our lab by site-directed mutagenesis. The amplified fragments were subcloned to the corresponding vectors to be fused with fluorescent proteins using XhoI and BamHI unique restriction sites. The PCR was perfomed with Pfu polymerase following the recommended protocol. The annealing temperature was optimized to obtain sufficient yield of well-defined product.

PCR mixture:
2µl appropriate template, e.g. 200x diluted purified plasmid
2µl appropriate forward primer (c = 5µM) (see 4.2.3.)
2µl appropriate reverse primer (c = 5µM) (see 4.2.3.)
38µl dH_2O
1µl dNTP
5µl 10X buffer for Pfu polymerase (Promega)
0,8µl Pfu polymerase (Promega)

4.4.2.2 DNA cleavage by restriction enzymes

Each reaction contained 2µl BamHI (20U), 1µl XhoI (5U), 8µl 10X Yellow Buffer and, if possible, 2µg of DNA (plasmic, PCR product). The total volume was brought to 42µl with dH_2O. Restriction reactions were incubated for 3-3,5h at 37°C.

4.4.2.3 Agarose gel electrophoresis and isolation of DNA

DNA fragments were separated by size on agarose gel electrophoresis. A 0,7% gel was prepared from agarose powder and TAE buffer. The UV-sensitive Gel Red Nucleic Acid Stain (10 000x diluted in water, by Biotium) was added for later visualization. Each sample was mixed with 6X Loading Dye and applied into a well in the gel. 5µl of Easy ladder I marker (Meridian Bioscience) and 5µl of GeneRuler™ DNA ladder Mix (Thermo Scientific) were also loaded and the electrophoresis ran in TAE buffer under 98V for approx. 1h 15min. After finishing, the separated fragments were visualized in a UV transilluminator, cut out of the gel and purified by PureLink™ Quick Gel Extraction Kit (Promega) according to official instructions.
Isolated and purified DNA fragments were separated by size on 1% agarose gel electrophoresis for control and quantification needed for ligation. The samples were loaded onto the gel with

the help of 6X Loading Dye, Gel Red Nucleic Acid Stain was added for visualization and electrophoresis ran for approx. 1h 15min under 98V. DNA fragments were then detected by Gene Box (Syngene) in comparison to the quantifying marker Easy Ladder I and quantified to determine the ligation mixture composition for each cloning.

4.4.2.4 Cloning mutated genes into plasmids

Using results from the quantification and relative molecular weights of inserted fragment and vector, the ligation mixture was prepared to contain insert and vector in 3:1 ratio of molecules. Every reaction was supplemented with 1µl of T4 DNA ligase (400.000 units/ml) and 4µl of 10X Ligase Reaction buffer, and dH_2O was added accordingly to bring every reaction to a total of 41µl. Ligation ran for 6h in 16°C. T4 DNA ligase was then deactivated by heat shock (10min in 65°C) and 4µl (1:10) of 3M NaAc (pH adjusted to 5,2) and 100µl of cold 96% ethanol were added to precipitate the DNA. The mixture was stored at -20°C overnight.

The next day, the ligation mixture was centrifuged for 30min at 10 000g at 4°C. Supernatant was discarded and the pellet was left to dry for 30-50min at lab temperature. The dried reaction mixture was rehydrated with 18µl dH_2O and 2µl Red Buffer (Thermo Scientific). Appropriate restriction enzymes (0,5µl, 5U) were then added to reduce the original plasmids used for the cloning; HindIII for the NPM constructs and EcoRI for the NCL constructs. The restriction was carried out for 2h at 37°C. The enzymes were then inactivated by incubation at 80°C for 20 min. The 4-10µl of ligation mixture was then used to transform competent *E. coli* cells, see 4.4.1.2.

4.4.2.5 Isolation of plasmid DNA by "boiling miniprep" for tentative analysis

Random colonies were chosen from agar plates with Kanamycin (Kan; see chapter 4.2) and transferred to agar plates for further cultivation; incubated overnight at 37°C and then stored in the fridge. For further analysis, individual clones were streaked to new agar plates and incubated overnight at 37°C. The next day the multiplied clone colonies were transferred to a test tube and resuspended in 150µl of STET medium. Mixed properly, the samples were boiled for 50s and centrifuged for 8min at 10 000g at lab temperature. The pellet was removed with picks, and isopropanol was added to each supernatant in approx. 1:1 ratio. After incubation for 1,5h at -20°C, the samples were centrifuged for 8min at 10 000g at 4°C. The supernatant was discarded, and the pellets were left to dry fully at room temperature for about 40min. Each sample was then resuspended in 20-25µl of TE buffer and finally analyzed on agarose gel electrophoresis.

(modified from (Malke, 1990)).

4.4.2.6 High-purity isolation of plasmids with Promega kit

Clones of the correct size chosen from testing by the gel electrophoresis were streaked with sterile microbiology picks onto new agar plates to obtain individual colonies. The plates were incubated at 37°C overnight. The next day a single colony was inoculated into liquid LB medium with Kan and incubated at 37°C on the shaker overnight. The next day, a portion of

the culture was used to prepare bacterial stocks and stored at -80°C, see 4.4.1.3. Plasmid DNA was isolated from the rest with PureYield™ Plasmid Miniprep System kit (Promega) according to protocol.

4.4.2.7 Spectrophotometric methods

The concentration and purity of DNA was determined by NanoDrop (ND-1000 Spectrophotometer). The appliance was cleaned, calibrated and blanked with dH_2O, and 2µl of each sample were used for measuring.

4.4.2.8 Sequencing

Reaction mixture for sequencing of the resulting plasmids included 300ng of plasmid, 1µl of appropriate sequencing primer (5µM), and dH_2O to obtain 8µl final volume. The sequencing was done by Laboratory OMICS – Genomics (Fac Sci, Charles Uni, https://natur.cuni.cz/en/biology/departments-and-work-places/service-facilities/laboratory-omics-genomics).

4.4.3 Cell lines cultivation

HeLa, Jurkat, MV4-11, and MOLM-13 cell lines were cultivated in RPMI medium, OCI-AML2 and OCI-AML3 in alpha-MEM medium, and HEK-293T in DMEM medium. Media contents are specified in chapter 4.2.

All the lines were cultivated in cell culture flasks in an incubator with 5% CO2 at 37°C and 80% humidity; passage was done in a sterile laminar flow box 3x a week, adherent cells being trypsinized to detach from the surface.

When needed, cells were counted, and viability was measured by mixing 1:1 with Trypan Blue solution by Cell Counter (BioRad).

4.4.3.1 Transfection with recombinant plasmids

In a sterile microtube, 100µl of jetPrime (Polyplus transfection) buffer, 1µg of plasmid DNA and 2µl of jetPrime reagent were mixed. After vortexing vigorously, the mixture was left to incubate at room temperature for approx. 20min and then added carefully to 2ml cell cultures (approx. 60-80% confluency) in microscopy wells. After a 4h incubation, the medium was exchanged for a fresh batch and the culture was further incubated for 24h or more at 37°C.

4.4.3.2 Immunofluorescent staining of fixed cells

Approx. $1x10^6$ cells per sample were centrifuged (300g, 6min), supernatants were discarded, and medium residues were removed by washing with PBS. Cleaned pellets were resuspended in 150µl PBS and the suspensions were pipetted onto cover glasses. The samples were incubated for 20-30min in a moist chamber to give the cells time to settle onto the surface. Residual liquid was removed with filter paper and the cells were fixed with 4% paraformaldehyde by incubation in a moist chamber overnight at 4°C.

The following day, the samples were rinsed with PBS and then incubated in 0,5% Triton for 10 min in room temperature for cell permeabilization. Then the samples were soaked in PBS with 0,2% Tween-20 (PBS-Tween) 3x for 5min and then incubated for 60min with the solutions of a mix of primary antibodies in PBS-Tween.
Subsequently, the samples were soaked in PBS-Tween 3x for 5min again and incubated with AlexaFluor-conjugated secondary antibodies for 60min in the dark, then the samples were rinsed twice with PBS-Tween still in the dark and finally rinsed once with PBS without Tween-20. A drop of fixating agent (Prolong) was put onto the slides and cover glasses were carefully placed on top. The fixating was left to harden overnight.

4.4.4 Cell-monitoring methods

4.4.4.1 Live-cell fluorescence microscopy

Cells were grown on a glass bottom Petri dish (D29-14–1,5-N, Cellvis) 24h prior to transfection with appropriate plasmids. After the 24h incubation period, control or doxorubicin-treated cells were observed in regular intervals (usually 30min) for several hours (usually 5h) or overnight (usually 16h). Fluorescence was observed under the confocal laser scanning microscope FV1000 with UPLSAPO 60x NA 1.35 oil immersion objective (Olympus). Data were processed with the FluoView FV10-ASW v3.1 software. For eGFP and mRFP1 fluorescence, 488nm and 543nm excitation lasers were used and emission was detected with FV12-MHBY filter cube.

4.4.4.2 Monitoring of doxorubicin presence in cells

Cells were seeded in Petri dish with coverslip for the microscopy measurements. After overnight cell attachment into the dish surface, doxorubicin was added to the dish to final concentration of 4μM and monitored by confocal microscope. Fluorescence induced by 488nm-laser beam was observed by a high-sensitivity detector capturing signal passing through FV12-MHBY filter cube, in the emission range of 575-675nm.

4.4.4.3 Fluorescent Activated Cell Sorting (FACS)

Treated and control samples (containing approx. $5x10^5$ cells) were harvested the same way as for SDS-PAGE. Adherent cells were trypsinized and moved into centrifugation tubes with the entire volume of medium. Suspension cells were counted and were placed into centrifugation tubes in volumes with approx. $5x10^5$ cells. From this point, both cell types were processed equally – as follows. Cells were centrifuged (300g, 5min), resuspended in 1ml of PBS, halved into FACS test tubes and centrifuged again. For each sample, one tube was resuspended in 0,5ml of appropriate medium with 20μM H_2DCFDA and the second one only in 0,5ml of medium and all samples were incubated for 30 min at 37°C with 5%CO_2. Then they were centrifuged again, resuspended in 300ul PBS with 1μM propidium iodide and immediately analyzed by flow cytometer.

4.4.4.4 Electrical cell-substrate impedance sensing (ECIS)

Impedance measurements were performed using the ECIS ZΘ device (Applied Biophysics) (Šašinková et al., 2021). The wells incubated with 200µl culture medium, and the baseline was monitored for several hours before cell addition. Cells were seeded at 120 000 cells/well and monitored overnight, then doxorubicin was added for another 20–24h. One well from each plate was left empty, filled only with medium, and the signal from this well was used as the baseline for the other wells of the same plate. The impedance signal is automatically decomposed into resistance and capacitance. The ECIS records were exported to Microsoft Excel and processed using the GraphPad Prism software: the background was set to zero at a time point corresponding to cell seeding, and the baseline was subtracted. The curves shown in the graphs represent the averages from duplicate wells, which were run in parallel.

4.4.4.5 roGFP

This method was executed by Mgr. Dita Strachotová, PhD. at the Faculty of Mathematics and Physics, Charles University. For more photophysics information, see chapter 2.5.

4.4.5 Working with proteins

4.4.5.1 Cell lysate preparation for SDS-PAGE

Adherent cells:

The medium from 5ml wells with adherent cells was discarded, the cells were rinsed with PBS twice and finally incubated with 300µl of 0,25% Trypsin-EDTA at 37°C for approx. 2,5min. 5ml of the medium (type depending on cell lines) was added to inactivate the trypsin and everything was transferred into 15ml test tubes and centrifuged for 5min at 300g.

Suspension cells:

Cell count and viability was determined by Cell Counter (BioRad) using Trypan Blue staining. Then approximately $5x10^6$ viable cells was transferred into 15-ml test tube and centrifuged 5min, 300g, RT.

After centrifugation, the protocol is the same for all cell lines: supernatant was discarded, pellet was resuspended in 1ml of PBS and transferred to 1,5ml microtubes, then centrifuged for 5min at 250g. Supernatant was discarded, and the sample was resuspended in 150µl of sample buffer and heated to 93°C for 5min.

After cooling down for at least 15min at -20°C, the sample was centrifuged for 4h at 180 000g at 4°C. Supernatant was transferred to a new microtube and stored in -20°C. When needed, the samples were taken out of the freezer, incubated again in 93°C for 5min and after quickly centrifuging again, they were analyzed on SDS-PAGE.

4.4.5.2 SDS-PAGE, Western blot

SDS-PAGE was prepared according to standard protocol (for composition of gels see Chapter 4.2.1), 2µl of Precision PlusProtein Dual Color Standard (Bio-Rad) were used as a molecular weight marker. The samples were loaded in volumes of 7µl; 10 µl in case of immunoprecipitation samples. Electrophoresis ran at max 200V and 100mA for approx. 1h.

After the electrophoresis, the separated proteins were transferred to a PVDF membrane by Western blotting using BioRad kit (standard protocol, blotting buffer specified in 4.2).
Strips were cut out of the membrane according to the assumed positions of desired proteins, localized by comparison to the visible ladder bands. Then the membrane pieces were blocked by PBS with 0,2% Tween-20 and 5% non-fat milk (in amounts determined by ratio 1g/20ml PBS) for 1h at room temperature while gently shaking. Primary antibodies were then added in correct concentrations, usually 1:500-1000, and incubated overnight at 4°C. The next day, the membranes were rinsed 6x in 5min intervals in PBS-Tween-20 solution. Appropriate secondary antibodies were added in concentrations 1:20 000-1:50 000 and incubated for 1h in the same solution at room temperature. Then the membranes were rinsed again (same way as before). After a 5min incubation in ECL substrate (ECL Prime Western Blotting Detection Reagent, Amersham), the appearing luminescent signal was detected in G:BOX Chemi XX6 System in the GeneSys software.

4.4.5.3 Co-immunoprecipitation

Cells of HEK-293T cell line were seeded into 5ml Petri dishes, transfected by respective plasmids after 24h, non-controls were treated with 4µM doxorubicin after 48h. After 72h, all cells were rinsed with chilled PBS, removed from the surface with a scraper, transferred to a test tube and washed with more PBS. The cell pellet was incubated in lytic buffer for 30min on ice and then centrifuged (20 000g, 10min, 4°C). Supernatant (cell lysate) from each sample was removed, halved and each half was added to either agarose nanoparticles with GFP-Trap (a peptide with high affinity to eGFP) or p53-Trap (a peptide with high affinity to p53 protein, which is present in larger quantities in HEK-293T). The suspensions were gently rotated for 60min at 4°C to allow the nanoparticles and respective proteins to bind together. Subsequently, the nanoparticles were washed several times with washing buffer, eventually resuspended in 100µl 2x sample buffer, boiled at 93°C for 10min and centrifuged (2500g, 2min, 4°C). The resulting supernatant was kept at -20°C until needed for SDS-PAGE.

4.4.6 Statistical analysis

To estimate the differences between fluorescence intensity ratio trends after doxorubicin treatment of cells transfected with various NPM mutants, we subjected the data to 2way-ANOVA with multiple comparisons using GraphPad software version 10.2.3. Tukey´s multiple comparison test revealed significant differences (p-value <0,05) among the samples in individual time points. These differences are marked in graphs with symbols explained in appropriate figure legends.

5 Results

5.1 Construct plasmids for different mutated NPM and NCL variants labeled by eGFP or mRFP

Mutations ensuring substitution of cysteines were planned to be inserted into genomic sequences of NPMwt and NCLwt in plasmids designed for fusion with fluorescent proteins. The C275S mutation was introduced to the NPM sequence using elongated adapted primers, see 4.2.3. Plasmid pmVenus-C1:NCL-C543S was available in the lab and used as a template for construction of peGFP-C2 and pmRFP1-C2-based plasmids for green and red labeling of NCL. Since constructs used for eGFP and mRFP1 labeling were based on –C2 line of the cloning vectors, both fragments were amplified by PCR using appropriate primers maintaining open reading frame. After that, we have decided to also prepare NPM-C275A to examine if and how the different substitutions change the behavior of NPM variants during nucleolar stress. We adapted the primer used for construction of NPM-C275S, but otherwise the molecular cloning protocol was identical. To tie our work to existing research of the AML-typical mutant A, we also created a "double mutant" – mRFP1_NPM-CS-mutA (mutA contains an extra cysteine compared to wt; see chapter 2.4.1.1). Here we used an already prepared construct containing the codon for the C275S mutation and we proceeded similarly as in (Brodská et al. 2016). The Y271C mutation was present in original plasmids used in the lab before being repaired the NPMwt sequence; the mutation existed in a commercially available ORF clone (Ultimate ORF Clone IOH 27892). This mutation substitutes the tyrosine at position 271 of NPMwt sequence for an additional cysteine, which offers another perspective when studying potential role of cysteines in redox sensing by nucleolus.

Typical steps of cloning procedure are illustrated in Figs. 7, 8 and 9. The linearized vectors used for molecular cloning were prepared by restriction cutting with XhoI and BamHI of constructs already available in the laboratory. These constructs were chosen in a way that prevented interference with the desired constructs; we used the peGFP-C2:NCLwt plasmid for construction of mutated NPM construct, and peGFP-C2:NPMwt for mutated NCL construct. PCR-amplified fragments and linearized vectors were separated and purified by agarose electrophoresis using Wizard SV Gel and PCR Clean-Up System (Promega). Resulting fragments and vectors are shown in Fig. 7. Corresponding vector and fragment were then ligated using T4 DNA Ligase (NEB) and transformed into competent cells. Resulting clones were tested first for their size on the agarose gel using the Boiling, see Fig. 8. Chosen clones were then amplified and purified by PureYield™ Plasmid Miniprep System (Promega) and again checked by agarose electrophoresis, As shown in Fig. 9, we obtained only one construct exhibiting appropriate plasmid size for the NPM-C275S construct and all three obtained NCL-C543S constructs were of correct size. Among the final NPM clones, we can see a construct with size identical to NCL clones, which means that the plasmid used for restriction cutting of the vector went through the cloning, which confirmed the usefulness of the chosen cloning strategy.

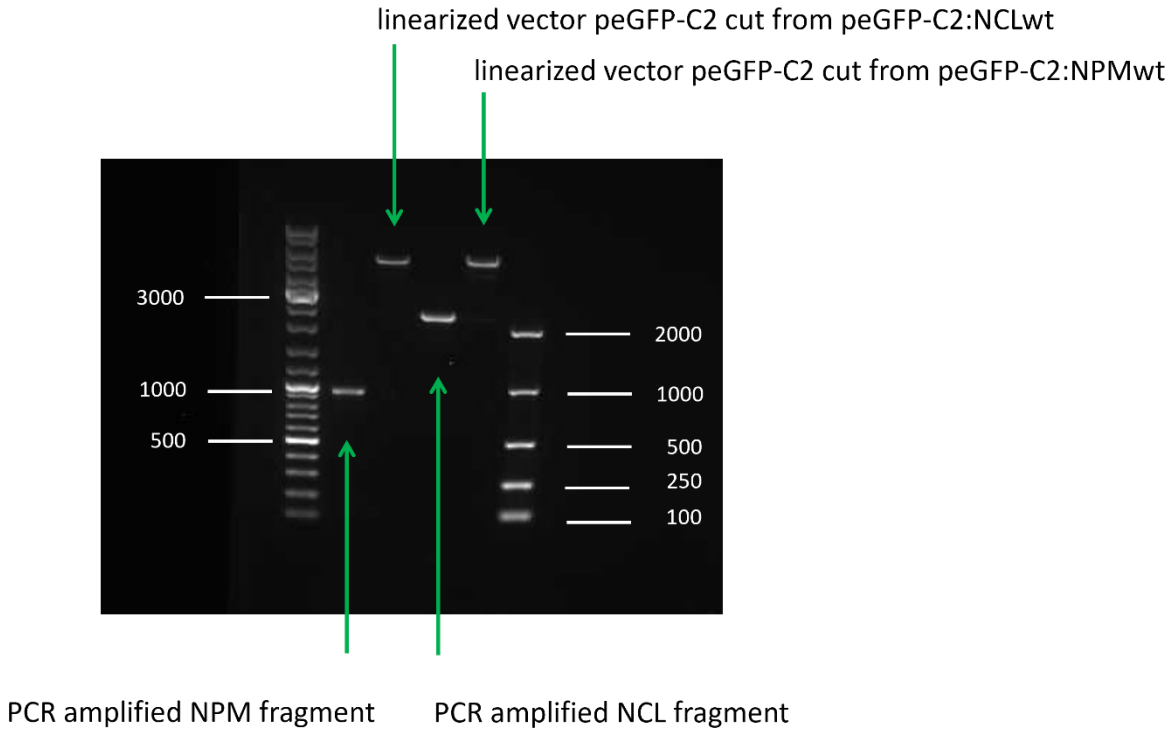

Figure 7: analysis of fragments and vectors prior to ligation

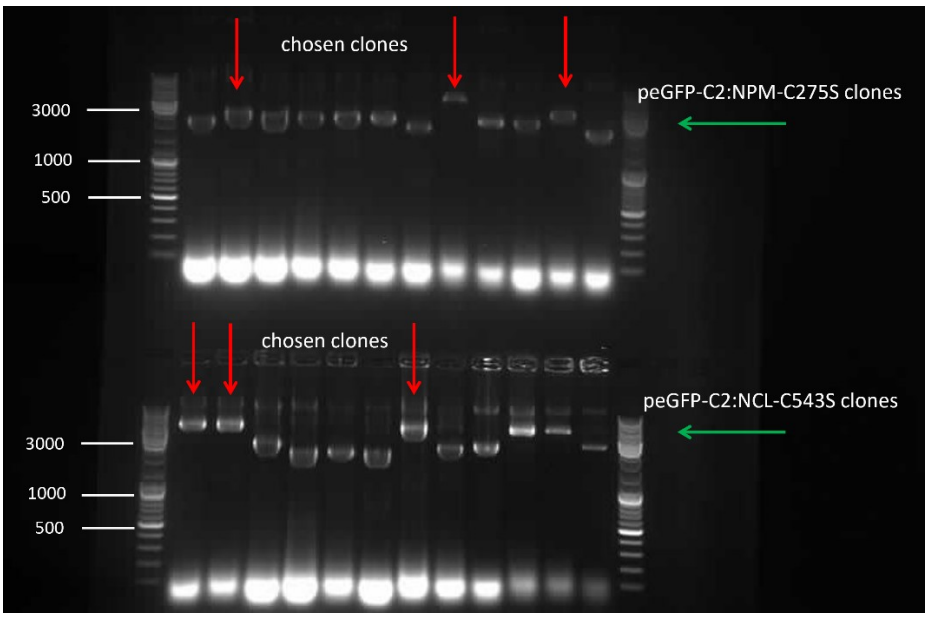

Figure 8: selection of promising clones

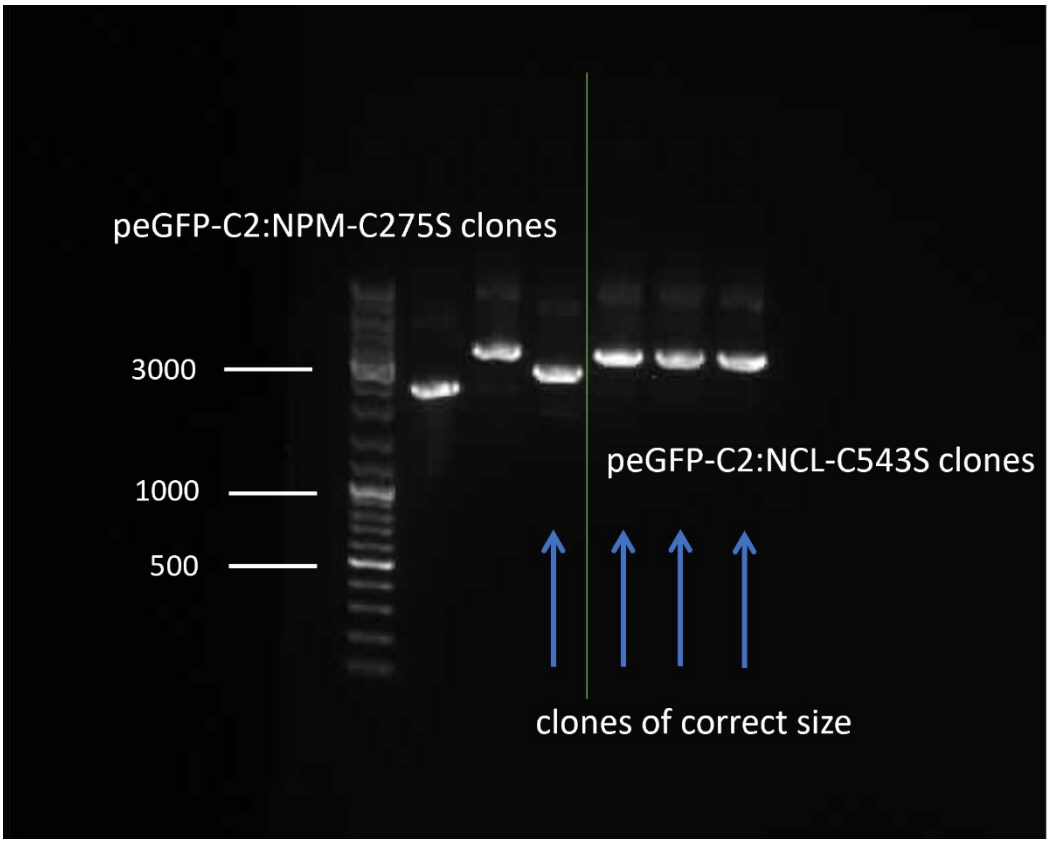

Figure 9: assessment of size of final constructs; the second NPM clone correlates in size with the NCL ones

Construction of plasmids for labeling with mRFP1 was carried out similarly as for the eGFP-labeling; only for the double mutated construct containing the altered C-terminus, the already prepared peGFP-C2:NPM-C275S plasmid was used as a template for the PCR amplification as in (Brodska et al., 2016). All prepared plasmid constructs were verified by sequencing.

For construction of roGFP1 and roGFP2-labeled plasmids, the already available constructs were used as DNA templates for PCR-mediated amplification of fragments corresponding to NPMwt, NPMmutA and NPM-C275S using appropriate primers designed to maintain the open reading frame. The fragments were subsequently cut with XhoI and BamHI restrictases, purified with the Wizard SV Gel and PCR Clean-Up System (Promega) and ligated to linearized vectors serving for fusion with the redox-sensitive fluorescent proteins, proGFP1-C1 and proGFP2-C1, cut also with the same combination of restriction enzymes. Molecular cloning was successful for all desired constructs and these were verified by sequencing.

5.2 Subject cells to different stress stimuli in a controlled manner, observe reactions of fluorescently labeled constructs, choose a stressor that induces delocalization of the constructs to nucleoplasm; verify the works and hypotheses of Yang et al. (Yang et al. 2016) concerning glutathionylation of NPM Cys275 under stress conditions

5.2.1 Stressor choosing

After having created green (eGFP or "g") and red (mRFP1 or "r") labeled wt versions and C275S mutants for NPM, we transfected them into HeLa cells and following the work of Yang et al. (Yang et al., 2016), we subjected the cells to 500µM H_2O_2.

In physiological conditions, both NPM and NCL are localized preferentially in the nucleoli of cells. Both are also present in the nucleoplasm in much lower amounts, but NCL in a higher concentration than NPM. Below is a picture to provide a visual conception (Fig. 10).

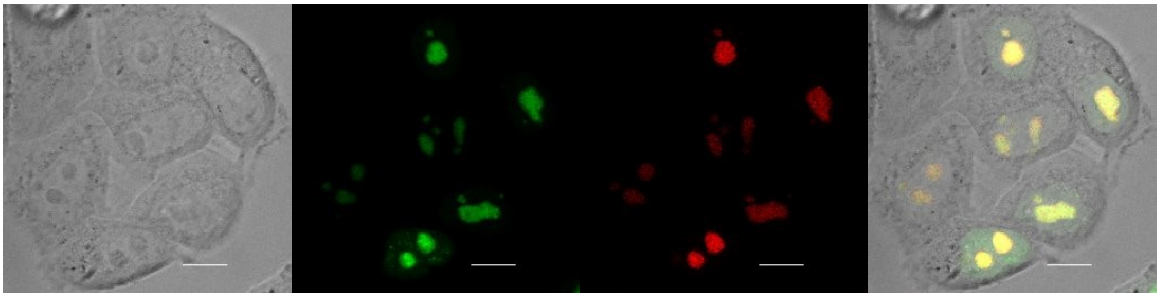

Figure 10: mRFP1_NPMwt (rNPM wt) in red and eGFP_NCLwt (gNCL wt)t in green localized in HeLa, bar represents 10µm

Yang et al. (Yang et al., 2016) provided the following pictures of a single cell (for each variant), stating that they observed a diminishing signal in the nucleolus of wt and no change in C275S (Figs. 11, 12).

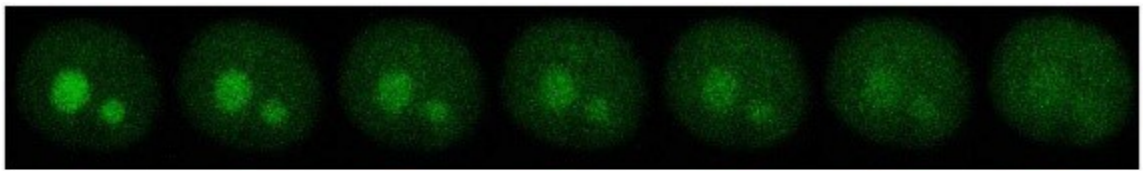

Figure 11: from Yang et al. (Yang et al., 2016); changes in the localization of NPM wt after adding 500µM H_2O_2

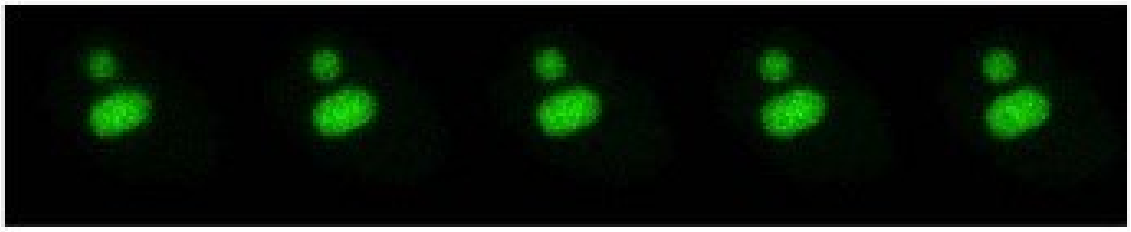

Figure 12: from Yang et al.(Yang et al., 2016); changes in the localization of NPM C275S after adding 500µM H_2O_2, images taken in 5min intervals

Our results of NPM variants response to addition of H_2O_2 are illustrated in Figs. 13, 14, 15. Similarly to Yang et al. (Yang et al., 2016), we saw no change in the signal of C275S-transfected

HeLa cells. However, unlike Yang et al. (Yang et al., 2016), we have not observed any changes to the intensity and localization of signal in NPMwt-transfected cells either. This remained true even in HEK-293T cells that have a higher expression of exogenous proteins and thus provide a better chance to detect weak fluorescent signal from the nucleoplasm.

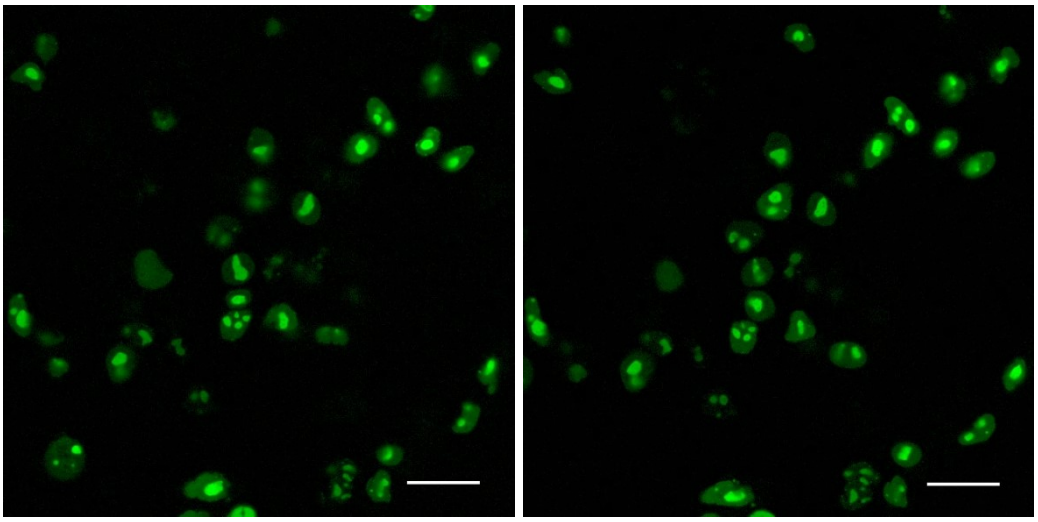

Figure 13: gNPM wt in HeLa without stress (left) and after overnight treatment with 500µM H_2O_2 (right); bar represents 30µm

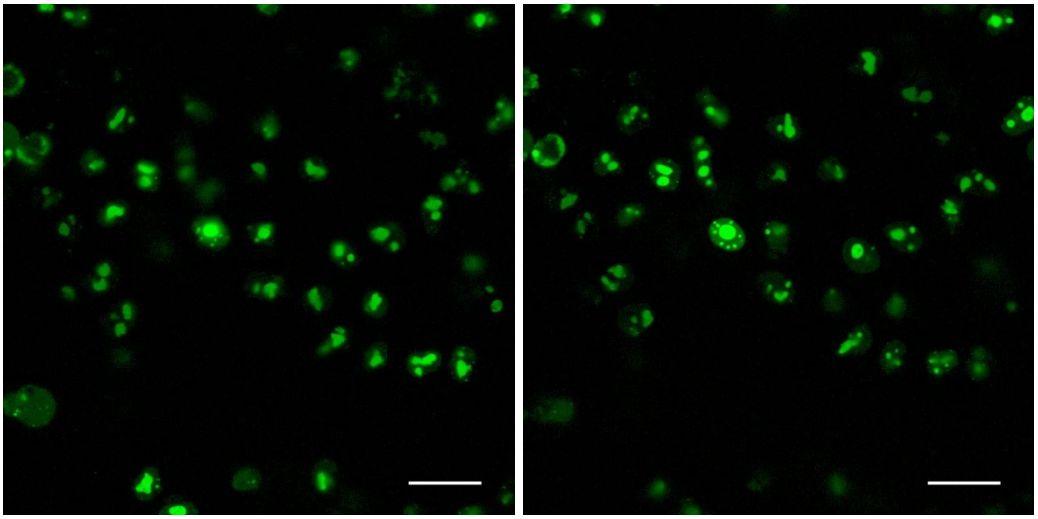

Figure 14: gNPM C275S in HeLa without stress (left) and after overnight treatment with 500µM H_2O_2 (right); bar represents 30µm

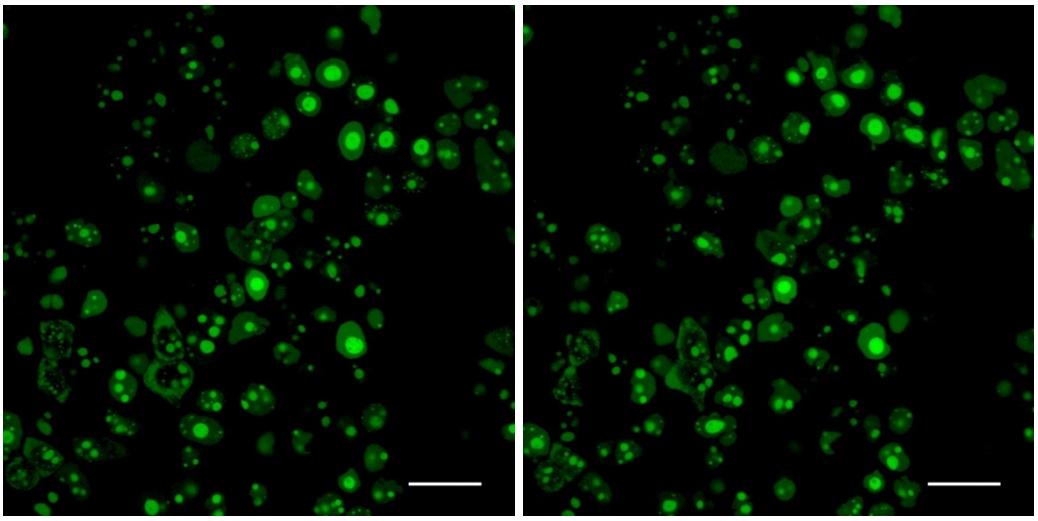

Figure 15: gNPM wt in HEK-293T without stress (left) and after overnight treatment with 500μM H_2O_2(right); bar represents 30μm

Based on these negative results, we analyzed lysates of cells subjected to H_2O_2 treatment by western blotting to assess markers of cell damage (Fig. 16). However, we did not reveal any signs of apoptosis (PARP fragmentation, caspase-3 activation) even with two times higher H_2O_2 concentration, although we detected weak indication of DNA damage (increased phosphorylation of H2A.X on Serine p139, commonly marked as γH2A.X).

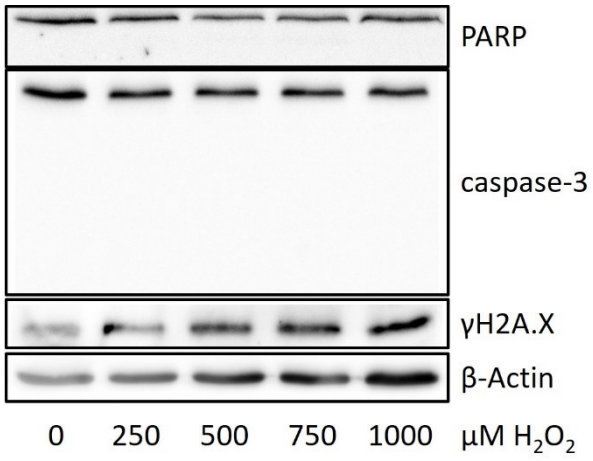

Figure 16: Western blot showing effect of overnight H_2O_2 treatment on markers of DNA damage and apoptosis in HeLa cells. β-Actin is used as a loading control.

Yang et al. also mention UV irradiation as a commonly used stressor (Yang et al., 2016). But again, we have not obtained convincing visual results in cells, despite expected cell damage, as documented in previous results of our lab (Strachotová et al., 2023)

5.2.2 Doxorubicin-induced nucleolar stress

Since genotoxic drugs such actinomycin D or doxorubicin are also studied in our laboratory, we tried to treat cells with doxorubicin, which is a common chemotherapeutic drug used in

acute leukemia therapy as well as for other types of cancer (see chapter 2.6). As seen in Figs. 17 through 20, the addition of 4µM doxorubicin led to an obvious increase of NPM and NCL presence in the nucleoplasm of HeLa cells. The effect was visible within a few hours and even more pronounced after overnight incubation. Both green and red variants responded similarly. We therefore decided to choose doxorubicin for our further research.

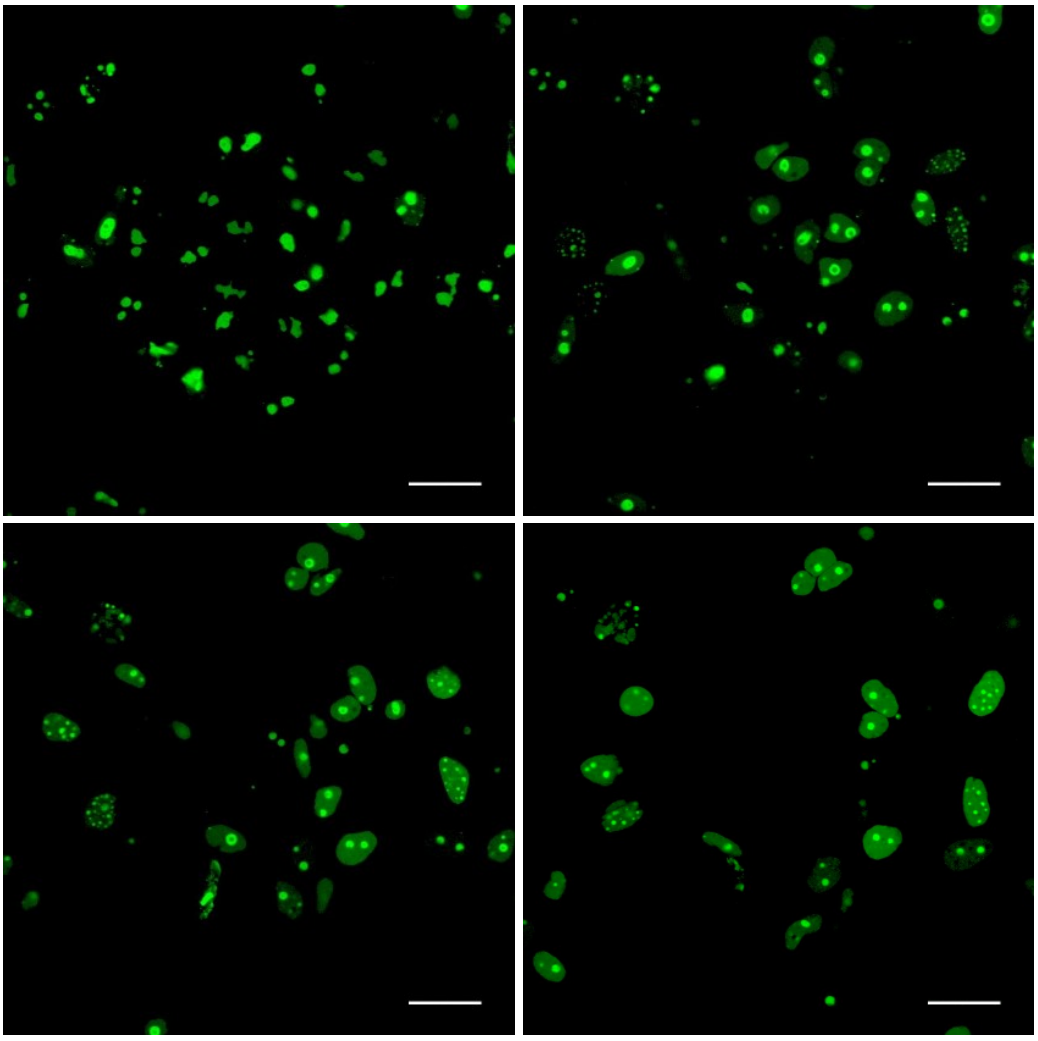

Figure 17: gNPM wt before adding doxorubicin (top left), 5h after (top right), 10h after (bottom left), and overnight (14 h; bottom right)); bar represents 30µm

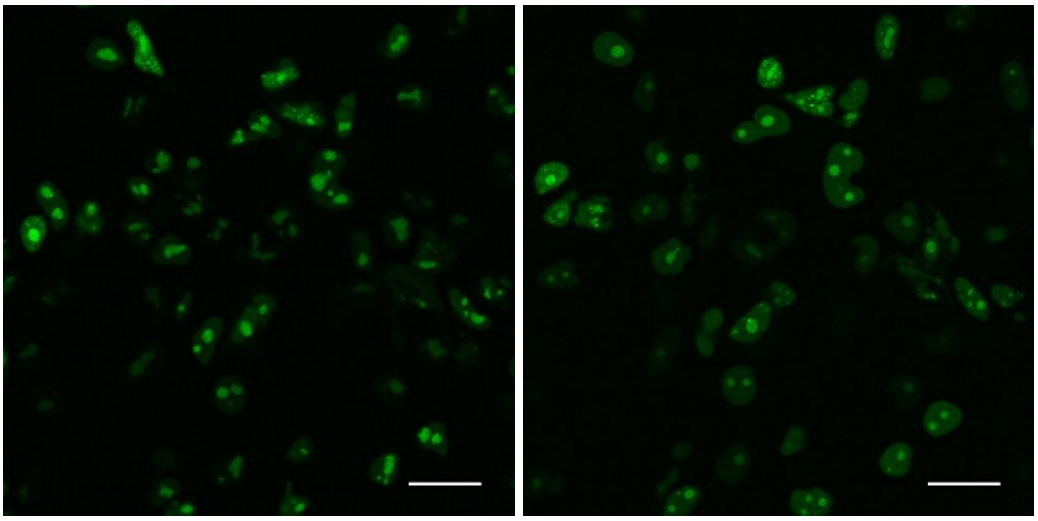

Figure 18: gNCL wt before adding doxorubicin (left), and 3,5h after (right); bar represents 30µm

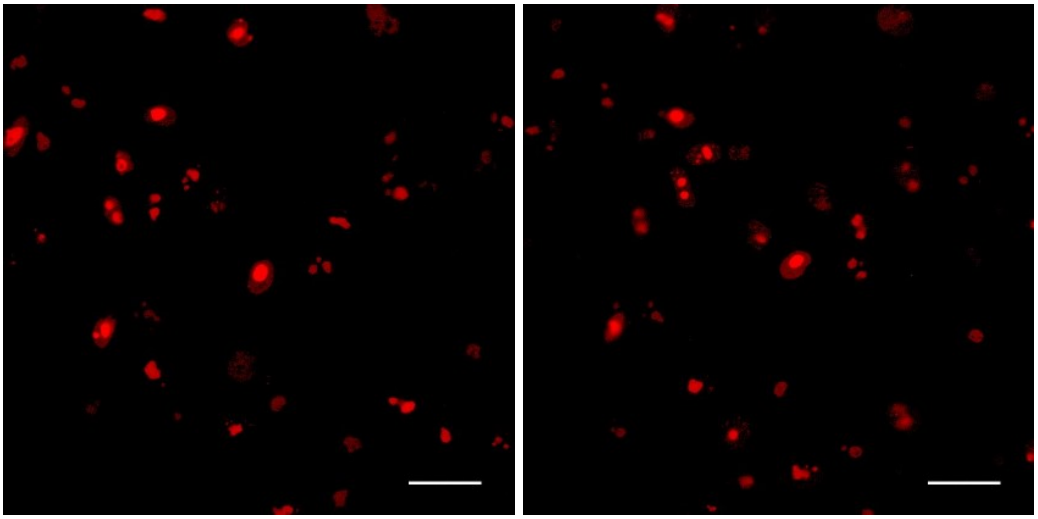

Figure 19: rNPM wt before adding doxorubicin (left), and 2h after (right); bar represents 30µm

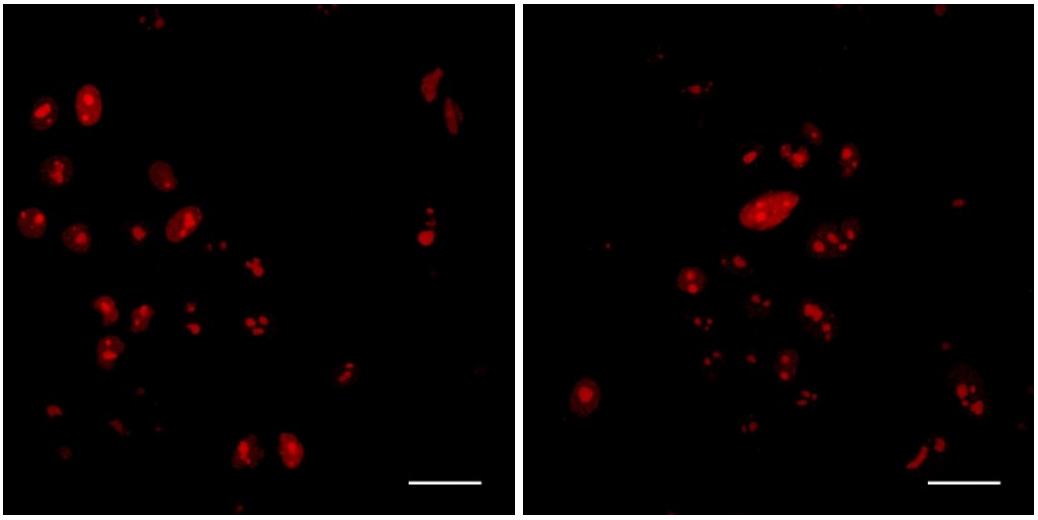

Figure 20: rNCL wt before adding doxorubicin (left), and overnight (right); bar represents 30µm

5.2.3 Doxorubicin in untransfected cells

To determine the optimal conditions for our experiments, we tested the effect of different doxorubicin concentrations and evaluated it by monitoring general markers of apoptosis with Western blot. As seen below (Fig. 21), 2µM doxorubicin did not activate all of the markers after 24h: p53 is present and activated (activation confirmed by increased phosphorylations (pS392 (Cox & Meek, 2010), pS46 (Smeenk et al., 2011), pS15 (Loughery et al., 2014)), so is γH2A.X (phosphorylated form of histone which indicates double strand breaks), but active caspase-3 is not detected, and PARP is not cleaved. Both 4µM and 8µM concentrations activated all of the markers. We then chose the 4µM as the lowest possible concentration to induce the investigated phenomena while not causing excessive damage in a shorter period of time.

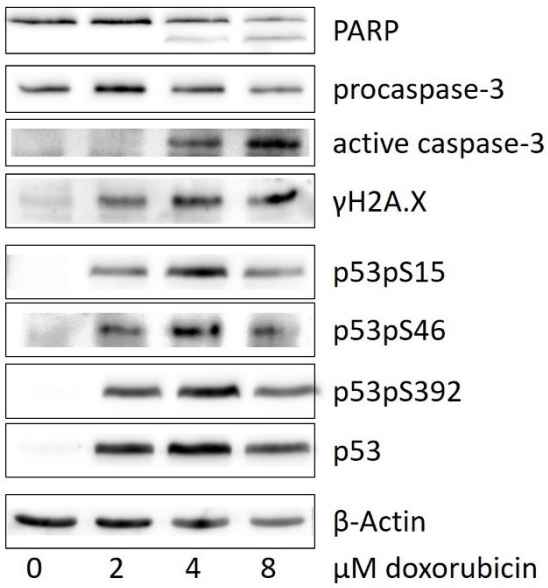

Figure 21: *markers of apoptosis in HeLa cells on Western blot, untreated control and treated with different concentration of doxorubicin for 24h; β-Actin is used as a loading control.*

To further establish the general reaction of cells to doxorubicin, we treated untransfected HeLa cells with 4µM doxorubicin and monitored them with several complementary methods. First, we observed the impact of doxorubicin on HeLa cell line properties. Using the natural fluorescence of doxorubicin (see chapter 2.6), we mapped how the drug enters the cells (Fig. 22).

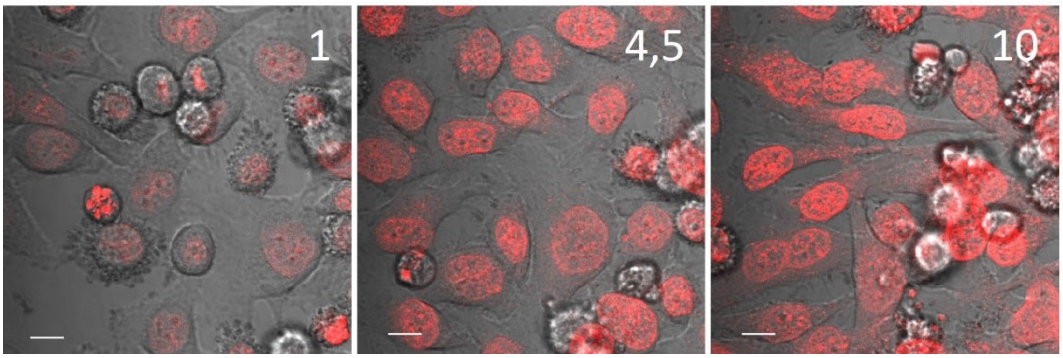

Figure 22: doxorubicin (red) entering HeLa cells, documented under microscope; bar represents 10µm, numbers are hours of doxorubicin treatment

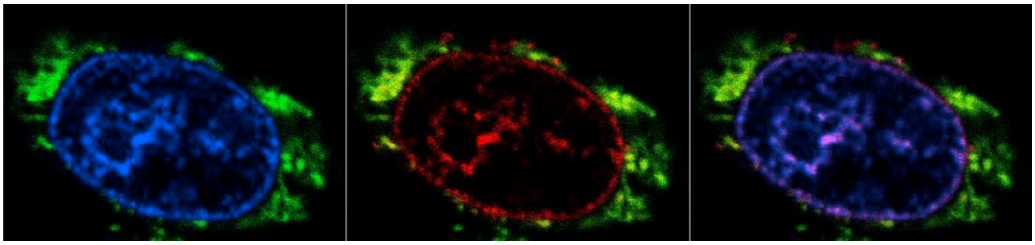

Figure 23: doxorubicin (red) co-localization with DNA (Hoechst33342, blue) in HeLa cell, third picture is overlayed red and blue; mitochondria are co-stained with MitoTracker Green (green).

Within approximately the first hour, we can see the drug concentrating in DNA, which is further specified in Fig. 23, where the cells were co-stained with Hoechst33342 to mark DNA in the nucleus and MitoTracker Green to visualize mitochondria. After this initial targeted accumulation, doxorubicin starts expanding into the rest of the nucleus and somewhere between the 4,5h and 6h mark, it eventually also starts to enter the cytoplasm. After about 10h, the vitality of the cell starts to be noticeably compromised, as they lose adherence, and later enter apoptosis.

Doxorubicin effect on cell adhesivity is possible to alternatively observe using microimpedance measurement, as illustrated in Fig 24. In this method('s results), capacitance is linked to the surface of contact of the cells with the well (in inverse proportion) and resistance is a marker of narrowness/tightness of the contact (direct proportion).
In the first part of each graph (20h), we can see the freshly transferred cells adhering to the well surface. After 20h, 4µM doxorubicin was added to one sample (in red) and another was kept untreated as a control (in black). We can notice capacitance rise and resistance decrease in the treated sample, meaning that the cells are adhering even more tightly and are spreading to a larger surface. This correlates with both our observation of doxorubicin entering cells and cells changing shape under the microscope. Next, the trend is inversed, again confirming what can be seen in the microscope: the cells condense and eventually lose contact with the surface completely. This loss of contact happens around the same time when some cells start to die, showcasing doxorubicin's cytotoxic properties.

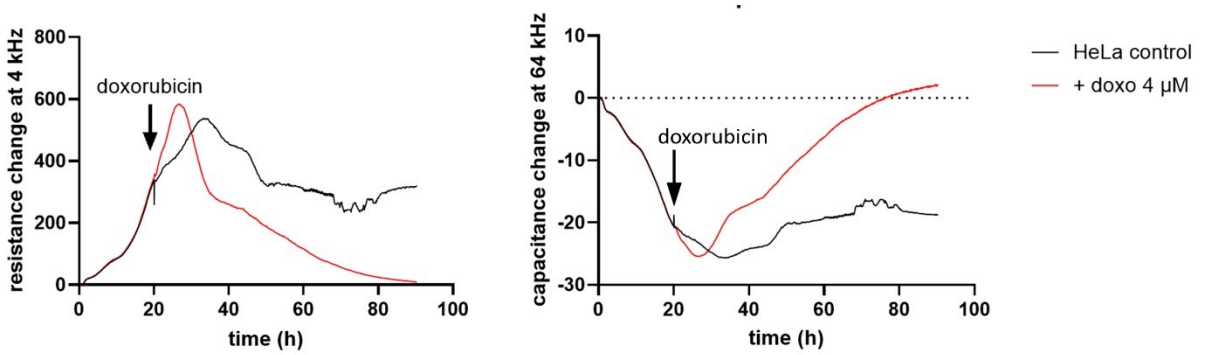

Figure 24: monitoring of doxorubicin-induced adhesivity changes using microimpedance signal measurement (ECIS method). Left: resistance, right: capacitance signal

5.2.4 Endogenous NPM, NCL reacting to doxorubicin

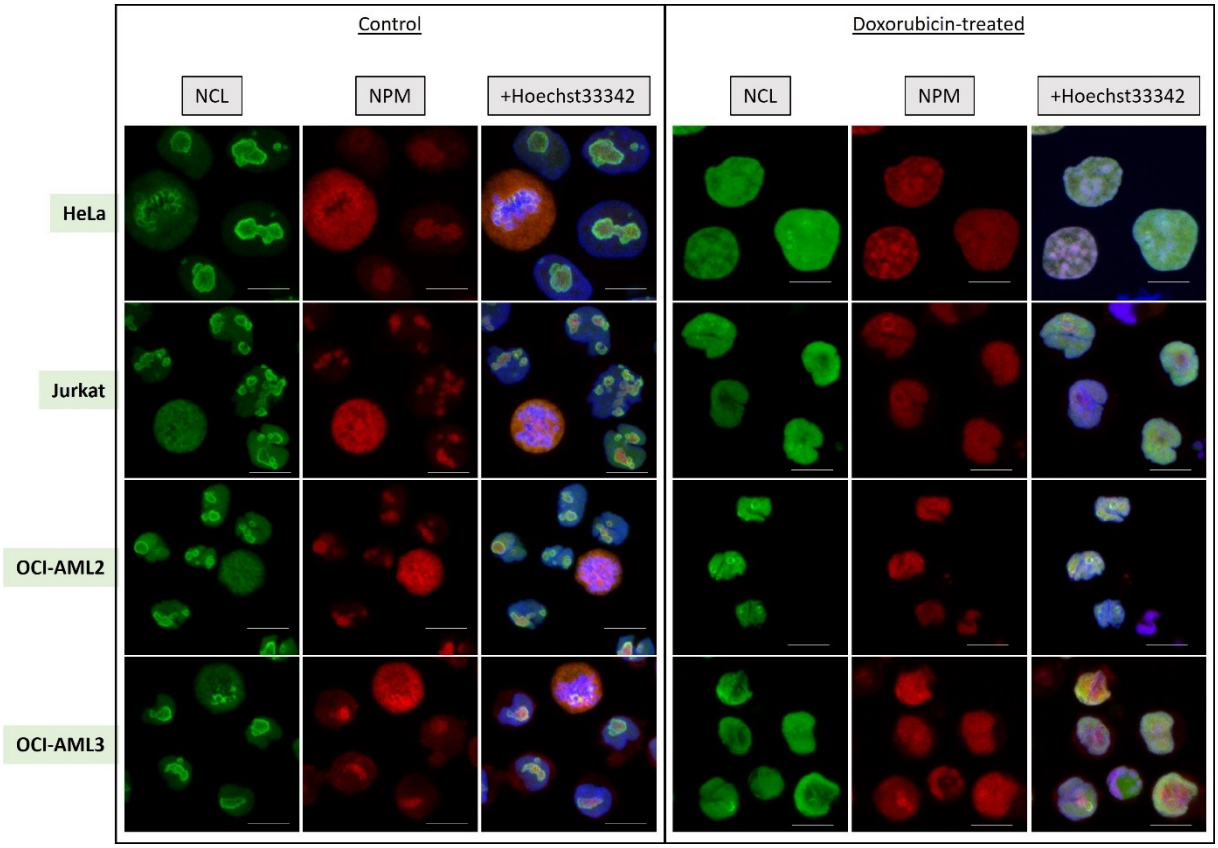

Figure 25: PFA-fixed cells with visualized endogenous NPM (red), NCL (green), and nuclei (blue, Hoechst33342); change in localization after doxorubicin treatment; bar represents 10 µm.

Next, we investigated the effect of doxorubicin on the localization of endogenous nucleolar proteins (Fig. 25). Besides HeLa, we also tested suspension cell lines derived from leukemia patients: OCI-AML2, OCI-AML3 and Jurkat, in order to estimate the applicability of our results in leukemia research. Cells have been PFA-fixed, NPM has been visualized by AlexaFluor555, NCL by AlexaFluor488 and nuclei by Hoechst33342 staining. Again, we can see doxorubicin caused considerable delocalization of both endogenous proteins in all investigated cell lines.

Comparing images of transfected and non-transfected HeLa cells, we can state that endogenous and exogenous forms of each protein are localized similarly and react to doxorubicin generally in the same manner. This confirmation allows us to (cautiously) apply results obtained from experiments using exogenous proteins to their endogenous forms.

5.2.5 Redox changes as a reaction to doxorubicin

Similarly to choosing doxorubicin concentration for HeLa earlier, we established that the sufficient doxorubicin concentration for Jurkat and other leukemia cells is only 1µM. The Western blot below (Fig. 26) also shows that apoptosis is induced by doxorubicin not only in p53-dependent manner, as Jurkat cells lack p53, but all of the apoptosis (cleaved PARP, active caspase, Bcl-2 fragmentation) and DNA-damage (γH2AX) markers are still present.

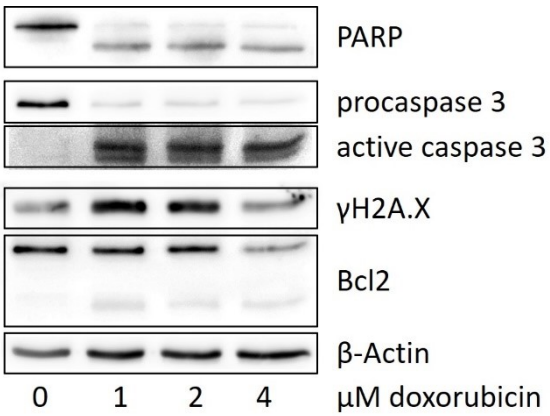

Figure 26: markers of apoptosis in Jurkat cell line after 24h-doxorubicin treatment; β-Actin is used as a loading control

Given their identical response in nucleolar proteins delocalization, we also screened the panel of cell lines for the doxorubicin-induced appearance of reactive oxygen species (ROS). Results of flow cytometric ROS assessment using ROS-sensitive fluorogenic probe H_2DCFDA are presented in Fig 27. Concurrent propidium iodide staining allowed us to distinguish the population of dead (PI-positive) cells.

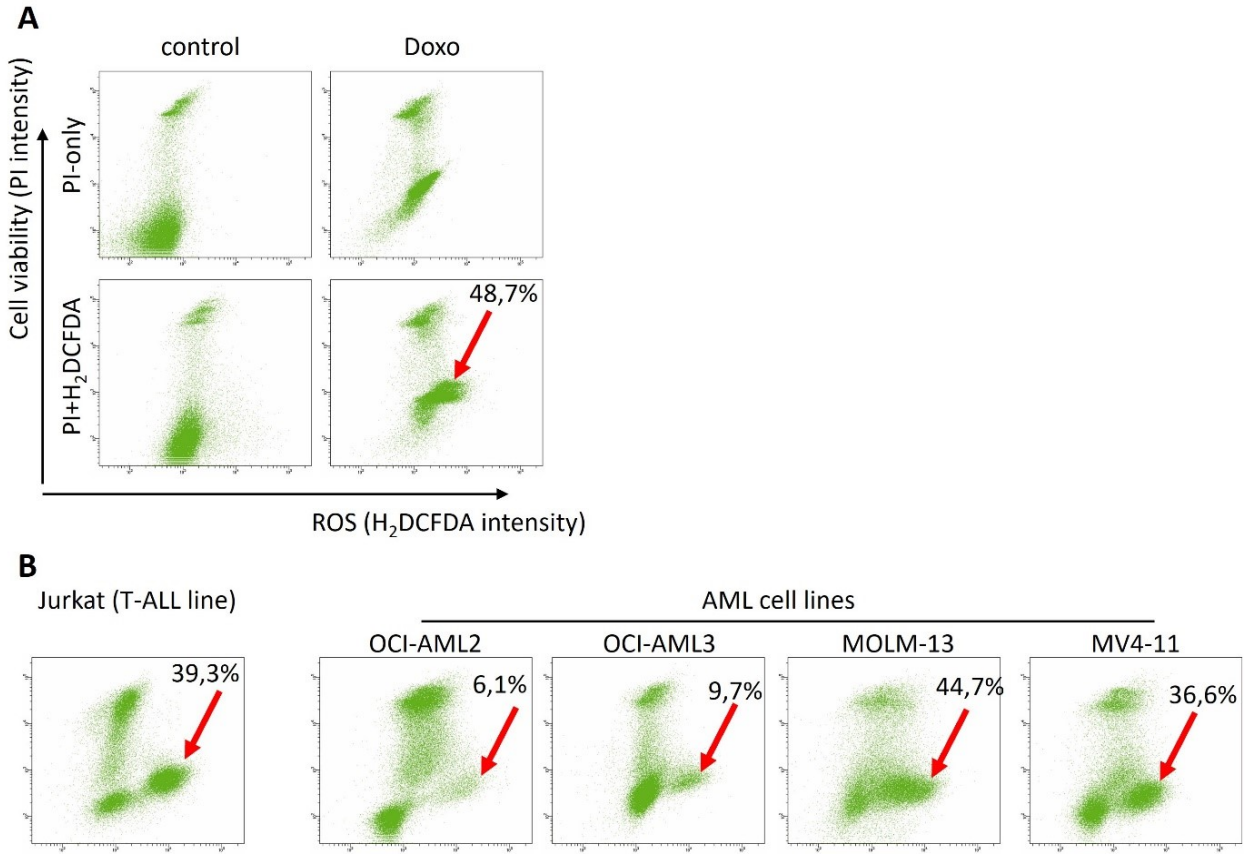

Figure 27: flow cytometric evaluation of ROS generation by doxorubicin in panel of cell lines. A. control (left) and doxorubicin-treated (right) HeLa cells were stained with propidium iodide alone (upper row) or together with H_2DCFDA (lower row). B. similar results of H_2DCFDA/PI-stained cells of leukemic cell lines. Arrows indicate ROS-positive population, numbers denote fraction of ROS-positive cells in sample.

The graphs indicate that a population of cells with increased ROS concentrations appeared in all of the cell lines. Differences in a fraction of cells in ROS-positive population likely depend on the cell sensitivity to doxorubicin as well as they are time-dependent (subsequently passing from H_2DCFDA-negative/PI-negative through H_2DCFDA-positive/PI-negative to H_2DCFDA-negative/PI-positive population). It is then fairly safe to say that doxorubicin generally causes an increase in ROS production. Heterogeneity of the ROS concentration inside individual samples corresponds to our observations of NPM and NCL localizations in doxorubicin treated HeLa, suggesting these two phenomena occurring simultaneously after doxorubicin treatment might be interlinked.

5.2.6 Differences between the behavior of wild type proteins and mutants

5.2.6.1 Nucleophosmin

Having established all of the aforementioned trends of cells and both endogenous and exogenous proteins reacting to doxorubicin, we introduced plasmids for mutated versions of proteins into the equation (and into cells) again.

The first difference appeared even before the doxorubicin treatment: although very faint, the signal was present in the nucleoplasm of the wild-type, but there was none in that of C275S (Fig. 28).

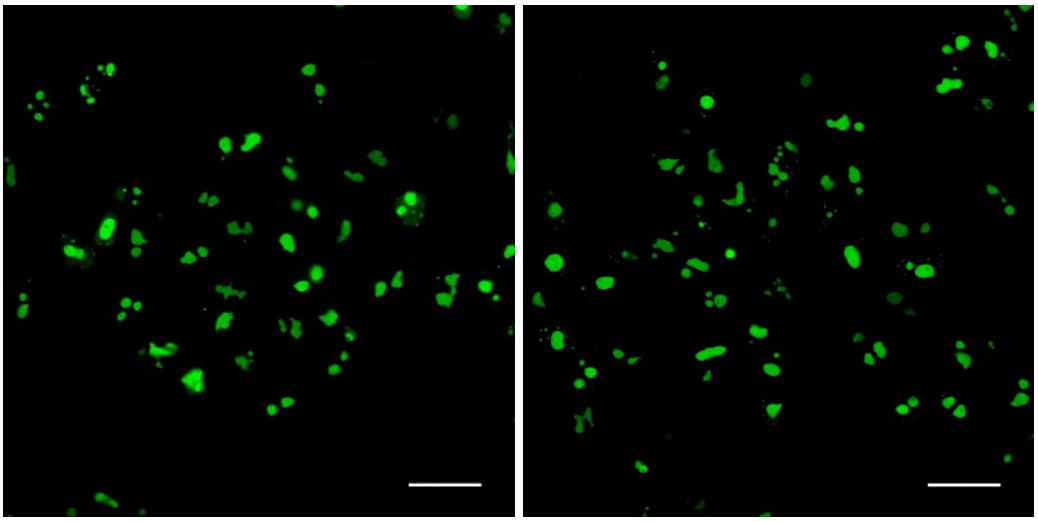

Figure 28: localization of gNPM wt (left) and C275S (right) in untreated HeLa cells

In contrast to Yang et al. (Yang et al., 2016) there was very little noticeable change in the localization of the signal within the first 30min (Figs. 29, 30) and there was also little to no difference between the behavior of wild-type and C275S in this timeframe.

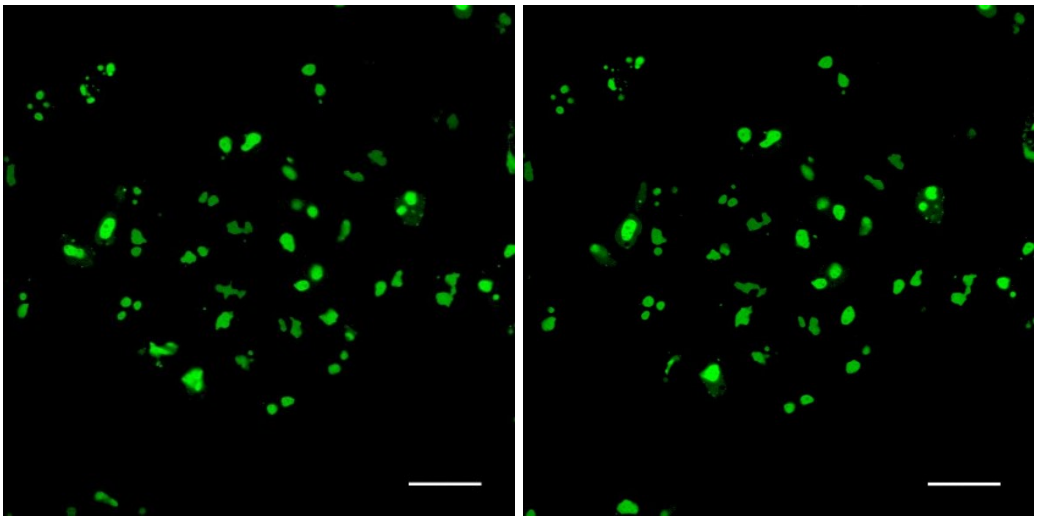

Figure 29: gNPM wt before adding doxorubicin (left), after 30min (right); bar represents 30µm

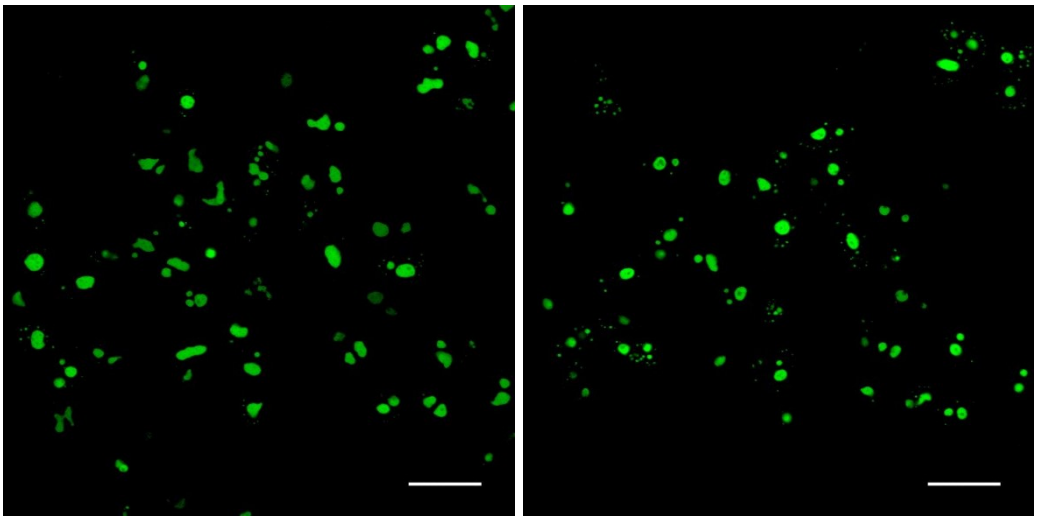

Figure 30: gNPM C275S before adding doxorubicin (left), after 30min (right); bar represents 30µm

After the first hour (which means after the third frame), however, the signal started to grow stronger in the nucleoplasm of the wild-type variant, while it remained the same (which was close to or absolutely zero) in C275S (Fig. 31). This trend continued for the rest of the 5h observation.

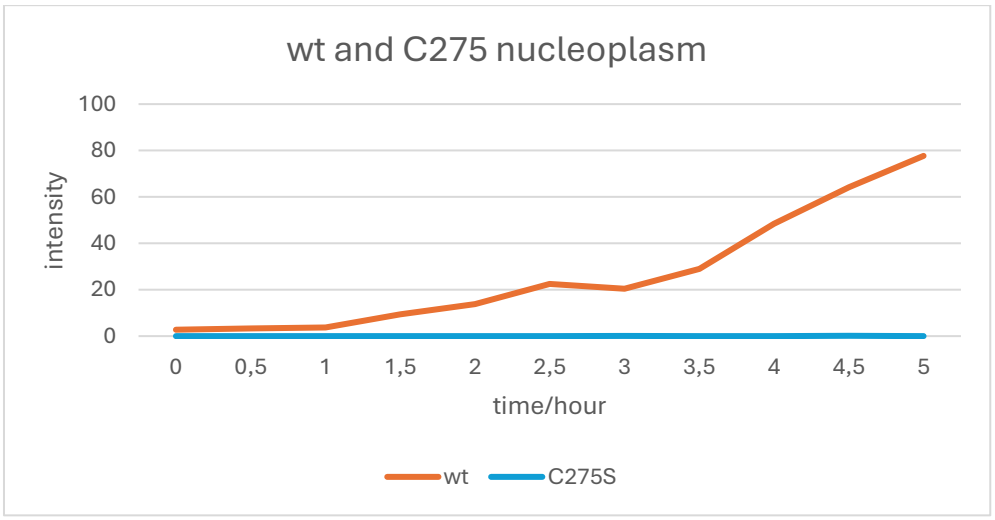

Figure 31: eGFP fluorescence intensity in nucleoplasm of HeLa cells transfected with NPMwt (orange line) or C275S mutant (blue line) during 4µM doxorubicin treatment; values are averages from 6 cells

While the signal in wt's nucleoplasm kept steadily increasing and finally plateaued at around 9h, the signal in C275S nucleoplasm remained extremely low until about the 10h mark and then started to slowly grow (Fig. 32).

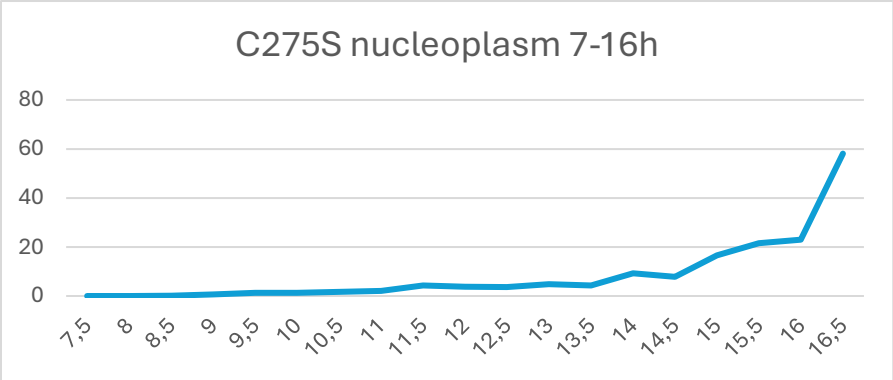

Figure 32: changes of fluorescence in nucleoplasm of cells with gNPM C275S between 7,5. and 16,5h of doxorubicin treatment; eGFP values are averages from 6 cells

There was also a visual difference between the cells transfected with each variant after the doxorubicin treatment (Figs. 33, 34): cells with wt looked more homogeneous throughout the experiment. Cells with C275S were changing more heterogeneously – at first, small, concentrated spots of signals appeared in the nucleoplasm of some of the cells, and later, several cells developed a signal in the entire nucleoplasm. Towards the end, these were the majority of cells that did not lose adherence or die.

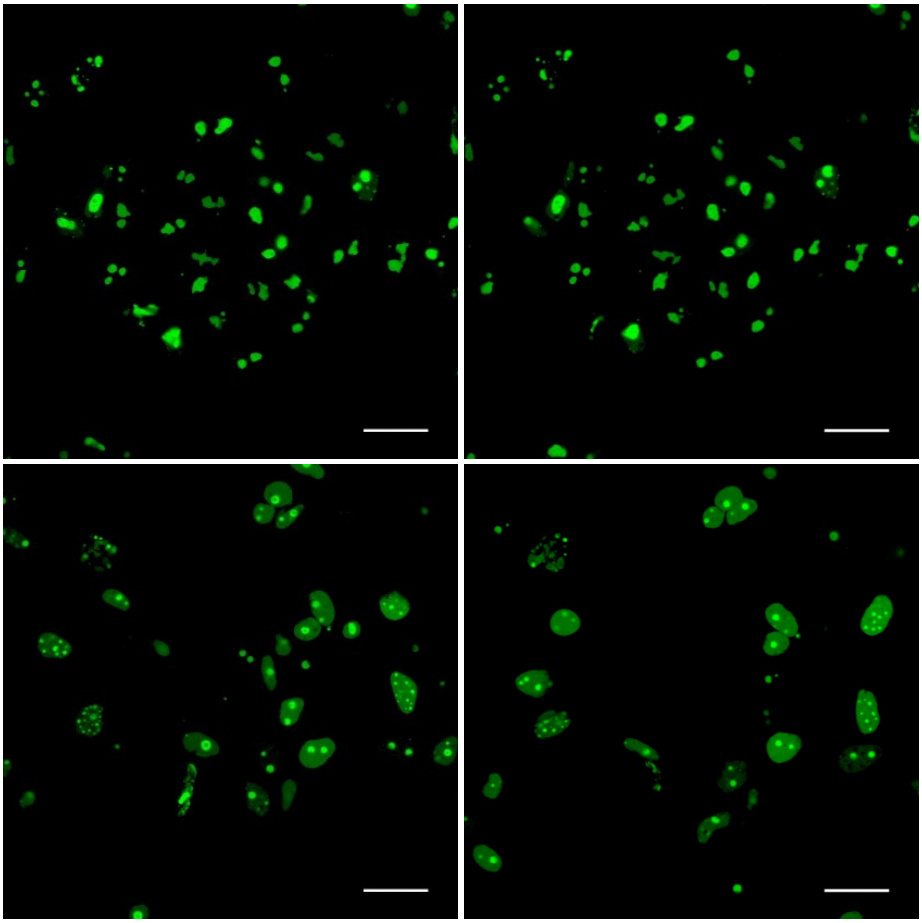

Figure 33: gNPM wt before adding doxorubicin (top left), after 5h (top right), 10h (bottom left), and overnight (14 h; bottom right); bar represents 30µm

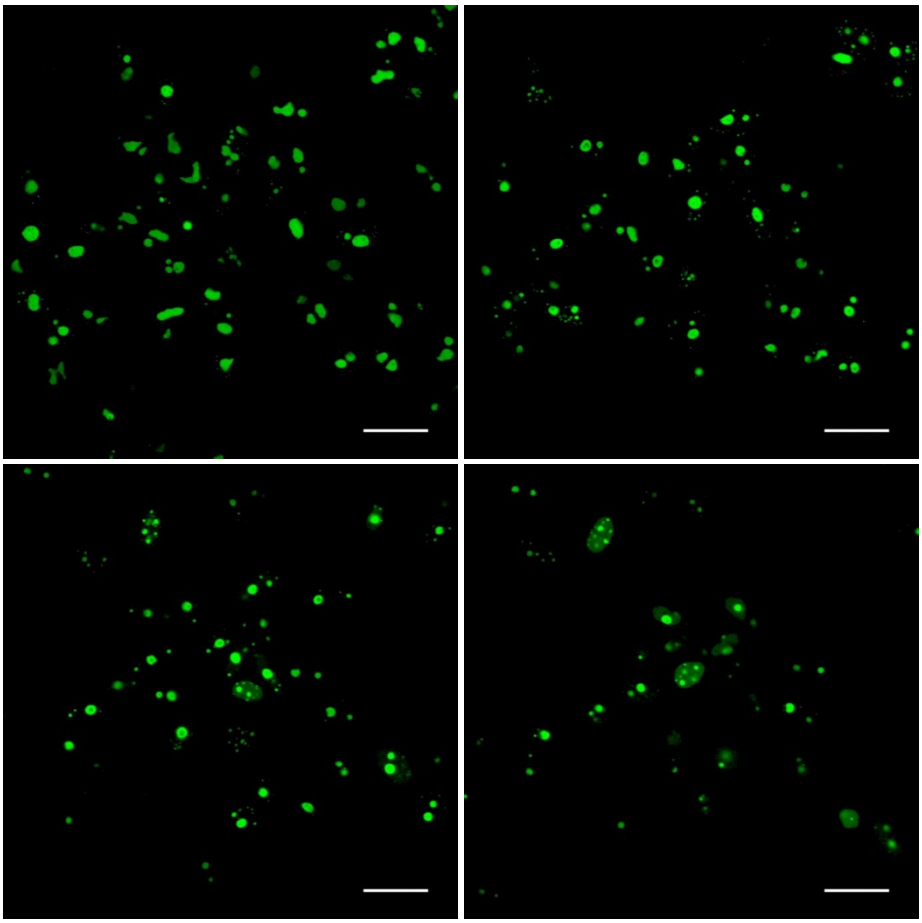

Figure 34: gNPM C275S before adding doxorubicin (top left), after 5h (top right), 10h (bottom left), and overnight (14 h; bottom right); bar represents 30µm

Yang et al. only used the C275S mutant. Serine is supposed to resemble the cysteine the most in the primary protein structure. The change from cysteine to serine is expected to cause minimal changes in the protein conformation. At the same time, the inserted serine residue can serve as an additional target for another posttranslational modification, phosphorylation. We decided to also use a mutant with a different substitution, Cys275 to alanine (C275A), which is the "simplest" amino acid (has no functional groups in the side chain, is unlikely to cause significant changes in protein polarity, charge, structure etc.). Interestingly, the localization of this variant in both intact and doxorubicin-treated cells was very similar to that of NPMwt (compare Fig. 33 and Fig. 35).

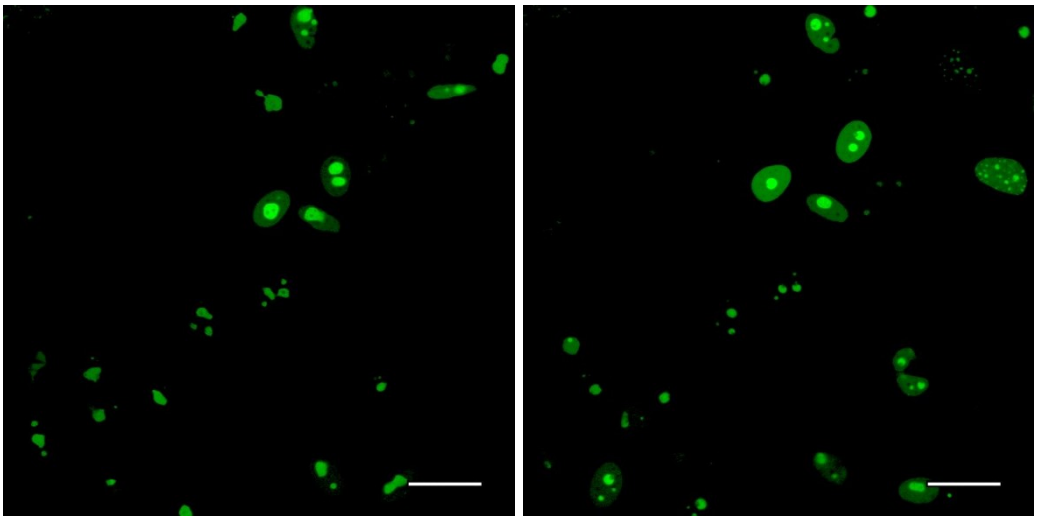

Figure 35: gNPM C275A before adding doxorubicin (left); after 5h (right); bar represents 30µm

Our last NPM variant was a mutant where a cysteine was added, not removed (Fig. 36). This was the Y271S mutant that was used in the lab before its repair to the NPMwt sequence (see Results section 1)). This variant differs substantially from other constructs, as its fraction localized to the nucleoplasm is clearly higher than that of other variants. Again, doxorubicin caused its delocalization into the nucleoplasm.

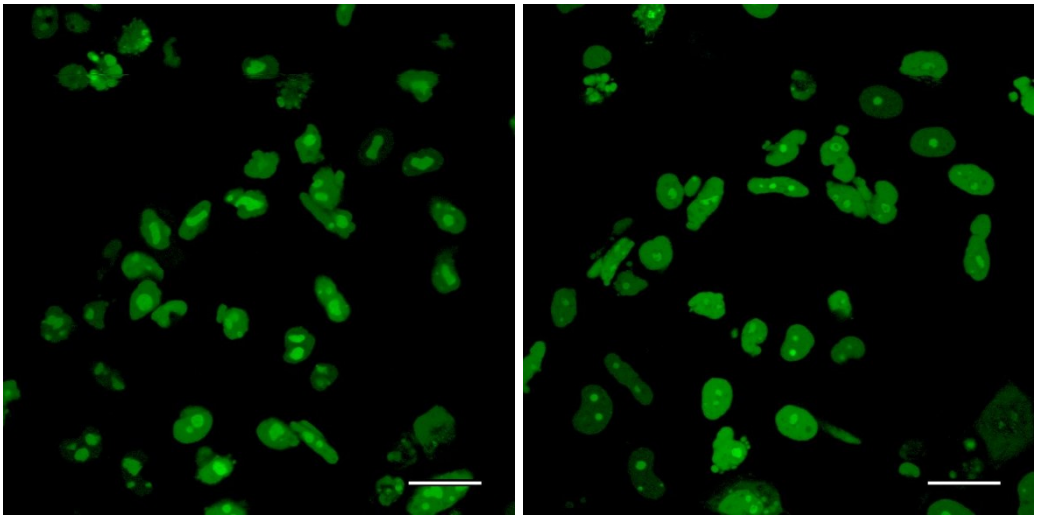

Figure 36: Y271C before adding doxorubicin (left); after 5h (right); bar represents 30µm

After scanning each of the variants for 5h in 30min intervals, we measured the changes in the signal intensity of nucleoli and nucleoplasm. The graphs below (Figs. 38 to 41) show the average intensity of twenty regions of interest (ROI) in twenty cells (or rather 40 ROI with 20 in nucleolus and 20 in nucleoplasm; example of placement in Fig. 37). Since the hypothesis states that the proteins should delocalize from the nucleolus into the nucleoplasm, we measured the signal in both of these compartments (A and B respectively), and to account for the differences in absolute values between the variants, we also plotted the ratio between nucleoplasm and nucleoli signals (C).

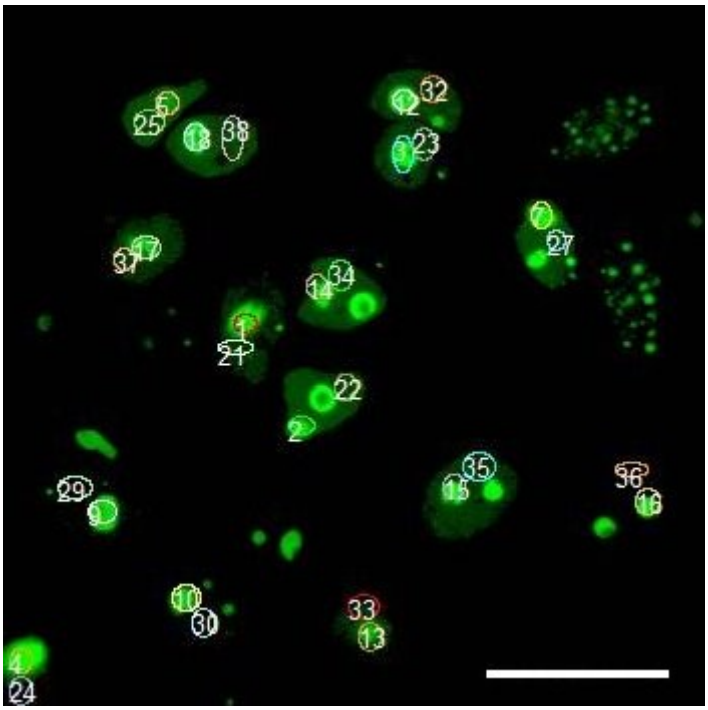

Figure 37: examples of final ROI placement in gNPM wt time measurement, placing of ROI was adjusted in each frame according to the movement of cells; bar represents 30µm

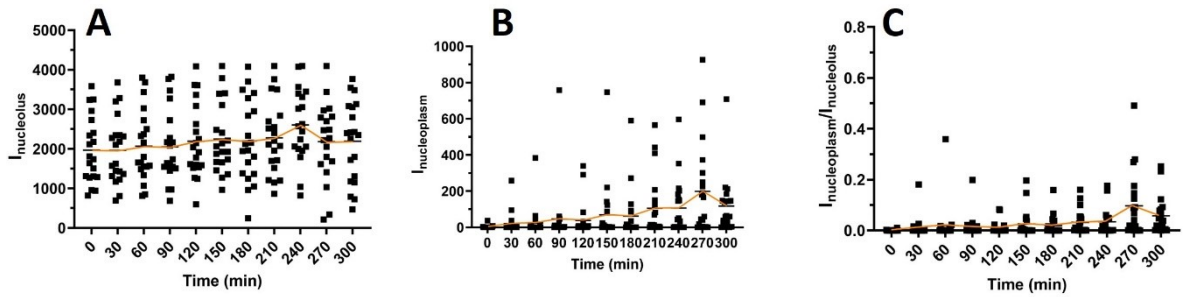

Figure 38: evolution of fluorescent signal of NPM wt in nucleolus (A) and nucleoplasm (B) in doxorubicin-treated cells, and the ratio of both values (C); each dot represents a cell, orange line connects mean values

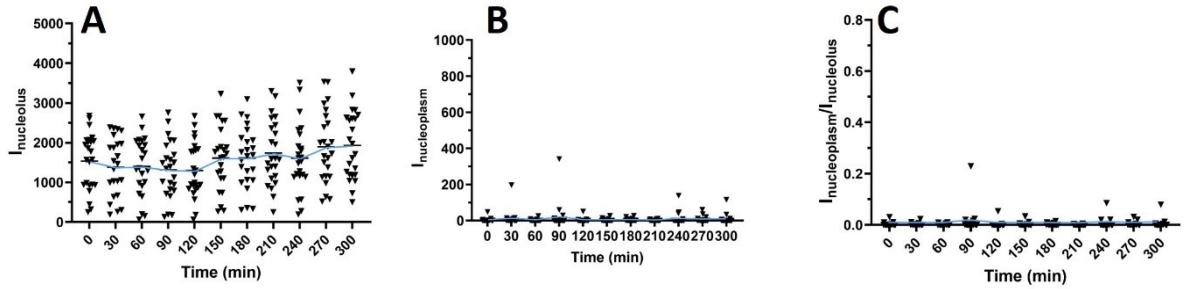

Figure 39: evolution of fluorescent signal of NPM C275S in nucleolus (A) and nucleoplasm (B) in doxorubicin-treated cells, and the ratio of both values (C); each dot represents a cell, blue line connects mean values

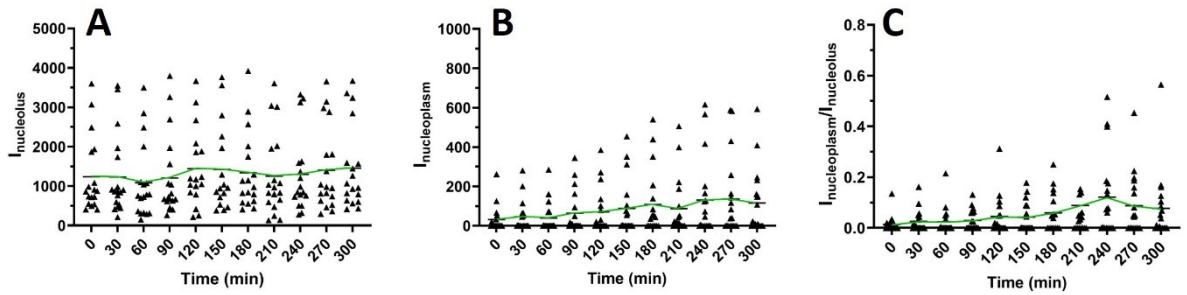

Figure 40: evolution of fluorescent signal of NPM C275A in nucleolus (A) and nucleoplasm (B) in doxorubicin-treated cells, and the ratio of both values (C); each dot represents a cell, green line connects mean values

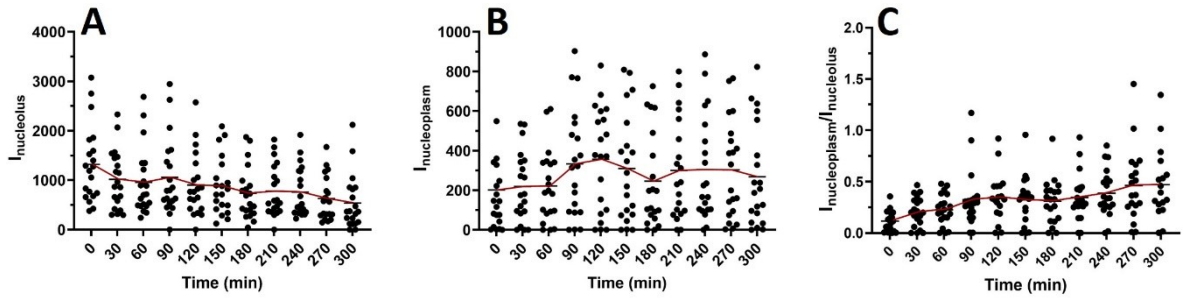

Figure 41: evolution of fluorescent signal of NPM Y271C in nucleolus (A) and nucleoplasm (B) in doxorubicin-treated cells, and the ratio of both values (C); each dot represents a cell, brown line connects mean values

While the spectrum of values is quite broad in almost all of the plots (exception being the virtually non-existent signal in C275S nucleoplasm and subsequent zeros in C275S ratio), the general trend is also fairly visible in most of them. Maximum values also generally follow the same trend as averages.

Below are plots of average values in each compartment (Figs. 42, 43) and their ratios (Fig. 44) with all of the four variants to better illustrate the differences between them.

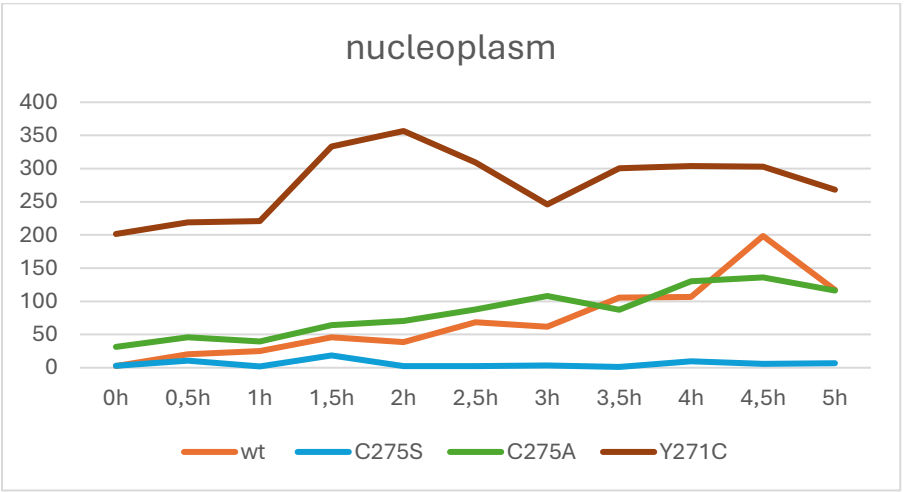

Figure 42: plot of fluorescence intensity changes in nucleoplasm of all NPM variants during doxorubicin treatment

The Y271C mutant has very clearly the highest nucleoplasm signal throughout the experiment. While C275S also clearly has the lowest signal, the difference in signals of wt and C275A are quite small.

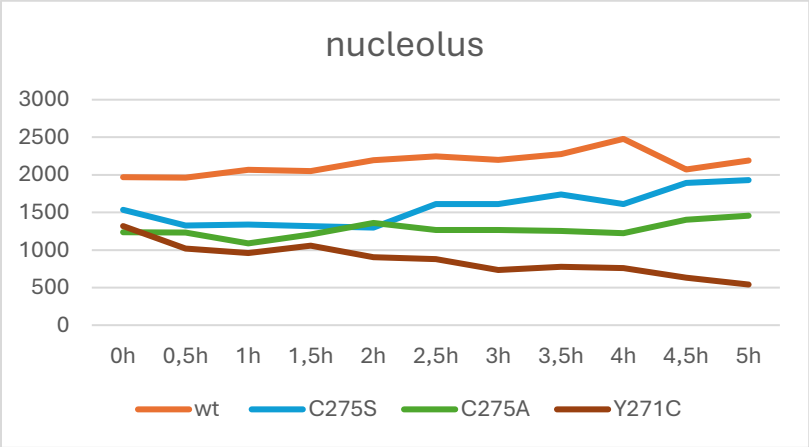

Figure 43: plot of fluorescence intensity changes in nucleolus of all NPM variants during doxorubicin treatment

Yang et al. (Yang et al., 2016) claim that the signal in the wt nucleoli decreased while it remained unchanged in C275S nucleoli after doxorubicin treatment. Our experiments, on the other hand, show a slight overall increase in three out of the four variants. Our results are also based on the observation of 20 cells instead of one.

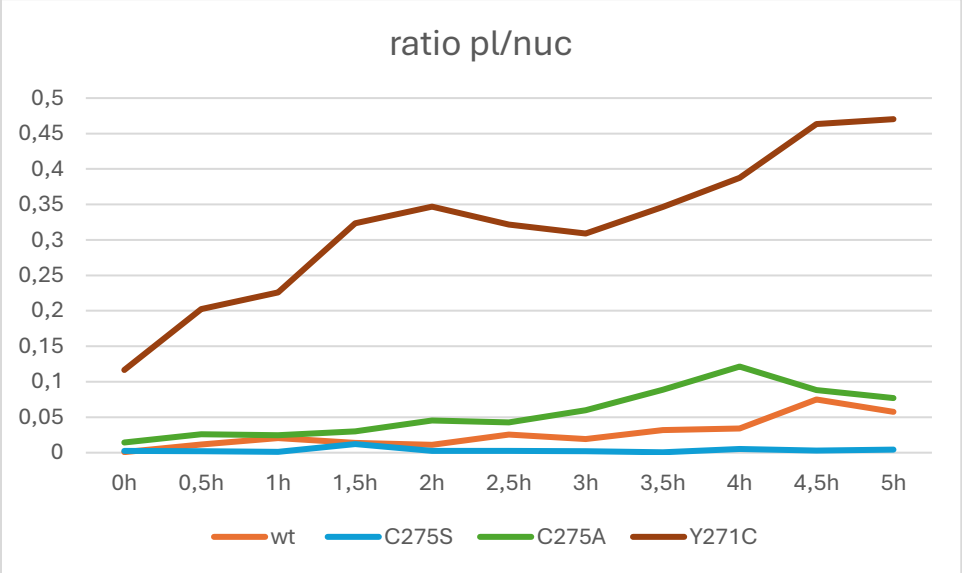

Figure 44: plot of ratios of fluorescence intensity changes in nucleoplasm and nucleolus of all NPM variants during doxorubicin treatment; "pl"=nucleoplasm, "nuc"=nucleolus

The Y271C construct remained the "odd one out" even when the difference in absolute values was removed by calculating a ratio. Since there were only slight changes in the fluorescence of nucleoli of the other three variants, the ratio curves approximately follow that of the nucleoplasm signal.

In Fig. 45 below, we determined the significance of difference between Y271C and the other three. The results were statistically significant (p<0,05) from the very beginning and the significance only grew as the experiments continued.

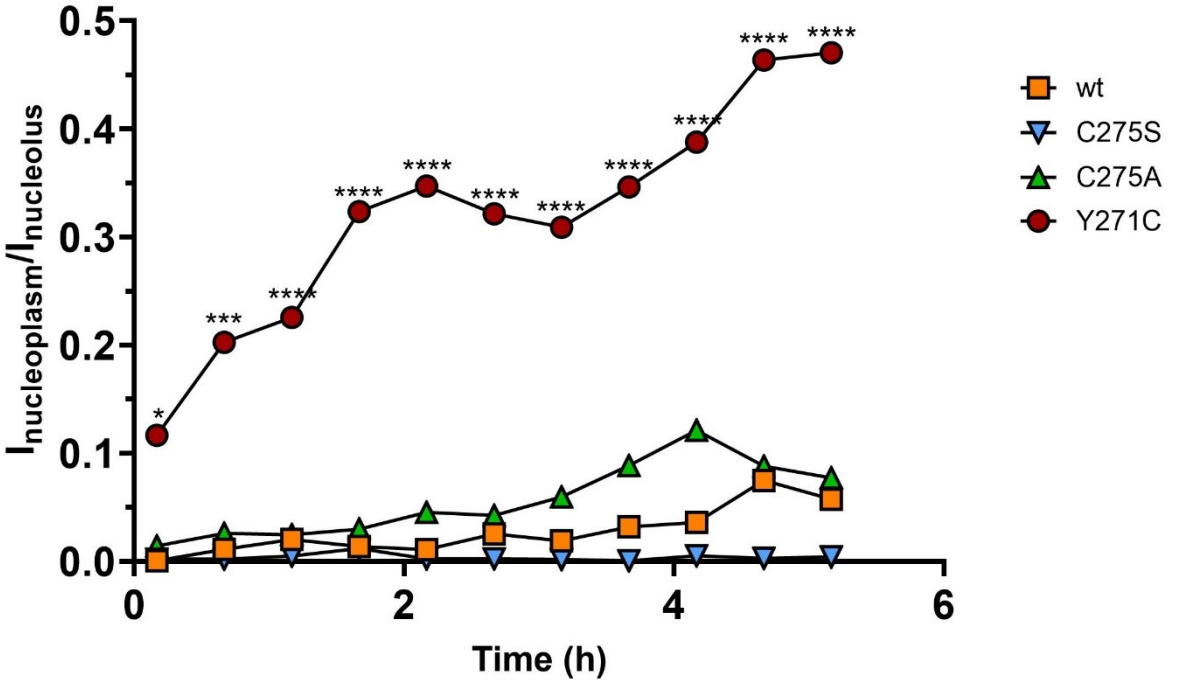

Figure 45: comparison of fluorescence intensity ratio trends of all NPM variants with significant differences between values for Y271C and other constructs marked by asterisks (: p<0,05; ***: p<0,001; ****: p<0,0001)*

To better understand the three other variants, we removed Y271C from the plot and in Fig. 46, we determined the significance of differences between each pair of the remaining three, from hour 2 – where the behavior starts to differ.

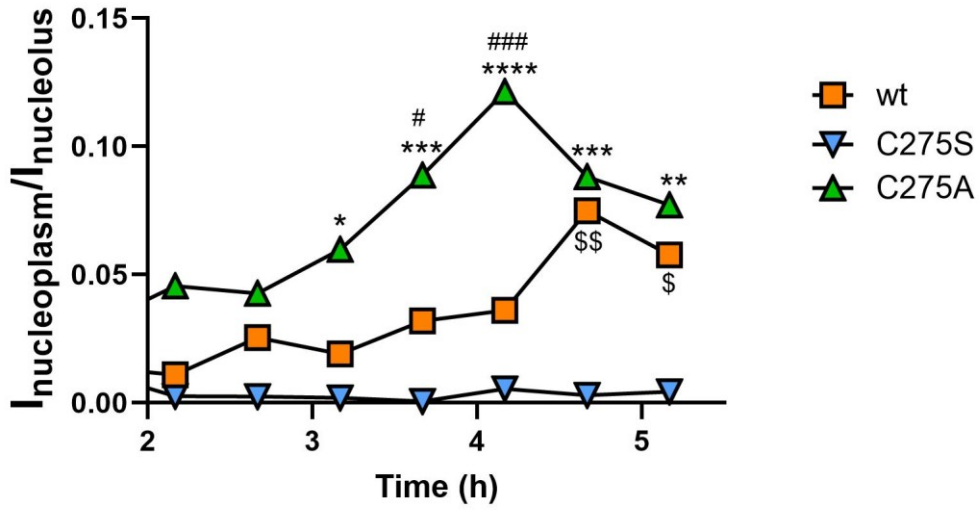

Figure 46: detailed graph of 2-5,5h time interval from Fig. 45. When significant, differences between wt and C275S (*), wt and C275A (#), and C275S and C275A ($) are marked with appropriate number of symbols (one: p<0,05; two: p<0,01; three: p<0,001; four: p<0,0001.

While generally not as high as in the case of Y271C, the significance was still notable, especially between wt and C275S variants. We can also see a similar trend of rising ratios (correlating approx. with rising signal in nucleoplasm) in wt and C275A, but in wt it occurs about 0,5-1h later. Considering the different result of comparing each of the cysteine-lacking mutants to wt, it is clear that the mere absence of a cysteine (or Cys275, to be more precise) does not determine a change in behavior. Nonetheless, more research would be needed to fully understand and conclude on these phenomena.

5.2.6.2 Nucleolin

To compare NPM and its behavior to another important nucleolar protein, nucleolin, we constructed a plasmid with a NCL variant with a cysteine (or the cysteine, as NCL only has one) substituted to serine – C543S. Localization of both in untreated cells was similar (Figs. 47, 48). We did observe a reaction to doxorubicin (delocalization to nucleoplasm, similarly to NPM) for both variants, but we were not able to see a large enough difference in the behavior of the wt and C543S forms. Analysis of fluorescence ratios is in Fig. 49.

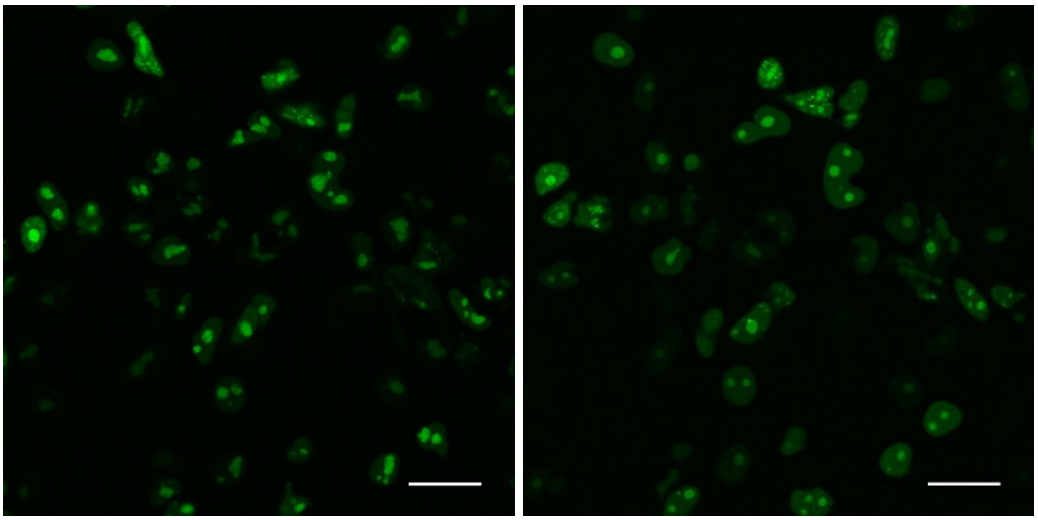

Figure 47: gNCL wt before adding doxorubicin, after 3,5h (right) (8th frame); bar represents 30µm

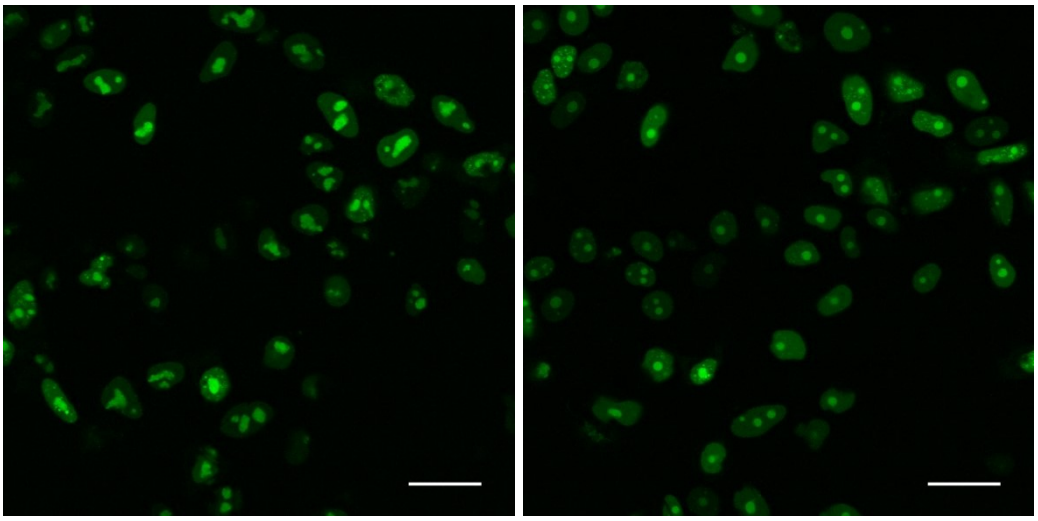

Figure 48: NCL C543S before adding doxorubicin (left); after 4,5h (10th frame); bar represents 30µm

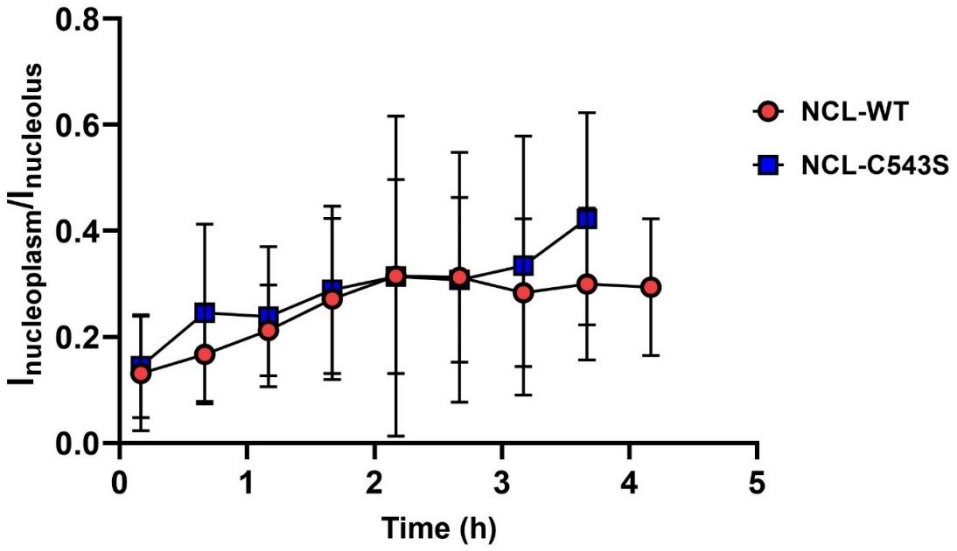

Figure 49: ratios of intensities in compartments of cells transfected by NCL wt (red) and NCL C543S (blue) during doxorubicin treatment

5.3 Examine the impact of studied NPM and NCL mutations on p53 regulation

It has been established that NPM is involved in activating p53, likely by interacting with Hdm2, which in turn starts to stabilize and activate p53. Yang et al. (Yang et al., 2016) suggested that since NPM C27S does not relocate, the activation of p53 will also be compromised. As seen on the Western blot below from HeLa transfected by each variant (Fig. 50), that does not seem to be the case: not only is p53 induced (stabilized) in both cultures by 4µM doxorubicin treatment, but the presence of phosphorylated forms also proves the activation of p53 in both.

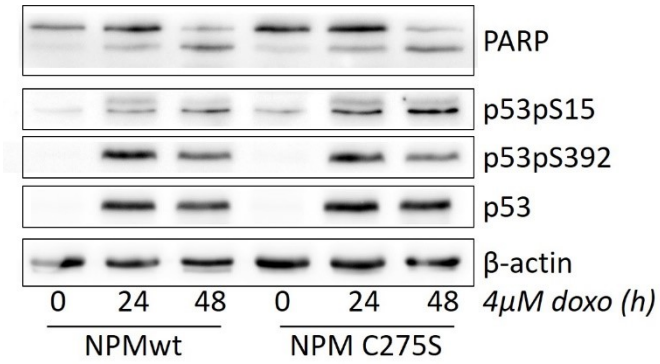

Figure 50: effect of 4μM doxorubicin treatment on PARP fragmentation and p53 activation of HeLa transfected with NPM wt or C275S mutant; β-Actin is used as a loading control

To compare with our second protein of interest, NCL, we repeated the experiment with HeLa cells transfected with each NCL variant (Fig. 51). The results were almost identical to those with NPM. We can conclude that the presence of cysteine-serine substitution did not interfere with the ability of doxorubicin to activate their interaction partner p53.

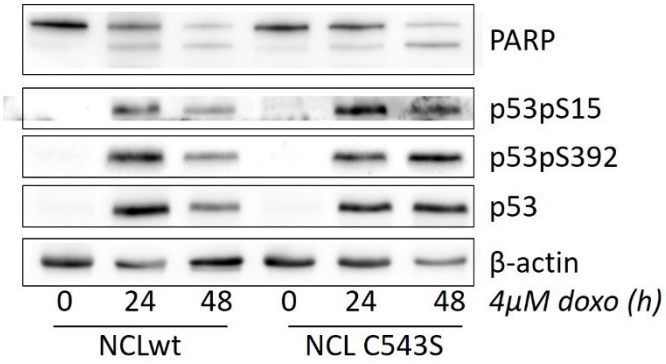

Figure 51: effect of 4μM doxorubicin treatment on PARP fragmentation and p53 activation of HeLa transfected with NCL wt or C543S mutant; β-Actin is used as a loading control

Next, we compared the reaction of cells transfected with both wt and C-S mutants with the reaction of untransfected cells (Fig. 52). Again, no substantial difference in p53 stabilization and activation has been detected.

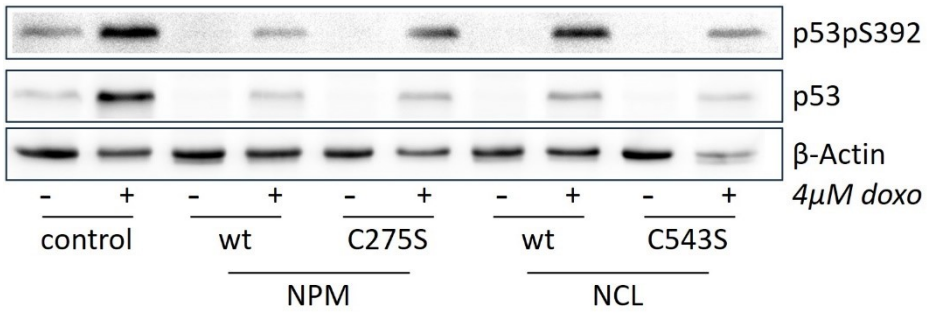

Figure 52: effect of 4μM doxorubicin treatment on p53 activation of HeLa cells: comparison of untransfected cells and cells transfected with wt variants or cysteine-serine mutants; β-Actin is used as a loading control

Finally, we repeated the experiment for NPM wt and C27S and added 3 more variants: C275A mutant, variant with C-terminal mutation type A (mutA) and a "double mutant", which we also prepared the plasmid for. After 48h in 4µM doxorubicin, p53 was activated in all the variants (Fig. 53).

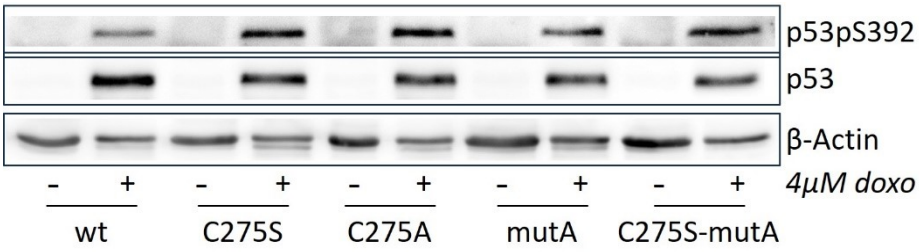

Figure 53: effect of 4µM doxorubicin treatment on p53 activation of HeLa cells: comparison of cells transfected with NPM variants; β-Actin is used as a loading control

Regarding the fact that introducing an exogenous protein does not interfere with the expression of endogenous ones, these results are to be considered somewhat tentative. Yang et al. (Yang et al., 2016) conducted their experiment on cells with a silenced endogenous variant, but for us, this exceeded the scope of the thesis.

Instead, we examined the potential influence of the cysteine-serine substitution in NPM and NCL on their interaction with p53 by co-immunoprecipitation. Previous studies of our laboratory showed that AML-associated NPM mutation disrupts interaction of NPM with NCL (Šašinková et al., 2018) but not with p53 (Holoubek et al., 2021). Similarly, our co-immunoprecipitation experiments proved interaction of NPM and NCL with p53, regardless of the mutation and doxorubicin treatment (Figs. 54, 55). Interestingly, the Y271C mutation seems to attenuate NPM interaction with both p53 and NCL, but not with endogenous NPM.

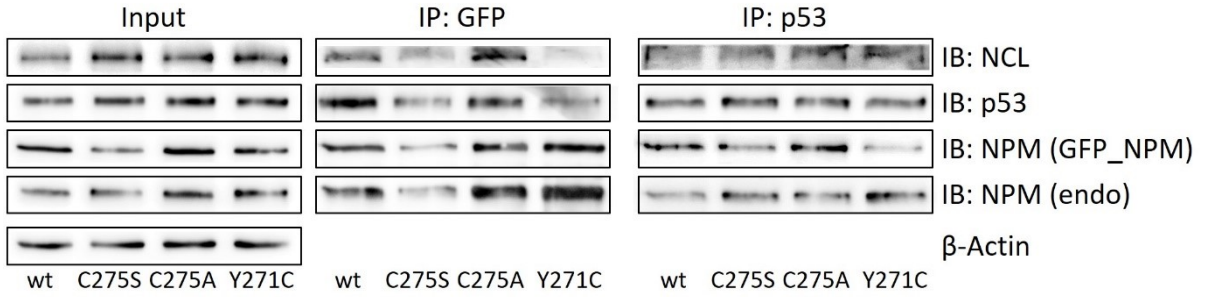

Figure 54: GFP- and p53- immunoprecipitation of HeLa cells transfected with NPM variants; Input~ whole cell lysate sample, IP=immunoprecipitation, IB=immunoblot

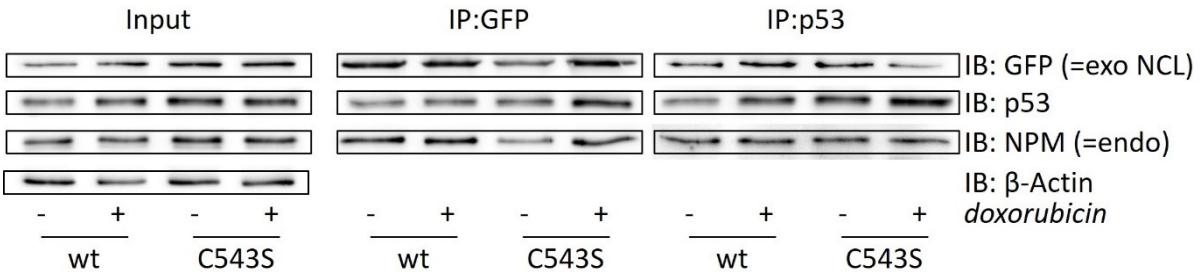

Figure 55: GFP- and p53- immunoprecipitation of HeLa cells transfected with NCL variants and treated with 4μM doxorubicin

5.4 Construct and test roGFP (NPM) sensors, monitor redox changes in cellular compartments

In the previous chapters, we proved doxorubicin-induced nucleolus-to-nucleoplasm delocalization of both proteins, all variants, as well as generation of ROS in doxorubicin-treated cells. Both of these phenomena were noticed in many, but not all cells in the samples, which represents the variability of cell states and reactions. To monitor redox state of the cells directly during treatment and to investigate whether the delocalization to nucleoplasm and ROS generation correlate, redox sensing roGFP1- and roGFP2-labeled variants of NPM wt were constructed. As the AML-related NPM mutant type A (C-terminal) has been previously shown to be sensitive to redox changes in the cytoplasm (G. Y. Liu et al., 2017) and to localize the genetically coded redox sensors specifically to cytoplasm, we also constructed a roGFP-labeled NPM mutA. To validate the application of the redox sensors in cells, first we used common oxidative reagent H_2O_2 to generate oxidative conditions inside cells. Fig. 56 illustrates the responses of roGFP1- and roGFP2-labeled proteins to 1mM H_2O_2 followed by addition of 5mM DTT as reductant.

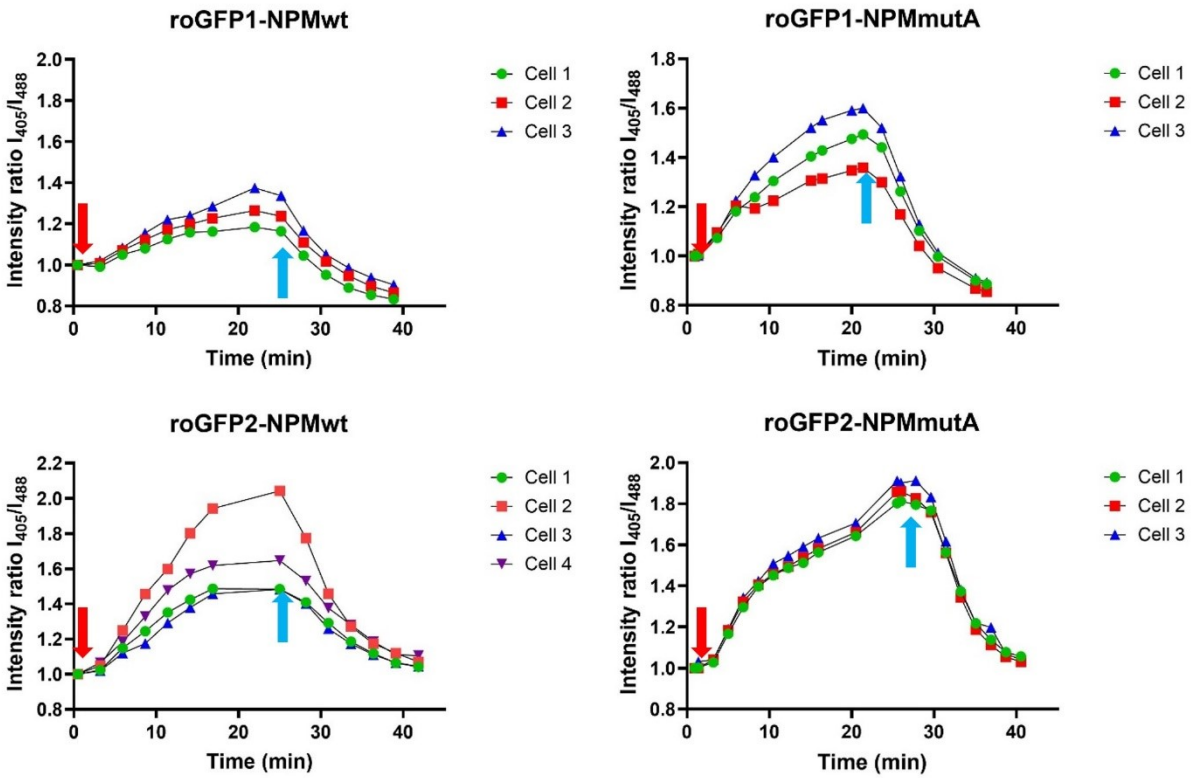

Figure 56: response of roGFP1 (upper row) and roGFP2 (lower row) labeled variants of NPMwt (left) and NPMmutA (right) to redox changes; red arrow: +1mM H2O2, blue arrow: + 5mM DTT; I_{405}/I_{488} denotes the ratio of fluorescence intensities detected after excitation at 405nm (I_{405}) and 488nm (I_{488}). Emission detected wit 520/35BP filter.

As can be seen, changes in redox state of the cells induced detectable response of both roGFP variants in the form of changes in the ratio of fluorescence intensity detected using 520/35BP filter from excitation at 405nm and 488nm (I_{405}/I_{488}) (Fig. 56).

As roGFP2 seems to exhibit a better response (larger range of detected values, the final state corresponds to the initial state), we chose to use the roGFP2 variant for our next experiment with roGFP-labeled C275S NPM mutant. As illustrated in Fig. 57, redox changes were detectable with this construct, although to a lesser extent than with NPMwt or NPMmutA. It corresponds to our previous results and the difference could be related to the absence of cysteine in the C275S mutant, but not enough experiments were performed to support any correlation. The presented dependencies represent pilot experiments carried out to test usefulness of prepared constructs in monitoring of cell redox state.

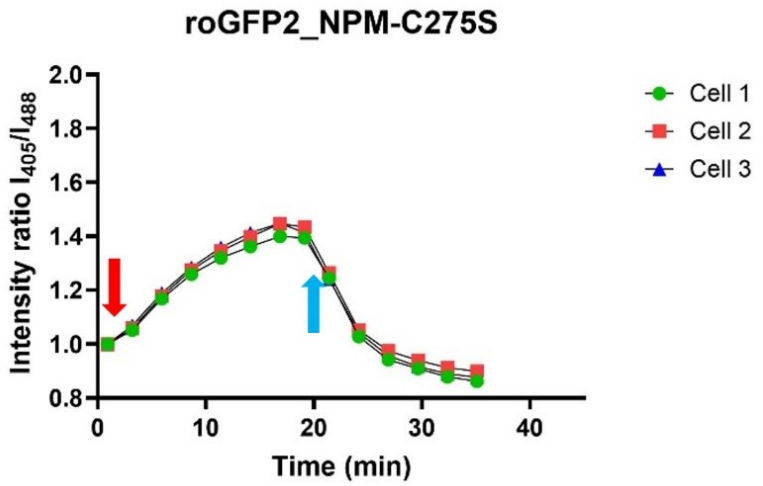

Figure 57: response of roGFP2-labeled NPM C275S to redox changes. Red arrow: +1mM H2O2, blue arrow: + 5mM DTT; I_{405}/I_{488} denotes ratio of fluorescence intensities excited by 405nm (I_{405}) and 488nm (I_{488}). Emission detected wit 520/35BP filter.

Despite the easily detected redox changes, no NPMwt delocalization has been detected in any sample (Fig. 58), which confirms our results from the first part of chapter 5.2 where we were not able to observe delocalization of NPM variants to nucleoplasm in response to H_2O_2 treatment.

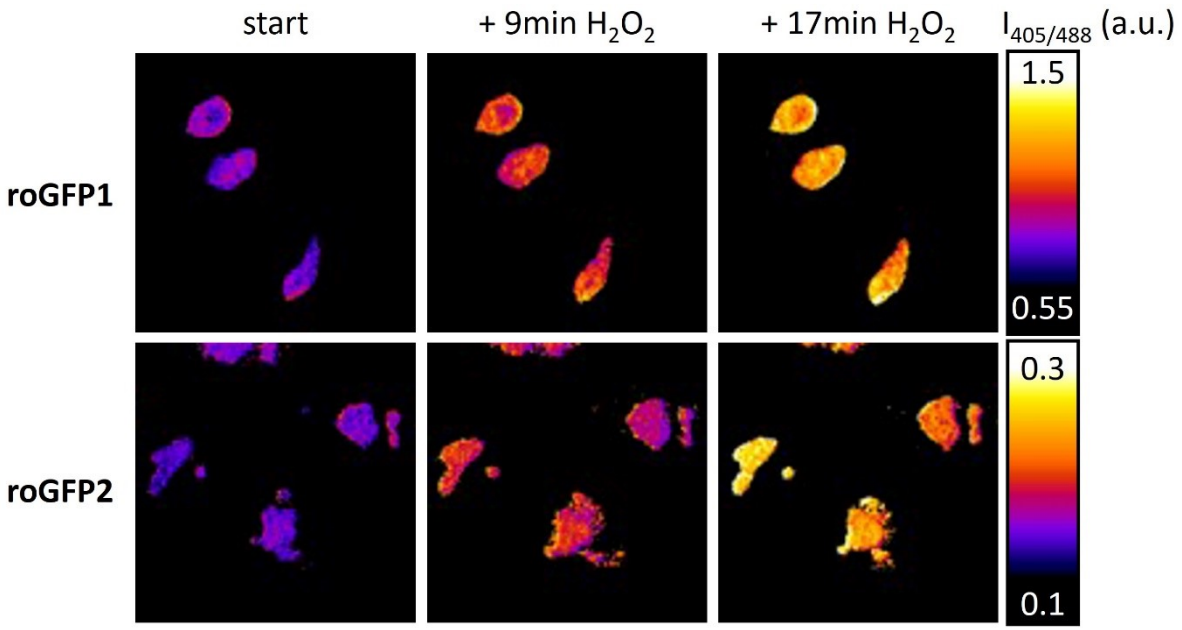

Figure 58: microscopy image of response of roGFP1 (upper row) and roGFP2 (lower row) labeled variants of NPMwt to H2O2 treatment. Color scale reflects changes in fluorescence intensity ratio (I_{405}/I_{488}).

Further research in this field will therefore target the reaction of roGFP2-labeled NPM forms in response to doxorubicin, which should answer the question whether the NPM delocalization and ROS generation occur simultaneously in the same cells. Such experiments should also confirm heterogeneity in redox responses of the cells to the treatment. However,

due to many technical difficulties (namely interference of doxorubicin fluorescence with roGFP fluorescence excited by 488 nm, although these might likely be separated using fluorescence lifetime imaging measurements (FLIM), and insufficient stabilization of z-position of the sample during longer experiments, which might be solved by a software addition), these experiments cannot be presented in this thesis.

6 Discussion

All of the plasmids constructed for this thesis were prepared by standard molecular cloning techniques well established in the laboratory under supervision of Dr. A. Holoubek. We were successful in the preparation of almost all the constructs needed; we did not obtain clones of correct size only for eGFP-labeled double mutant NPMmutA-C275S. However, as we were successful with mRFP1 variant, it is possible to use this construct as a template for further cloning if needed. Further cloning should also include the preparation of more roGFP-labeled plasmids, namely for both NCL variants and the remaining NPM variants, C275A or Y271C, to investigate role of cysteine content in induced redox changes inside the nucleolus. To mirror the research on NPM, it would also be beneficial to create a NCL C543A variant and a NCL variant with an extra cysteine.

Our main goal was to study the behavior of NPM and NCL under cellular (nucleolar) stress. Inspired by Yang et al. (Yang et al., 2016), we started by application of H_2O_2, which is known to cause oxidative stress. In contrast to expectations, we have not been able to confirm a stress-induced apoptosis in cells with Western blot, using double the H_2O_2 concentration compared to Yang et al. (Yang et al., 2016). Their microscopic evaluations also showed that the signal did not decrease with lower H_2O_2 concentrations (125 and 250µM), so suboptimal concentration can still be a part of the reason for the difference in our results. Nonetheless, as we were not successful in finding the optimal concentration, we chose not to investigate further.

In fluorescence confocal microscopy experiments with exogenous proteins produced from transfected plasmids, we did not observe significant translocation of NPMwt to the nucleoplasm in response to H_2O_2 treatment, which is supposed to accompany nucleolar stress. Since this study planned to preferentially target this kind of behavior of nucleolar phosphoproteins, we aimed to test other stressors that would ensure an observable translocation. The reason of the unexpected behavior in the presence of H_2O_2 may lie in the complexity of stress response: while the majority of signaling pathways go through the nucleolus, not all of them include NPM and/or NCL, and there is also doubt around the interpretation of the phenomena observed in Yang et al. (Yang et al., 2016). In our opinion, the parameter proposed in Yang et al. (decreasing signal in the nucleolus) does not fully reflect the nucleolar stress-induced translocation (Yang et al., 2016). Each of the stressors also causes a unique spectrum of damage: for example, H_2O_2 induces apoptosis via the mitochondrial pathway, whereas doxorubicin mainly induces DNA/RNA damage (Singh et al., 2007). However, Yang et al. suggest common mechanism comprising redox sensing in the nucleolus for majority of cell stresses (Yang et al., 2016).

We also briefly tested UV irradiation and actinomycin D as stressors, but neither produced satisfying or different enough results, so we discontinued the use and deemed it useless to further discuss the results.

In the experiments addressing the main aim, we initially tried to track different variants of NPM or NCL at the same time using labelling with fluorescent proteins of two colors, eGFP and mRFP1. The cells were transfected, as regularly used in the laboratory, with a mixture of

plasmids ensuring that cells produce a double-colored mixture of fluorescently labeled proteins. Unfortunately, the same NPM variants labeled with different fluorescent proteins did not behave completely in the same manner. The main difference lied in the original distribution of labeled proteins inside the nucleolus: the presence of the green labeled NPMwt was stronger in the nucleoplasm than of the red construct, which equaled null levels, even prior to doxorubicin treatment. In addition, the treatment then caused a stronger relative rise of fluorescence of the red construct.

We did not observe this kind of behavior for NCL construct. We then decided to observe each variant separately using cells transfected with one plasmid for production of single color-labeled proteins. Preferentially, we used the eGFP-linked constructs, as they provided clearer and more consistent results. The aforementioned issue concerning monitoring of more NPM variants at once could be solved by using a programmable microscopy table, which allows taking pictures of several wells in short sequence while maintaining the photographed positions in each well. Alas, we do not have one of those. We therefore monitored each sample individually, which brought some inconsistency in the process of sample observation, as the doxorubicin addition occurred at different time points in relation to the cell passage. Nonetheless, we tried to minimize these variations by maintaining the same time between cell seeding, transfection and doxorubicin addition.

We observed some difference between the behavior of NPM wt and C275S in the initial hours of the experiments, but they were different from the observation of Yang et al. (Yang et al., 2016). Rather than delocalizing from the nucleolus to the nucleoplasm, the amount of both variants appeared to grow (eventually) in both compartments, even though slower/later in case of C275S. Compared to the changes in the time frame 30mins to 2h observed by Yang et al. (Yang et al., 2016), the growth within several hours observed by us can be related to doxorubicin concentrating in the nucleolus taking more than an hour to start (see chapter 5.2). Another difference was in the nucleoplasm: in the results of Yang et al. (Yang et al., 2016), there is almost no observable signal in this compartment, throughout the experiment (and no discussion regarding the nucleoplasm either). In our results, the largest changes happened in the nucleoplasm, while the nucleolus signal remained generally almost constant.

We have also confirmed that there is no significant difference in terms of stabilization of p53 and/or inducing apoptosis (according to apoptosis markers). We were aware of the risk of p53 activity/regulation possibly being affected by human papilloma virus (HPV), which is regularly found in cervix carcinoma cells (including HeLa) (Ajay et al., 2012). However, DSMZ, the cell line culture bank from which we obtained our cells, declared that “several copies of HPV18 integrated as proviruses into the eukaryotic genome are incomplete and exhibit 2-3 kb deletions of the E2-L2 region”, and that “activation and transmission of the HPV-18 during handling of the cell line is improbable.” (dsmz.de, 2025). We therefore did not expect any alterations in p53 signalization caused by potential HPV infection.

Interestingly, when cysteine was substituted for alanine (C275A) rather than serine, the mutant variant behaved more similarly to the wild-type variant, and we observed translocation to the nucleoplasm. Since this variant also cannot be glutathionylated

at position 275, this observation indicates that this posttranslational modification must not be critical for the nucleolar stress-related behavior of NPM. This variant resides in the nucleoplasm noticeably more than wt or C275S even in untreated cells. This suggests that the substituting amino acid can play a crucial role in keeping NPM in the nucleolus, but also in the initial localization. This may be due to many factors, for example changes in the protein conformation, since the replacement of Cys275 with serine should be more conservative than with alanine, with respect to size and polarity of the exchanged amino acid and the introduction of different reactive groups (or lack thereof in the case of alanine). Further research on this topic could include more extensive testing of the reactivity of the mutated protein or modeling the possibly altered structure of the mutated variants. From this point of view, it was interesting to investigate another available mutant variant of NPM (Y271C). This variant has an extra cysteine rather than lacking one compared to wt; and following the hypothesis that cysteines may play a crucial role in the response of nucleolar proteins to (redox) stress, adding a cysteine should result in opposite behavior. In our research, this was partly true: the Y271C variant had clearly the highest initial concentration in the nucleoplasm out of all of the four variants and it was the only one where the concentration in the nucleolus stagnated or decreased slightly rather than increased. However, the concentration in the nucleoplasm followed a similar trend to wt and C275A.
The “double mutant” variant of NPM (mutA-C275S) was localized in the cytoplasm, in the same manner as the “single mutant” variant NPMmutA. We did not include the double-mutant variant in most of our research (the different localization being part of the reason why) but it might be an interesting tool to study redox changes in the cytoplasm.
In conclusion, once again, the hypothesis of cysteines and redox stress would benefit from much more experimental attention – there is probably a reason why NPM, NCL, fibrillarin and other nucleolar proteins have a much lower than average content of cysteines.

Another part of our main goal was to observe NCL wt and NCL C543S and to compare the results to corresponding NPM variants. We were able to observe and measure some differences between the NCL variants, but they were not statistically significant. The comparison of NCL wt/C543S and NPM C275S/NCL C543S is disproving the hypothesis about the importance of cysteines for redox sensing by the nucleolus and the meaning of glutathionylation of nucleolar phosphoproteins for delocalization in response to local redox changes in the nucleolus; although differences in function of NCL and NPM, even in redox sensing, may play a large role. It would also be valuable to mirror the rest of the NPM research with a NCL C543A variant and a NCL variant with an extra cysteine, but that was not possible with the thesis time frame.
All of the observed differences in behavior can also be supported by the mutation pathogenicity score of mutants calculated by AlphaFold (Jumper et al., 2021) is high (0.898 for C275S, 0.883 for C275A, 0.997 for Y271C, and 0.748 for NCL C543S; on the scale from 0 to 1, scores over 0.564 are considered high).

As for the stabilization of p53 by wt and lack thereof by C275S mutant, our immunoblot experiments show no noticeable difference in p53 regulation indicated by interaction between these proteins. It has to be said, however, that Yang et al. (Yang et al., 2016) conducted their research on cells with knocked-out endogenous NPM, which heightens the influence of exogenous protein variants. We did not conduct the knock-outs – it is also outside of the scope of this thesis.

In our co-IP experiments, we showed that the interaction of NCL and endogenous NPM as well as NCL and p53 was impacted neither by the C543S mutation nor by the doxorubicin treatment.

We were also not able to conduct as many experiments with leukemic cells as we initially hoped. We expected to replicate the results of Yang et al. (Yang et al., 2016), extend research on HeLa cells and then try to confirm our results in leukemic cells (lines or patient cells). However, after obtaining results mostly different from Yang's, we were forced to focus more on the initial research on HeLa. Despite the setback, we were able to show that after doxorubicin treatment, 4 AML cell lines (OCI-AML2 and 3, MV4-11 and MOLM-13) and 1 ALL line (Jurkat) all develop a population of cells with increased ROS concentration similarly to HeLa cells, and that apoptosis is induced in Jurkat despite lacking p53. We also confirmed doxorubicin-induced delocalization of endogenous forms of both proteins in leukemic cell lines. General mechanisms induced by doxorubicin treatment are thus likely identical for leukemic and HeLa cell lines, which is promising in terms of hopefully obtaining similar results on leukemic cells.

We also succeeded in creating roGFP plasmids with NPMwt, NPMmutA and NPM-C275S, and we conducted initial experiments with them. In collaboration with Mgr. Dita Strachotová, PhD. from the Faculty of Mathematics and Physics, Charles University, we measured the redox potential changes immediately after adding H_2O_2 and then DTT. The mutA variant seems to be reacting more strongly than wt (Fig. 56); the reason may lie in different environments in different compartments (wt being localized in nucleolus and nucleoplasm, mutA in cytoplasm), but also possibly in the extra cysteine added by the mutation of NPM C-terminus in mutA (Huang et al., 2013). Liu et al (G. Y. Liu et al., 2017) documented that NPM regulates expression of peroxiredoxins, namely PRDX6, thus modulating redox homeostasis. When mutated, cytoplasm-targeted NPM lowers ROS concentration by downregulation of PRDX6. Moreover, transient increase of ROS has been detected after treatment with small molecule NSC348884, designed to inhibit NPM oligomerization, which suggests transient NPM cytoplasmic relocation induced by this treatment (Liu et al. 2017). However, the relationship between cysteine number, protein localization and ROS concentration should be further investigated to elucidate these proceses.

All results obtained with roGFP are discussed in the Results chapter and these pilot experiments encourage further use of this new tool in collaborating departments. This may include constructing roGFP-labeled plasmids for other NPM or NCL variants, but more importantly implementing improved roGFP variants with better sensitivity and further experiments with doxorubicin and other stressors inducing the nucleolar stress.

In conclusion, we have not fully reproduced the results of Yang et al. (Yang et al., 2016), but we have proven that the studied mutations do have an influence over the reaction to doxorubicin-induced stress.

7 Conclusions

We created several new plasmids to study nucleolar stress in cells. Among these were also plasmids for roGFP1- and roGFP2-tagged NPM variants, which will be used in the lab in future projects.

We conducted experiments to observe the behavior of wt and mutated NPM and NCL in HeLa cells as a reaction to stress induced by the chemotherapeutic drug doxorubicin. We partly confirmed the works of Yang et al. (Yang et al., 2016), we extended their research with two new mutant variants of NPM and added some interesting observations.

To better understand the role of nucleolar proteins as a whole, we compared two NCL variants to corresponding NPM variants (wt to wt, C275S to C543S). We disproved our original hypothesis that NPM and NCL could behave similarly due to their similar functions. There is undoubtedly much room for further research, but our results add valuable building blocks.

To make further connections with oxidative stress, we documented the similarity of ROS level increase between HeLa and several leukemic cell-lines, and most importantly, we designed a new model system using redox sensitive fluorescent proteins to prove the hypothesis that NPM delocalization could correlate with redox changes in cellular compartments of HeLa cells.

Another topic of interest was the possible role of nucleolar proteins' cysteines in redox sensing by nucleolus. We addressed NCL not only because of its importance e.g. in AML, but also because it possesses only one cysteine residue in its structure, which is an exceptionally small portion. As we did not observe a significant effect of substituting this residue (with serine), we cannot conclude on the importance of cysteine content for redox sensing by nucleolus. Again, this will need further research using the newly tested roGFPs-based system with varying cysteine contents of nucleolar proteins.

Given the time frame of this thesis, it was not possible to answer all of the questions that were raised during the research, but we succeeded in elucidating and comparing the behavior of two important nucleolar proteins under conditions of nucleolar stress.

8 References

ACS web site. (2025). *Key Statistics for Acute Myeloid Leukemia (AML) | American Cancer Society*. https://www.cancer.org/cancer/types/acute-myeloid-leukemia/about/key-statistics.html

Ajay, A. K., Meena, A. S., & Bhat, M. K. (2012). Human papillomavirus 18 E6 inhibits phosphorylation of p53 expressed in HeLa cells. *Cell & Bioscience*, *2*(1), 2. https://doi.org/10.1186/2045-3701-2-2

Alpermann, T., Schnittger, S., Eder, C., Dicker, F., Meggendorfer, M., Kern, W., Schmid, C., Aul, C., Staib, P., Wendtner, C. M., Schmitz, N., Haferlach, C., & Haferlach, T. (2016). Molecular subtypes of NPM1 mutations have different clinical profiles, specific patterns of accompanying molecular mutations and varying outcomes in intermediate risk acute myeloid leukemia. *Haematologica*, *101*(2), e55–e58. https://doi.org/10.3324/HAEMATOL.2015.133819

Appelbaum, F. R., Gundacker, H., Head, D. R., Slovak, M. L., Willman, C. L., Godwin, J. E., Anderson, J. E., & Petersdorf, S. H. (2006). Age and acute myeloid leukemia. *Blood*, *107*(9), 3481–3485. https://doi.org/10.1182/BLOOD-2005-09-3724

Barford, D. (2004). The role of cysteine residues as redox-sensitive regulatory switches. *Current Opinion in Structural Biology*, *14*(6), 679–686. https://doi.org/10.1016/J.SBI.2004.09.012

Berger, C. M., Gaume, X., & Bouvet, P. (2015). The roles of nucleolin subcellular localization in cancer. *Biochimie*, *113*, 78–85. https://doi.org/10.1016/J.BIOCHI.2015.03.023

Boisvert, F. M., Van Koningsbruggen, S., Navascués, J., & Lamond, A. I. (2007). The multifunctional nucleolus. *Nature Reviews Molecular Cell Biology 2007 8:7*, *8*(7), 574–585. https://doi.org/10.1038/nrm2184

Borer, R. A., Lehner, C. F., Eppenberger, H. M., & Nigg, E. A. (1989). Major nucleolar proteins shuttle between nucleus and cytoplasm. *Cell*, *56*(3), 379–390. https://doi.org/10.1016/0092-8674(89)90241-9

Bouvet, P., Diaz, J. J., Kindbeiter, K., Madjar, J. J., & Amalric, F. (1998). Nucleolin interacts with several ribosomal proteins through its RGG domain. *The Journal of Biological Chemistry*, *273*(30), 19025–19029. https://doi.org/10.1074/JBC.273.30.19025

Brodska, B., Holoubek, A., Otevrelova, P., & Kuzelova, K. (2016). Low-Dose Actinomycin-D Induces Redistribution of Wild-Type and Mutated Nucleophosmin Followed by Cell Death in Leukemic Cells. *Journal of Cellular Biochemistry*, *117*(6), 1319–1329. https://doi.org/10.1002/jcb.25420 [doi]

Brodska, B., Kracmarova, M., Holoubek, A., & Kuzelova, K. (2017). Localization of AML-related nucleophosmin mutant depends on its subtype and is highly affected by its interaction with wild-type NPM. *PloS One*, *12*(4), e0175175. https://doi.org/10.1371/journal.pone.0175175 [doi]

Brodská, B., Šašinková, M., & Kuželová, K. (2019). Nucleophosmin in leukemia: Consequences of anchor loss. *The International Journal of Biochemistry & Cell Biology*, *111*, 52–62. https://doi.org/10.1016/J.BIOCEL.2019.04.007

Calo, E., Gu, B., Bowen, M. E., Aryan, F., Zalc, A., Liang, J., Flynn, R. A., Swigut, T., Chang, H. Y., Attardi, L. D., & Wysocka, J. (2018). Tissue-selective effects of nucleolar stress and rDNA damage in developmental disorders. *Nature*, *554*(7690), 112–117. https://doi.org/10.1038/NATURE25449

Cannon, M. B., & Remington, S. J. (2006). Re-engineering redox-sensitive green fluorescent protein for improved response rate. *Protein Science : A Publication of the Protein Society*, *15*(1), 45–57. https://doi.org/10.1110/PS.051734306

Cannon, M. B., & Remington, S. J. (2008). Redox-sensitive green fluorescent protein: probes for dynamic intracellular redox responses. A review. *Methods in Molecular Biology (Clifton, N.J.)*, *476*, 51–65. https://doi.org/10.1007/978-1-59745-129-1_4

Carugo, O. (2008). Amino acid composition and protein dimension. *Protein Science : A Publication of the Protein Society*, *17*(12), 2187. https://doi.org/10.1110/PS.037762.108

Carvalho, C., Santos, R., Cardoso, S., Correia, S., Oliveira, P., Santos, M., & Moreira, P. (2009). Doxorubicin: the good, the bad and the ugly effect. *Current Medicinal Chemistry*, *16*(25), 3267–3285. https://doi.org/10.2174/092986709788803312

Castillo-Villanueva, A., Reyes-Vivas, H., & Oria-Hernández, J. (2023). Comparison of cysteine content in whole proteomes across the three domains of life. *PLOS ONE*, *18*(11), e0294268. https://doi.org/10.1371/JOURNAL.PONE.0294268

Chen, Y., Wu, Z., Wang, L., Lin, M., Jiang, P., Wen, J., Li, J., Hong, Y., Zheng, X., Yang, X., Zheng, J., Gale, R. P., Yang, T., & Hu, J. (2023). Targeting nucleolin improves sensitivity to chemotherapy in acute lymphoblastic leukemia. *Cellular Oncology (Dordrecht, Netherlands)*, *46*(6), 1709–1724. https://doi.org/10.1007/S13402-023-00837-2

Christian, S., Pilch, J., Akerman, M. E., Porkka, K., Laakkonen, P., & Ruoslahti, E. (2003). Nucleolin expressed at the cell surface is a marker of endothelial cells in angiogenic blood vessels. *The Journal of Cell Biology*, *163*(4), 871. https://doi.org/10.1083/JCB.200304132

Cong, R., Das, S., & Bouvet, P. (2011). *The Nucleolus: Vol. Chapter 9* (M. O. J. Olson, Ed.). Springer New York. https://doi.org/10.1007/978-1-4614-0514-6

Cong, R., Das, S., Ugrinova, I., Kumar, S., Mongelard, F., Wong, J., & Bouvet, P. (2012). Interaction of nucleolin with ribosomal RNA genes and its role in RNA polymerase I transcription. *Nucleic Acids Research*, *40*(19), 9441–9454. https://doi.org/10.1093/NAR/GKS720

Cox, M. L., & Meek, D. W. (2010). Phosphorylation of serine 392 in p53 is a common and integral event during p53 induction by diverse stimuli. *Cellular Signalling*, *22*(3), 564–571. https://doi.org/10.1016/J.CELLSIG.2009.11.014

Créancier, L., Prats, H., Zanibellato, C., Amalric, F., & Bugler, B. (1993). Determination of the functional domains involved in nucleolar targeting of nucleolin. *Molecular Biology of the Cell*, *4*(12), 1239–1250. https://doi.org/10.1091/MBC.4.12.1239

Desai, M., & Sun, B. (2024). Positions of cysteine residues reveal local clusters and hidden relationships to Sequons and Transmembrane domains in Human proteins. *Scientific Reports 2024 14:1*, *14*(1), 1–14. https://doi.org/10.1038/s41598-024-77056-8

Dooley, C. T., Dore, T. M., Hanson, G. T., Jackson, W. C., Remington, S. J., & Tsien, R. Y. (2004). Imaging dynamic redox changes in mammalian cells with green fluorescent protein indicators. *The Journal of Biological Chemistry*, *279*(21), 22284–22293. https://doi.org/10.1074/JBC.M312847200

Dorr, R. T., Dordal, M. S., Koenig, L. M., Taylor, C. W., & McClosky, T. M. (1989, December 15). *High levels of doxorubicin in the tissues of a patient experiencing extravasation during a 4-day infusion - PubMed*. Cancer 64(12). https://pubmed.ncbi.nlm.nih.gov/2819656/

dsmz.de. (2025). *Leibniz Institute DSMZ: Details*. https://www.dsmz.de/collection/catalogue/details/culture/ACC-57

Falini, B., Mecucci, C., Tiacci, E., Alcalay, M., Rosati, R., Pasqualucci, L., La Starza, R., Diverio, D., Colombo, E., Santucci, A., Bigerna, B., Pacini, R., Pucciarini, A., Liso, A., Vignetti, M., Fazi, P., Meani, N., Pettirossi, V., Saglio, G., … Martelli, M. F. (2005). Cytoplasmic nucleophosmin in acute myelogenous leukemia with a normal karyotype. *The New England Journal of Medicine*, *352*(3), 254–266. https://doi.org/10.1056/NEJMOA041974

Ginisty, H., Amalric, F., & Bouvet, P. (1998). Nucleolin functions in the first step of ribosomal RNA processing. *The EMBO Journal*, *17*(5), 1476–1486. https://doi.org/10.1093/EMBOJ/17.5.1476

Ginisty, H., Serin, G., Ghisolfi-Nieto, L., Roger, B., Libante, V., Amalric, F., & Bouvet, P. (2000). Interaction of nucleolin with an evolutionarily conserved pre-ribosomal RNA sequence is required for the assembly of the primary processing complex. *The Journal of Biological Chemistry*, *275*(25), 18845–18850. https://doi.org/10.1074/JBC.M002350200

Ginisty, H., Sicard, H., Roger, B., & Bouvet, P. (1999). Structure and functions of nucleolin. *Journal of Cell Science*, *112 (Pt 6)*(6), 761–772. https://doi.org/10.1242/JCS.112.6.761

Go, Y. M., Chandler, J. D., & Jones, D. P. (2015). The Cysteine Proteome. *Free Radical Biology & Medicine*, *84*, 227. https://doi.org/10.1016/J.FREERADBIOMED.2015.03.022

Grimwade, D., Ivey, A., & Huntly, B. J. P. (2016). Molecular landscape of acute myeloid leukemia in younger adults and its clinical relevance. *Blood*, *127*(1), 29–41. https://doi.org/10.1182/BLOOD-2015-07-604496

Grisendi, S., Bernardi, R., Rossi, M., Cheng, K., Khandker, L., Manova, K., & Pandolfi, P. P. (2005). Role of nucleophosmin in embryonic development and tumorigenesis. *Nature*, *437*(7055), 147–153. https://doi.org/10.1038/NATURE03915

Hariharan, N., & Sussman, M. A. (2014). Stressing on the nucleolus in cardiovascular disease. *Biochimica et Biophysica Acta*, *1842*(6), 798–801. https://doi.org/10.1016/J.BBADIS.2013.09.016

Henderson, A. S., Warburton, D., & Atwood, K. C. (1972). Location of ribosomal DNA in the human chromosome complement. *Proceedings of the National Academy of Sciences of*

the United States of America, *69*(11), 3394–3398. https://doi.org/10.1073/PNAS.69.11.3394

Hindley, A., Catherwood, M. A., McMullin, M. F., & Mills, K. I. (2021). Significance of NPM1 Gene Mutations in AML. *International Journal of Molecular Sciences*, *22*(18). https://doi.org/10.3390/IJMS221810040

Holoubek, A., Strachotova, D., Wolfova, K., Otevrelova, P., Belejova, S., Roselova, P., Benda, A., Brodska, B., & Herman, P. (2025). Correlation of p53 oligomeric status and its subcellular localization in the presence of the AML-associated NPM mutant. *PLoS One*, in press. https://doi.org/10.1371/journal.pone.0322096

Holoubek, Al., Strachotová, D., Otevřelová, P., Roselová, P., Heřman, P., & Brodská, B. (2021). AML-Related NPM Mutations Drive p53 Delocalization into the Cytoplasm with Possible Impact on p53-Dependent Stress Response. *Cancers (Basel)*, *13*(13), 33266. https://doi.org/10.3390/cancers13133266

Hortobágyi, G. N. (1997). Anthracyclines in the treatment of cancer. An overview. *Drugs*, *54 Suppl 4*(SUPPL. 4), 1–7. https://doi.org/10.2165/00003495-199700544-00003

Hua, L., Yan, D., Wan, C., & Hu, B. (2022). Nucleolus and Nucleolar Stress: From Cell Fate Decision to Disease Development. *Cells*, *11*(19). https://doi.org/10.3390/CELLS11193017

Huang, M., Thomas, D., Li, M. X., Feng, W., Chan, S. M., Majeti, R., & Mitchell, B. S. (2013). Role of cysteine 288 in nucleophosmin cytoplasmic mutations: sensitization to toxicity induced by arsenic trioxide and bortezomib. *Leukemia*, *27*(10), 1970–1980. https://doi.org/10.1038/LEU.2013.222

Issa, A., Schlotter, F., Flayac, J., Chen, J., Wacheul, L., Philippe, M., Sardini, L., Mostefa, L., Vandermoere, F., Bertrand, E., Verheggen, C., Lafontaine, D. L. J., & Massenet, S. (2024). The nucleolar phase of signal recognition particle assembly. *Life Science Alliance*, *7*(8). https://doi.org/10.26508/LSA.202402614

James, A., Wang, Y., Raje, H., Rosby, R., & DiMario, P. (2014). Nucleolar stress with and without p53. *Nucleus (Austin, Tex.)*, *5*(5), 402–426. https://doi.org/10.4161/NUCL.32235

Julka, P. K., Chacko, R. T., Nag, S., Parshad, R., Nair, A., Oh, D. S., Hu, Z., Koppiker, C. B., Nair, S., Dawar, R., Dhindsa, N., Miller, I. D., Ma, D., Lin, B., Awasthy, B., & Perou, C. M. (2008). A phase II study of sequential neoadjuvant gemcitabine plus doxorubicin followed by gemcitabine plus cisplatin in patients with operable breast cancer: prediction of response using molecular profiling. *British Journal of Cancer*, *98*(8), 1327–1335. https://doi.org/10.1038/SJ.BJC.6604322

Jumper, J., Evans, R., Pritzel, A., Green, T., Figurnov, M., Ronneberger, O., Tunyasuvunakool, K., Bates, R., Žídek, A., Potapenko, A., Bridgland, A., Meyer, C., Kohl, S. A. A., Ballard, A. J., Cowie, A., Romera-Paredes, B., Nikolov, S., Jain, R., Adler, J., … Hassabis, D. (2021). Highly accurate protein structure prediction with AlphaFold. *Nature*, *596*(7873), 583–589. https://doi.org/10.1038/S41586-021-03819-2

Kantarjian, H., Thomas, D., O'Brien, S., Cortes, J., Giles, F., Jeha, S., Bueso-Ramos, C. E., Pierce, S., Shan, J., Koller, C., Beran, M., Keating, M., & Freireich, E. J. (2004). Long-term follow-up results of hyperfractionated cyclophosphamide, vincristine, doxorubicin, and dexamethasone (Hyper-CVAD), a dose-intensive regimen, in adult acute lymphocytic leukemia. *Cancer*, *101*(12), 2788–2801. https://doi.org/10.1002/CNCR.20668

Kauffman, M., Kauffman, M., Zhu, H., Jia, Z., & Li, Y. (2016). Fluorescence-Based Assays for Measuring Doxorubicin in Biological Systems. *Reactive Oxygen Species (Apex, N.C.)*, *2*(6). https://doi.org/10.20455/ROS.2016.873

Kciuk, M., Gielecińska, A., Mujwar, S., Kołat, D., Kałuzińska-Kołat, Ż., Celik, I., & Kontek, R. (2023). Doxorubicin-An Agent with Multiple Mechanisms of Anticancer Activity. *Cells*, *12*(4). https://doi.org/10.3390/CELLS12040659

Kennis, J. T. M., Larsen, D. S., Van Stokkum, I. H. M., Vengris, M., Van Thor, J. J., & Van Grondelle, R. (2004). Uncovering the hidden ground state of green fluorescent protein. *Proceedings of the National Academy of Sciences of the United States of America*, *101*(52), 17988–17993. https://doi.org/10.1073/PNAS.0404262102

Komínková, M., Zítka, O., & Kizek, R. (2015). Poměr GSH/GSSG u biologických organismů. *Journal of Metallomics and Nanotechnologies*, *2*(2), 46–48.

Kurki, S., Peltonen, K., Latonen, L., Kiviharju, T. M., Ojala, P. M., Meek, D., & Laiho, M. (2004). Nucleolar protein NPM interacts with HDM2 and protects tumor suppressor protein p53 from HDM2-mediated degradation. *Cancer Cell*, *5*(5), 465–475. https://doi.org/S1535610804001102 [pii]

Lafita-Navarro, M. C., & Conacci-Sorrell, M. (2023). Nucleolar stress: From development to cancer. *Seminars in Cell & Developmental Biology*, *136*, 64–74. https://doi.org/10.1016/J.SEMCDB.2022.04.001

Lee, S. B., Kim, C. K., Lee, K. H., & Ahn, J. Y. (2012). S-nitrosylation of B23/nucleophosmin by GAPDH protects cells from the SIAH1-GAPDH death cascade. *The Journal of Cell Biology*, *199*(1), 65–76. https://doi.org/10.1083/JCB.201205015

Li, Y. P., Busch, R. K., Valdez, B. C., & Busch, H. (1996). C23 interacts with B23, a putative nucleolar-localization-signal-binding protein. *European Journal of Biochemistry*, *237*(1), 153–158. https://doi.org/10.1111/J.1432-1033.1996.0153N.X

Liang, J., Zhang, Z., Zhao, H., Wan, S., Zhai, X., Zhou, J., Liang, R., Deng, Q., Wu, Y., & Lin, G. (2018). Simple and rapid monitoring of doxorubicin using streptavidin-modified microparticle-based time-resolved fluorescence immunoassay. *RSC Advances*, *8*(28), 15621–15631. https://doi.org/10.1039/C8RA01807C

Liu, G. Y., Shi, J. X., Shi, S. L., Liu, F., Rui, G., Li, X., Gao, L. Bin, Deng, X. L., & Li, Q. F. (2017). Nucleophosmin Regulates Intracellular Oxidative Stress Homeostasis via Antioxidant PRDX6. *Journal of Cellular Biochemistry*, *118*(12), 4697–4707. https://doi.org/10.1002/JCB.26135

Liu, L. F., Rowe, T. C., Yang, L., Tewey K M, & Chen, G. L. (1983, December 25). *Cleavage of DNA by mammalian DNA topoisomerase II - PubMed*. J Biol Chem 258(24). https://pubmed.ncbi.nlm.nih.gov/6317692/

Loughery, J., Cox, M., Smith, L. M., & Meek, D. W. (2014). Critical role for p53-serine 15 phosphorylation in stimulating transactivation at p53-responsive promoters. *Nucleic Acids Research*, *42*(12), 7666. https://doi.org/10.1093/NAR/GKU501

Lu, L., Yi, H., Chen, C., Yan, S., Yao, H., He, G., Li, G., Jiang, Y., Deng, T., & Deng, X. (2018). Nucleolar stress: is there a reverse version? *Journal of Cancer*, *9*(20), 3723. https://doi.org/10.7150/JCA.27660

Maehama, T., Nishio, M., Otani, J., Mak, T. W., & Suzuki, A. (2023). Nucleolar stress: Molecular mechanisms and related human diseases. *Cancer Science*, *114*(5), 2078–2086. https://doi.org/10.1111/CAS.15755

Malke, H. (1990). J. SAMBROCK, E. F. FRITSCH and T. MANIATIS, Molecular Cloning, A Laboratory Manual (Second Edition), Volumes 1, 2 and 3. 1625 S., zahlreiche Abb. und Tab. Cold Spring Harbor 1989. Cold Spring Harbor Laboratory Press. $ 115.00. ISBN: 0-87969-309-6. *Journal of Basic Microbiology*, *30*(8), 623–623. https://doi.org/10.1002/JOBM.3620300824

Minotti, G., Recalcati, S., Mordente, A., Liberi, G., Calafiore, A. M., Mancuso, C., Preziosi, P., & Cairo, G. (1998). The secondary alcohol metabolite of doxorubicin irreversibly inactivates aconitase/iron regulatory protein-1 in cytosolic fractions from human myocardium. *FASEB Journal : Official Publication of the Federation of American Societies for Experimental Biology*, *12*(7), 541–552. https://doi.org/10.1096/FASEBJ.12.7.541

Miseta, A., & Csutora, P. (2000). Relationship Between the Occurrence of Cysteine in Proteins and the Complexity of Organisms. *Molecular Biology and Evolution*, *17*(8), 1232–1239. https://doi.org/10.1093/OXFORDJOURNALS.MOLBEV.A026406

Mitra, A., Barua, A., Huang, L., Ganguly, S., Feng, Q., & He, B. (2023). From bench to bedside: the history and progress of CAR T cell therapy. *Frontiers in Immunology*, *14*. https://doi.org/10.3389/FIMMU.2023.1188049

Muñoz-Velasco, I., Herrera-Escamilla, A. K., & Vázquez-Salazar, A. (2025). Nucleolar origins: challenging perspectives on evolution and function. *Open Biology*, *15*(3), 240330. https://doi.org/10.1098/RSOB.240330

Nagura, E., Kimura, K., Yamada, K., Ota, K., Maekawa, T., Takaku, F., Uchino, H., Masaoka, T., Amaki, I., Kawashima, K., Ohno, R., Nomura, T., Hattori, J. ichi, Kawamura, S., Shibata, A., Shirakawa, S., & Hamajima, N. (1994). Nation-wide randomized comparative study of doxorubicin, vincristine and prednisolone combination therapy with and without L-asparaginase for adult acute lymphoblastic leukemia. *Cancer Chemotherapy and Pharmacology*, *33*(5), 359–365. https://doi.org/10.1007/BF00686263

Ogawa, L. M., Buhagiar, A. F., Abriola, L., Leland, B. A., Surovtseva, Y. V., & Baserga, S. J. (2021). Increased numbers of nucleoli in a genome-wide RNAi screen reveal proteins that link the cell cycle to RNA polymerase I transcription. *Molecular Biology of the Cell*, *32*(9), 956. https://doi.org/10.1091/MBC.E20-10-0670

Olausson, K. H., Nistér, M., & Lindström, M. S. (2012). p53 -Dependent and -Independent Nucleolar Stress Responses. *Cells*, *1*(4), 774–798. https://doi.org/10.3390/CELLS1040774

Olson, M. O. J. (2004). Sensing cellular stress: another new function for the nucleolus? *Science's STKE : Signal Transduction Knowledge Environment*, *2004*(224). https://doi.org/10.1126/STKE.2242004PE10

Otake, Y., Soundararajan, S., Sengupta, T. K., Kio, E. A., Smith, J. C., Pineda-Roman, M., Stuart, R. K., Spicer, E. K., & Fernandes, D. J. (2007). Overexpression of nucleolin in chronic lymphocytic leukemia cells induces stabilization of bcl2 mRNA. *Blood*, *109*(7), 3069–3075. https://doi.org/10.1182/BLOOD-2006-08-043257

Pelcovits, A., & Niroula, R. (2013, April 1). *Acute Myeloid Leukemia: A Review - PubMed*. R I Med J 103(3). https://pubmed.ncbi.nlm.nih.gov/32236160/

Pichiorri, F., Palmieri, D., De Luca, L., Consiglio, J., You, J., Rocci, A., Talabere, T., Piovan, C., Lagana, A., Cascione, L., Guan, J., Gasparini, P., Balatti, V., Nuovo, G., Coppola, V., Hofmeister, C. C., Marcucci, G., Byrd, J. C., Volinia, S., … Croce, C. M. (2013). In vivo NCL targeting affects breast cancer aggressiveness through miRNA regulation. *The Journal of Experimental Medicine*, *210*(5), 951–968. https://doi.org/10.1084/JEM.20120950

Rickards, B., Flint, S. J., Cole, M. D., & LeRoy, G. (2007). Nucleolin is required for RNA polymerase I transcription in vivo. *Molecular and Cellular Biology*, *27*(3), 937–948. https://doi.org/10.1128/MCB.01584-06

Rieker, C., Engblom, D., Kreiner, G., Domanskyi, A., Schober, A., Stotz, S., Neumann, M., Yuan, X., Grummt, I., Schütz, G., & Parlato, R. (2011). Nucleolar disruption in dopaminergic neurons leads to oxidative damage and parkinsonism through repression of mammalian target of rapamycin signaling. *The Journal of Neuroscience : The Official Journal of the Society for Neuroscience*, *31*(2), 453–460. https://doi.org/10.1523/JNEUROSCI.0590-10.2011

Rodrigues, A., MacQuarrie, K. L., Freeman, E., Lin, A., Willis, A. B., Xu, Z., Alvarez, A. A., Ma, Y., Perez White, B. E., Foltz, D. R., & Huang, S. (2023). Nucleoli and the nucleoli-centromere association are dynamic during normal development and in cancer. *Molecular Biology of the Cell*, *34*(4). https://doi.org/10.1091/MBC.E22-06-0237

Russo, A., & Russo, G. (2017). Ribosomal Proteins Control or Bypass p53 during Nucleolar Stress. *International Journal of Molecular Sciences*, *18*(1). https://doi.org/10.3390/IJMS18010140

Šašinková, M., Heřman, P., Holoubek, A., Strachotová, D., Otevřelová, P., Grebeňová, D., Kuželová, K., & Brodská, B. (2021). NSC348884 cytotoxicity is not mediated by inhibition of nucleophosmin oligomerization. *Scientific Reports*, *11*(1), 1084. https://doi.org/10.1038/s41598-020-80224-1

Šašinková, M., Holoubek, A., Otevřelová, P., Kuželová, K., & Brodská, B. (2018). AML-associated mutation of nucleophosmin compromises its interaction with nucleolin. *The International Journal of Biochemistry & Cell Biology*, *103*, 65–73. https://doi.org/10.1016/j.biocel.2018.08.008

Scherl, A., Couté, Y., Déon, C., Callé, A., Kindbeiter, K., Sanchez, J. C., Greco, A., Hochstrasser, D., & Diaz, J. J. (2002). Functional proteomic analysis of human nucleolus. *Molecular Biology of the Cell*, *13*(11), 4100–4109. https://doi.org/10.1091/MBC.E02-05-0271

Schieber, M., & Chandel, N. S. (2014). ROS function in redox signaling and oxidative stress. *Current Biology : CB*, *24*(10). https://doi.org/10.1016/J.CUB.2014.03.034

Schmidt-Zachmann, M. S., & Nigg, E. A. (1993). Protein localization to the nucleolus: a search for targeting domains in nucleolin. *Journal of Cell Science*, *105 (Pt 3)*(3), 799–806. https://doi.org/10.1242/JCS.105.3.799

Shen, N., Yan, F., Pang, J., Wu, L. C., Al-Kali, A., Litzow, M. R., & Liu, S. (2014). A nucleolin-DNMT1 regulatory axis in acute myeloid leukemogenesis. *Oncotarget*, *5*(14), 5494. https://doi.org/10.18632/ONCOTARGET.2131

Sherif, H. A., Magdy, A., Elshesheni, H. A., Ramadan, S. M., & Rashed, R. A. (2021). Treatment outcome of doxorubicin versus idarubicin in adult acute myeloid leukemia. *Leukemia Research Reports*, *16*, 100272. https://doi.org/10.1016/J.LRR.2021.100272

Sies, H., Berndt, C., & Jones, D. P. (2017). Oxidative stress. *Annual Review of Biochemistry*, *86*(Volume 86, 2017), 715–748. https://doi.org/10.1146/ANNUREV-BIOCHEM-061516-045037/CITE/REFWORKS

Sies, H., Mailloux, R. J., & Jakob, U. (2024). Fundamentals of redox regulation in biology. *Nature Reviews. Molecular Cell Biology*, *25*(9), 701–719. https://doi.org/10.1038/S41580-024-00730-2

Singh, M., Sharma, H., & Singh, N. (2007). Hydrogen peroxide induces apoptosis in HeLa cells through mitochondrial pathway. *Mitochondrion*, *7*(6), 367–373. https://doi.org/10.1016/J.MITO.2007.07.003

Smeenk, L., van Heeringen, S. J., Koeppel, M., Gilbert, B., Janssen-Megens, E., Stunnenberg, H. G., & Lohrum, M. (2011). Role of p53 serine 46 in p53 target gene regulation. *PloS One*, *6*(3). https://doi.org/10.1371/JOURNAL.PONE.0017574

Smetana, K., Chan, P. K., Marinov, Y., Souček, J., Hrkal, Z., & Busch, H. (2004). A short note on the nucleolar size and density in apoptotic leukemic granulocytic precursors (HL-60 cells). *Life Sciences*, *75*(7), 791–796. https://doi.org/10.1016/j.lfs.2003.12.028

Sritharan, S., & Sivalingam, N. (2021). A comprehensive review on time-tested anticancer drug doxorubicin. *Life Sciences*, *278*. https://doi.org/10.1016/J.LFS.2021.119527

Strachotová, D., Holoubek, A., Wolfová, K., Brodská, B., & Heřman, P. (2023). Cytoplasmic localization of Mdm2 in cells expressing mutated NPM is mediated by p53. *The FEBS Journal*, *290*(17), 4281–4299. https://doi.org/10.1111/FEBS.16810

Sulima, S. O., Hofman, I. J. F., De Keersmaecker, K., & Dinman, J. D. (2017). How Ribosomes Translate Cancer. *Cancer Discovery*, *7*(10), 1069–1087. https://doi.org/10.1158/2159-8290.CD-17-0550

Takeuchi, J., Kyo, T., Naito, K., Sao, H., Takahashi, M., Miyawaki, S., Kuriyama, K., Ohtake, S., Yagasaki, F., Murakami, H., Asou, N., Ino, T., Okamoto, T., Usui, N., Nishimura, M., Shinagawa, K., Fukushima, T., Taguchi, H., Morii, T., … Ohno, R. (2002). Induction therapy by frequent administration of doxorubicin with four other drugs, followed by intensive consolidation and maintenance therapy for adult acute lymphoblastic leukemia: the JALSG-ALL93 study. *Leukemia*, *16*(7), 1259–1266. https://doi.org/10.1038/SJ.LEU.2402526

Terwilliger, T., & Abdul-Hay, M. (2017). Acute lymphoblastic leukemia: a comprehensive review and 2017 update. *Blood Cancer Journal*, *7*(6). https://doi.org/10.1038/BCJ.2017.53

Tewey, K. M., Rowe, T. C., Yang, L., Halligan, B. D., & Liu, L. F. (1984). Adriamycin-induced DNA damage mediated by mammalian DNA topoisomerase II. *Science (New York, N.Y.)*, *226*(4673), 466–468. https://doi.org/10.1126/SCIENCE.6093249

Thiede, C., Koch, S., Creutzig, E., Steudel, C., Illmer, T., Schaich, M., & Ehninger, G. (2006). Prevalence and prognostic impact of NPM1 mutations in 1485 adult patients with acute myeloid leukemia (AML). *Blood*, *107*(10), 4011–4020. https://doi.org/10.1182/BLOOD-2005-08-3167

Thorn, C. F., Oshiro, C., Marsh, S., Hernandez-Boussard, T., McLeod, H., Klein, T. E., & Altman, R. B. (2011). Doxorubicin pathways: pharmacodynamics and adverse effects. *Pharmacogenetics and Genomics*, *21*(7), 440–446. https://doi.org/10.1097/FPC.0B013E32833FFB56

Varadi, M., Bertoni, D., Magana, P., Paramval, U., Pidruchna, I., Radhakrishnan, M., Tsenkov, M., Nair, S., Mirdita, M., Yeo, J., Kovalevskiy, O., Tunyasuvunakool, K., Laydon, A., Žídek, A., Tomlinson, H., Hariharan, D., Abrahamson, J., Green, T., Jumper, J., … Velankar, S. (2024). AlphaFold Protein Structure Database in 2024: providing structure coverage for over 214 million protein sequences. *Nucleic Acids Research*, *52*(D1), D368–D375. https://doi.org/10.1093/NAR/GKAD1011

Willi, J., Küpfer, P., Eviquoz, D., Fernandez, G., Katz, A., Leumann, C., & Polacek, N. (2018). Oxidative stress damages rRNA inside the ribosome and differentially affects the catalytic center. *Nucleic Acids Research*, *46*(4), 1945–1957. https://doi.org/10.1093/NAR/GKX1308

Xu, G., Hao, Z., Xiao, W., Tan, R., Yuan, M., Xia, Y., & Liu, Y. (2023). Zymosan A Improved Doxorubicin-Induced Ventricular Remodeling by Evoking Heightened Cardiac Inflammatory Responses and Healing in Mice. *Journal of the American Heart Association*, *12*(18). https://doi.org/10.1161/JAHA.123.030200

Yang, K., Wang, M., Zhao, Y., Sun, X., Yang, Y., Li, X., Zhou, A., Chu, H., Zhou, H., Xu, J., Wu, M., Yang, J., & Yi, J. (2016). A redox mechanism underlying nucleolar stress sensing by nucleophosmin. *Nature Communications*, *7*. https://doi.org/10.1038/NCOMMS13599

Yao, Y., Zhou, Y., Zhuo, N., Xie, W., Meng, H., Lou, Y., Mao, L., Tong, H., Qian, J., Yang, M., Yu, W., Zhou, D., Jin, J., & Wang, H. (2024). Co-mutation landscape and its prognostic impact on newly diagnosed adult patients with NPM1-mutated de novo acute myeloid leukemia. *Blood Cancer Journal*, *14*(1). https://doi.org/10.1038/S41408-024-01103-W

Zhang, J., Tsaprailis, G., & Bowden, G. T. (2008). Nucleolin stabilizes Bcl-X L messenger RNA in response to UVA irradiation. *Cancer Research*, *68*(4), 1046–1054. https://doi.org/10.1158/0008-5472.CAN-07-1927

Zhao, H., Huang, Y., Xue, C., Chen, Y., Hou, X., Guo, Y., Zhao, L., Hu, Z. huang, Huang, Y., Luo, Y., & Zhang, L. (2013). Prognostic significance of the combined score of endothelial expression of nucleolin and CD31 in surgically resected non-small cell lung cancer. *PloS One*, *8*(1). https://doi.org/10.1371/JOURNAL.PONE.0054674